SPRINGER BRIEFS IN
PETROLEUM GEOSCIENCE & ENGINEERING

Alexandre Mendonça Teixeira
Lara de Oliveira Arinelli
José Luiz de Medeiros
Ofélia de Queiroz Fernandes Araújo

Monoethylene Glycol as Hydrate Inhibitor in Offshore Natural Gas Processing

From Fundamentals to Exergy Analysis

Springer

SpringerBriefs in Petroleum Geoscience & Engineering

The SpringerBriefs series in Petroleum Geoscience & Engineering promotes and expedites the dissemination of substantive new research results, state-of-the-art subject reviews and tutorial overviews in the field of petroleum exploration, petroleum engineering and production technology. The subject focus is on upstream exploration and production, subsurface geoscience and engineering. These concise summaries (50–125 pages) will include cutting-edge research, analytical methods, advanced modelling techniques and practical applications. Coverage will extend to all theoretical and applied aspects of the field, including traditional drilling, shale-gas fracking, deepwater sedimentology, seismic exploration, pore-flow modelling and petroleum economics. Topics include but are not limited to:

- Petroleum Geology & Geophysics
- Exploration: Conventional and Unconventional
- Seismic Interpretation
- Formation Evaluation (well logging)
- Drilling and Completion
- Hydraulic Fracturing
- Geomechanics
- Reservoir Simulation and Modelling
- Flow in Porous Media: from nano- to field-scale
- Reservoir Engineering
- Production Engineering
- Well Engineering; Design, Decommissioning and Abandonment
- Petroleum Systems; Instrumentation and Control
- Flow Assurance, Mineral Scale & Hydrates
- Reservoir and Well Intervention
- Reservoir Stimulation
- Oilfield Chemistry
- Risk and Uncertainty
- Petroleum Economics and Energy Policy

Contributions to the series can be made by submitting a proposal to the responsible Springer contact, Charlotte Cross at charlotte.cross@springer.com or the Academic Series Editor, Prof Dorrik Stow at dorrik.stow@pet.hw.ac.uk.

More information about this series at http://www.springer.com/series/15391

Alexandre Mendonça Teixeira
Lara de Oliveira Arinelli • José Luiz de Medeiros
Ofélia de Queiroz Fernandes Araújo

Monoethylene Glycol as Hydrate Inhibitor in Offshore Natural Gas Processing

From Fundamentals to Exergy Analysis

Springer

Alexandre Mendonça Teixeira
Escola de Química - UFRJ
Federal University of Rio de Janeiro
Rio de Janeiro, Brazil

Lara de Oliveira Arinelli
Escola de Química - UFRJ
Federal University of Rio de Janeiro
Rio de Janeiro, Brazil

José Luiz de Medeiros
Escola de Química - UFRJ
Federal University of Rio de Janeiro
Rio de Janeiro, Brazil

Ofélia de Queiroz Fernandes Araújo
Escola de Química – UFRJ
Federal University of Rio de Janeiro
Rio de Janeiro, Brazil

ISSN 2509-3126 ISSN 2509-3134 (electronic)
SpringerBriefs in Petroleum Geoscience & Engineering
ISBN 978-3-319-66073-8 ISBN 978-3-319-66074-5 (eBook)
DOI 10.1007/978-3-319-66074-5

Library of Congress Control Number: 2017950161

Printed on acid-free paper

This Springer imprint is published by Springer Nature
The registered company is Springer International Publishing AG
The registered company address is: Gewerbestrasse 11, 6330 Cham, Switzerland

Preface

In the past two decades the exploration and production of natural gas in offshore fields has made impressive expansion, with several discoveries of fields involving many dozens of $MMsm^3/d$ of gas flow rate in the peak of production. Now, in certain parts of the globe, the frontier is on ultra-deep water offshore fields as in the Pre-Salt Basin in the south-east coast of Brazil.

Evidently, the main driving force behind these discoveries is not the natural gas per se, but, instead, the quest for offshore oil reservoirs. In this regard, the biggest new found Pre-Salt provinces are invariably associated to immense volumes of natural gas at high gas-oil ratios, ultra-high reservoir pressure and, in some instances, ultra-high CO_2 content above 45% mol. Such immense volumes of natural gas must be adequately explored, transported, processed and utilized, according to an economical and environmental sustainable way, in order to cope with stringent environmental constraints and with the enormous costs and investments of ultra-deep water production. In other words, in face of the huge reserves of associated natural gas, which must be produced to allow the oil production to flow, it is planned that the natural gas offshore production could pay for all costs of exploration & production in the main Pre-Salt fields, leaving the oil production as a net positive income of cash.

This, of course, is a very wishful-thinking image of the real problem, because several other massively important conjunctural variables must be taken into account, like the global economic slow-down and the prices of oil and gas, which are experimenting incredible global falls by the time this book was written.

Even so, the recent discoveries in the Pre-Salt Basin of Brazil are so huge, that they really can create a massive business of natural gas, which must be taken seriously in terms of rational use and engineering in order to abate at least a good share of the costs and risks of ultra-deep water offshore oil & gas production.

But if we are talking about massive gas production in cold ultra-deep waters, at extra high pressures on well-heads, located at hundreds of kilometers from the coast and even more from the main consuming centers, evidently we are also talking about gas transportation via subsea pipelines and flow assurance issues.

Such kind of talk evidently poses the discussion of technologies of Thermodynamic Hydrate Inhibition (THI) on the order of the day. It is then natural that one of the great global THI champions, namely, Monoethylene Glycol (MEG) should also be invited to the discussion. But MEG just cannot come alone, especially if massive flow rates of MEG have to be used, as THIs are normally spent with generosity. In other words, the entire infra-structure for MEG recovery and recycle on offshore rigs should also be addressed.

Well, is precisely at this point of our little discussion that we can put this book on the table.

The book is a consolidation of the recent works of our group (www.h2cin.org.br) on engineering, modeling, exergy analysis and thermodynamic analysis of technologies for recovery (reclamation) of Monoethylene Glycol (MEG) as thermodynamic hydrate inhibitor (THI) in the context of natural gas production in offshore fields. Indeed, the book is an expanded version of some of ours recent papers, particularly Teixeira et al. (2015, 2016).

In offshore platforms that operate MEG Loops, MEG reclamation is processed on MEG Recovery Units (MRUs). MRUs are very modular processing systems, that are attached on oil & gas platforms or FPSOs, in order to accomplish the task of regeneration of Rich MEG (used THI) to be re-injected as refreshed THI (Lean MEG).

MRUs per se are not very complex plants, but, as they have to be attached on offshore rigs, immediately some questions like engineering and energy consumption of MRU flowsheets, thermodynamic modeling of glycol systems, equipment size, equipment footprint and evaluation of the degree of energy degradation in MRU flowsheets gain some highlight and come naturally into the discussion.

These are the main topics of this book. But the chapters of the book dedicated to evaluation of energy degradation in offshore MRUs constitute its more sophisticated sector which should be perhaps worth of note. The subject of evaluation of energy degradation in MRUs was addressed via Exergy Analysis of offshore MRUs in Chap. 8, where the determination of the Exergy Efficiency of units and of the entire MRUs is done according to two formulations of the Reference Environmental Reservoir (RER), namely: the classical RER prescribing chemical equilibrium for the organic species and a new RER version which gave more useful results. But, since distillation operations constitute the main components of MRUs as great sinks of exergy destruction, a parallel Thermodynamic Analysis of distillation columns was also carried out in Chap. 7 with the intent of presenting tools to estimate the Thermodynamic Efficiency of steady-state distillation operations. In connection with this issue, it must be pointed out that Thermodynamic Efficiency of Process is not the same thing as Exergy Efficiency of Process. But both have a strong and direct interrelation and both vary alongside in the same direction and should have similar magnitudes in the same context of application.

These are a few previous words that, perhaps, can motivate the interested Reader on the subject of Exergy Analysis of MRUs and related topics, to go into this book.

Rio de Janeiro, Brazil

Alexandre Mendonça Teixeira
Lara de Oliveira Arinelli
José Luiz de Medeiros
Ofélia de Queiroz Fernandes Araújo

Contents

Abbreviations

AAHI	Anti-agglomerating hydrate inhibitors
ADC	Atmospheric distillation column of MRU
BOP	Blow-out preventer
C1	Methane, CH_4
C2	Ethane, C_2H_6
C3	Propane, C_3H_8
C3=	Propylene, C_3H_6
C4	Butane, C_4H_{10}
CAPEX	Capital expenditures
ChW	Chilled water (10 °C)
CMO	Constant molar overflow (McCabe-Thiele assumption)
CW	Cooling Water (25–40 °C) or (35–50 °C)
EE	Electric energy consumption (kW)
EOS	Equation of state
ExA	Exergy analysis
FLS	Flash-evaporator
FPSO	Floating production, storage and offloading
FS	Full-stream process
HC	Hydrocarbon
HSE	Health, safety and environment
HRWH	Heat recovery water heater
iC4	Isobutane, iC_4H_{10}
KHI	Kinetic hydrate inhibitor
LHS	Left hand side
MEG	Monoethylene glycol
MRU	MEG recovery unit
NG	Natural gas
OPEX	Operation expenditures
PFD	Process flow diagram
PHW	Pressurized hot water (200–110 °C) or (150–100 °C)

PR-EOS	Peng-Robinson EOS
RER	Reference environmental reservoir
RHS	Right hand side
SDC	Sub-atmospheric (vacuum) distillation column
SVLE	Solid–vapor–liquid equilibrium
SS	Slip-stream process
SW	Sea water (20–35 °C)
THI	Thermodynamic hydrate inhibitor
TP	Traditional MEG recovery process
TST-EOS	Twu-Sim-Tassone EOS
VLE	Vapor–liquid equilibrium

Nomenclature

a, b	: EOS parameters dependent of mixing rules
$\dot{B}$	: Exergy flow rate (kW)
$\bar{B}_{K_j}, \bar{B}_{F_j}$	: Molar exergies of streams K_j and F_j (kJ/mol)
B	: Bottoms product flow rate of distillation column (mol/s)
$\bar{C}_P$	: Molar heat capacity at constant pressure (kJ/K·mol)
$\hat{C}_P$	: Mass heat capacity at constant pressure (kJ/K·kg)
D	: Distillate product flow rate of distillation column (mol/s)
F	: Feed flow rate of distillation column (mol/s)
F_j	: Molar flow rate of jth inlet stream (mol/s)
(g)	: Standard state of pure ideal gas at 25 °C and 1 atm
$\bar{G}$	: Molar Gibbs free energy (kJ/mol)
$\bar{H}$	: Molar enthalpy (kJ/mol)
$\bar{H}_B$	: Molar enthalpy of bottoms product (kJ/mol)
$\bar{H}_D$	: Molar enthalpy of distillate product (kJ/mol)
$\bar{H}_D^V$	: Molar enthalpy of distillate as a saturated vapor (kJ/mol)
$\bar{H}_F$	: Molar enthalpy of the column feed (kJ/mol)
$\hat{H}$	: Mass enthalpy (kJ/kg)
K_j	: Molar flow rate of jth outlet stream (mol/s)
K_k	: Vapor–liquid equilibrium factor of component k
nc	: Number of components
P	: Absolute pressure (kPa)
q	: Mass flow rate (kg/s)
q_{CW}	: Mass flow rate of cooling water (CW) (kg/s)
q_{PHW}	: Mass flow rate of pressurized hot water (PHW) (kg/s)
$\dot{Q}_0$	: Heat transfer rate (System viewpoint) from R_H (kW)
Q	: Heat duty (kW) (System viewpoint)
Q^{REV}	: Reversible heat duty (kW) (System viewpoint)
Q_C	: Absolute value (>0) of condenser (cold) duty (kW)

Q_H : Absolute value (>0) of reboiler (hot) duty (kW)
R : Ideal gas constant ($8.314.10^{-3}$ kJ/mol·K)
R_H, R_V, R_k : Heat reservoir, volume reservoir and species k reservoir
REC_i : Distillation molar top recovery of species i (mol/s)
REC'_i : Distillation molar bottoms recovery of species i (mol/s)
$REC_i\%$: Distillation % top recovery of species i (%)
$REC'_i\%$: Distillation % bottoms recovery of species i (%)
RR : Column reflux ratio
$\bar{S}$: Molar entropy (kJ/K.mol)
$\bar{S}_B$: Molar entropy of bottoms product (kJ/K·mol)
$\bar{S}_D$: Molar entropy of distillate product (kJ/K·mol)
$\bar{S}_F$: Molar entropy of column feed (kJ/K·mol)
$\hat{S}$: Mass entropy (kJ/K·kg)
T : Absolute temperature (K)
T_r : Reduced temperature
TAPP : Thermal approach of heat exchange (°C)
$\dot{U}$: Rate of change of internal energy (kW)
$\bar{V}$: Molar volume (m^3/mol)
v : EOS molar volume (m^3/mol)
X : Component 1 mol fraction in binary liquid phase
X_k : Component k mol fraction in liquid phase
X_B : Component 1 mol fraction in binary bottoms product
X_{Bk} : Component k mol fraction in bottoms product
X_D : Component 1 mol fraction in binary distillate product
X_{Dk} : Component k mol fraction in distillate product
$\dot{W}$: Rate of shaft work done by System (kW)
$\dot{W}^{REV}$: Reversible rate of work done by System (kW)
$\dot{W}_V$: Rate of volume work done by System on R_V (kW)
Y : Component 1 mol fraction in binary vapor phase
Y_k : Component k mol fraction in vapor phase
Y_{kFj} : Mol fraction of species k in stream F_j
Z_k : Component k mol fraction in the column feed

Greek Symbols

α‘ : Volatility of species 1 relative to species 2
α_k : Volatility of component k relative to heavy key j
$\alpha(T)$: Specific EOS function of temperature for each component
β : Feed vapor fraction at column pressure
$\eta\%$: Percent exergy efficiency of process or unit
λ : Enthalpy of vaporization at column pressure (kJ/mol)
$\dot{\Xi}_k$: Rate of energy transfer from the reservoir of species k to the System (kW)

$\dot{\Omega}_k$: Net rate of creation of species k (mol/s) in the Universe
$\dot{\Omega}_V$: Net rate of creation of volume (m^3/s) in the Universe
$\dot{\Omega}_S$: Net rate of creation of entropy (kJ/K.s) in the Universe
μ_k : Chemical potential of species k (kJ/kmol)
ω_k : Acentric factor of species k

Subscripts

0 : Relative to Reference Environmental Reservoir (RER)
0 : Relative to reservoir R_H at T_0
B : Relative to bottoms product
c : Relative to critical point of a species
CW : Relative to the cooling water (CW) stream
D : Relative to distillate product
F : Relative to column feed
i, k : Indexes of component
i, j : Light and heavy key components of a distillation cut
j : Index of stream
PHW : Relative to the pressurized hot water (PHW) stream

Superscripts

∞, H_2O : Infinite dilution in water
∞ : Relative to pinch condition (minimum column reflux)
0 : Relative to Reference Environmental Reservoir (RER)
CW : Relative to the cooling water (CW) stream
f : Pure component formation at standard conditions
IN : Entering condition of a stream
LOST : Related to work lost by irreversibilities
nfs : Number of feed streams
nps : Number of product streams
nwi : Number of power streams imported by the System
nwe : Number of power streams exported by the System
OUT : Exiting condition of a stream
PHW : Relative to the pressurized hot water (PHW) stream
REV : Under reversible operation
w : Relative to exergy flows constituted by pure mechanical energy like an electricity current

Chapter 1
Introduction

Abstract Offshore exploration and production of natural gas has increased all over the globe due to the high offer of this energy resource in ocean basins. Along with this quest a lot of challenges have emerged. Particularly, a major concern is related to flow assurance, i.e., to ensure successful natural gas flow in pipelines and processing facilities and guarantee continuous production without flow restriction. In this sense, gas hydrate formation is considered as the most critical aspect in flow assurance strategies, particularly in deepwater offshore fields. Gas hydrate plugs can signify tremendous safety and economic impacts on gas flowline operation and can stop production completely for several days or months, and even result in pipeline loss in the worst case. Further, the removal and remediation of plugs of gas hydrate, once they are formed, can be a very costly and time-consuming process, which emphasizes the importance of preventive measures like the inhibition of hydrate formation. Hence, this chapter presents the main topics of this book by making a quick overview about hydrates, hydrate inhibitors, MEG injection, closed MEG loop system, MEG recovery processes, and exergy contextualization.

In the past few decades, humanity has crossed natural boundaries in search of energetic resources as occurred in the exploration and production in deepwater offshore environments. Around a third of the oil and gas extracted worldwide comes from offshore sources, and it is likely to continue to rise over the coming decades due to abundant oil and gas deposits deep in the oceans (World Ocean Review 3 2014). Further, as many oil and gas fields in shallow waters have becoming more or less exhausted, companies tend to penetrate greater depths to access this energy resource.

Offshore exploration and production of natural gas has increased all over the globe due to the high offer of this energy resource in ocean basins. Along with this quest a lot of challenges have emerged. Particularly, a major concern is related to flow assurance, i.e., to ensure successful natural gas flow in pipelines and processing facilities and guarantee continuous production without flow restriction.

In the context of natural gas production the presence of water in contact with light hydrocarbon species of natural gas—CH_4, C_2H_6, C_3H_8, C_4H_{10}—defines the scenario for the appearance of solid gas hydrates. Gas hydrate formation is

A. Mendonça Teixeira et al., *Monoethylene Glycol as Hydrate Inhibitor in Offshore Natural Gas Processing*, SpringerBriefs in Petroleum Geoscience & Engineering,
DOI 10.1007/978-3-319-66074-5_1

considered as the most critical aspect in flow assurance strategies, particularly in deepwater offshore fields.

Hydrocarbon gas hydrate formation in flowlines occurs as consequence of favorable thermodynamic conditions, which can be materialized basically by the occurrence of the three first factors below and severely aggravated by the fourth factor:

- Presence of production liquid water or vapor water saturation along with the gas.
- Conditions of high pressure in flowlines.
- Low external pipe temperature close to 0 °C due to the high depth involved (Gupta and Singh 2012).
- Frequent line shutdowns and flow interruptions under exposure to the three above factors.

As the above conditions are typically found in deepwater subsea gas pipelines, measures for prevention, control and abatement of such gas hydrate compounds is mandatory in offshore gas production.

Gas hydrate plugs can signify tremendous safety and economic impacts on gas flowline operation and can stop production completely for several days or months, and even result in pipeline loss in the worst case. Further, the removal and remediation of plugs of gas hydrate, once they are formed, can be a very costly and time-consuming process, which emphasizes the importance of preventive measures like the inhibition of hydrate formation (Nazeri et al. 2012).

Therefore, the need for avoiding hydrate formation in natural gas flowlines is evident. Not only do hydrates act chronically progressively restricting flow and gradually imposing higher compressor costs due to head losses, but they can also form solid plugs that can suddenly cause damages to equipment like automatic valves and heat transfer surfaces.

In this sense, a common alternative to overcome gas hydrate issues is the continuous injection of hydrate inhibitors in well-heads, so that the inhibitor flows together with production fluids, thus preventing or retarding hydrate formation and consequently avoiding significant safety hazards in production facilities and preventing loss of production.

There are several categories of commercial agents for gas hydrate inhibition, namely:

- Thermodynamic hydrate inhibitors (THIs): Act displacing the thermodynamic equilibrium of hydrate formation to unfavorable conditions via stabilizing the water in the liquid aqueous phase by adding a liquid or solid solute that reduces the chemical potential of water, which is equivalent to say that the hydrate boundary is shifted to lower temperatures. The THIs are very hydrophilic substances that must be present at high concentration ($>20\%$ *w*/*w*) in the liquid aqueous phase (high dosage hydrate inhibitors) so that they can interact strongly with water in the aqueous phase reducing its fugacity and activity. Examples of THIs are glycols like mono-ethylene glycol (MEG), di-ethylene glycol (DEG) and tri-ethylene glycol (TEG); small chain alcohols like methanol (MeOH) and

ethanol (EtOH); and hydrophilic inorganic salts like NaCl and KCl. THIs are not very dependent of temperature to be effective and can be used in ample ranges of temperatures, excepting the most viscous agents like TEG and DEG which are problematic at very low temperatures. THIs are somewhat indifferent to the presence of liquid hydrocarbons (condensate) provided the water content is high enough to stabilize them in the aqueous phase. Nevertheless the excess of condensate can affect the processing costs of using certain organic THIs that may dissolve in the organic liquid losing hydrophilic action and bringing separation concerns for their recovery.

- Kinetic hydrate inhibitors (KHIs): Act slowing down or retarding the kinetics of hydrate nucleation and, consequently, its crystal growth, despite the existence of favorable hydrate thermodynamic conditions. The KHIs are low dosage hydrate inhibitors (<1% w/w) in the aqueous liquid phase—like amines and fatty acids—that adhere to the very first nucleating particles of formed solid hydrates retarding its successful nucleation and growth via surface phenomena. Temperature can affect strongly the performance of KHIs, because low temperatures are obstacles to the anti-nucleating action of these agents, besides the fact that some are very viscous species that may present problems at low temperatures. KHIs do not require the presence of liquid hydrocarbons (condensate) jointly with water to be effective.
- Anti-agglomerating hydrate inhibitors (AAHIs): The AAHIs do not interfere with the thermodynamic favorability or with the kinetics of nucleation of gas hydrate formation. They merely are low dosage hydrate inhibitors that act as dispersing agents at low concentration, like surfactants or detergents. AAHIs avoid the growth of hydrate plugs by dispersing or emulsifying the small crystals as they form in the aqueous phase, hindering crystals sticking together and creating obstacles to the appearance of large crystals of hydrates that are the true troublemakers. The efficacy of the AAHIs is dependent of the presence of liquid hydrocarbons (condensate) jointly with water to be effective because this conjunction enhances the emulsification of solid hydrates.

Regarding the recent developments of technologies of gas hydrate inhibition, the achievements in the past decade of new technologies of kinetic hydrate inhibitors (KHIs) and anti-agglomerating hydrate inhibitors (AAHIs) are very impressive and worth of note (Pickering et al. 2001).

An appealing factor is that low dosage hydrate inhibitors, like KHIs and AAHIs, are receiving recent commercial attention due to their more pragmatic and practical way of utilization. The underlying point is that there is no need of recovery of KHIs and AAHIs after use. That is, there is no necessity of investments in recovery plants or separation processes. This is in frontal contrast with the category of THIs, which, classically, is the most used one in terms of global scale, but depends heavily of recovery technologies. In connection with this, it must be pointed out that the subject of this work is only the THIs category, specifically the technologies involved with the use of MEG as THIs.

In the category of thermodynamic hydrate inhibition (THIs), MEG injection has been widely used owing to its advantageous features when compared to other THIs, such as low losses to vapor phase, low solubility in condensate phase, high depression of water freezing point, high depression of temperatures for gas hydrate formation, good performance at very low (glacial) temperatures, not too low viscosity, and good attenuation of corrosion potential.

In connection with the notion that THIs are High Dosage Hydrate Inhibitors, which must be easily recovered in order to be cost-effective, the recovery of MEG is comparatively a simple process. In other words, MEG can be effectively regenerated and recycled with low losses, configuring a cost-effective choice for hydrate inhibition (Haghighi et al. 2009). Due to the high cost of replacing the large amounts of hydrate inhibitors used within the natural gas processing system, there is a strong economic drive to recycle and recirculate MEG.

Moreover, the latest MEG reclamation plant designs are cheaper to build, safer and easy to operate. Up-to-date MRUs have simpler equipment and offer substantially better performance, especially in terms of reliability, high recovery of MEG, low energy consumption, low carbon emission, and adequate disposal of salt and water back into the sea with environmentally acceptable levels of contamination, and they also comply with the best Health, Safety and Environment (HSE) standards (Nazzer and Keogh 2006). All those features are advantageous for offshore environment, rendering MEG as the preferred THIs.

After injection, MEG flows along with the production fluids towards the platform, where the three-phase incoming stream is split into:

- An aqueous bottom phase, comprising mainly MEG, water, and salts.
- An intermediate hydrocarbon liquid phase (condensate).
- An upper vapor phase of saturated natural gas with low water content.

The aqueous denser phase, after removal of hydrocarbons in a pretreatment step, is also known as Rich MEG, i.e., aqueous MEG containing at least 25% w/w of water and salts (Bikkina et al. 2012).

The Rich MEG stream is sent to the MEG Recovery Unit (MRU) in order to be stripped of water, salts and other impurities. The recovered MEG is known as Lean MEG and normally contains a minimum of 80% w/w MEG. Lean MEG is returned to be reinjected into the well-heads, thereby completing the MEG loop.

Currently, there are three main technologies for offshore MRUs, namely, traditional atmospheric distillation process (TP), full-stream process (FS), and slipstream process (SS) (Teixeira et al. 2015, 2016).

Depending on the adopted MRU technology and process conditions, there will be different requirements of heating, cooling, and electric energy (EE) for the MRU operation. Since only MRUs located on offshore platforms are considered here, it is critical to minimize heating, cooling, and EE requirements and also the extent of energy degradation.

A better understanding of MRU technologies is attained when a more complete thermodynamic point of view is taken. In this sense, a comprehensive analysis of a

complex thermodynamic processing system includes both energy and exergy analyses in order to obtain a more complete picture of its processing performance.

Exergy analysis (ExA) has been recognized in the field of chemical and thermoelectric plants as a powerful tool to assess degradation of energy quality. ExA quantifies the percentage of destroyed exergy via process irreversibilities, as well as the percentage of lost exergy accompanying waste (material and energy) streams. ExA also assesses the primary sinks responsible for exergy destruction due to process inefficiencies (Boroumandjazi et al. 2013). Moreover, ExA might also be used as the criteria for optimization of process design in order to minimize energy requirements and energy degradation. ExA is then conducted for MRU processes in order to give insights regarding degradation of energy quality.

Hence, this work contributes to a better understanding of hydrate inhibition using MEG injection in offshore fields by discussing relevant features concerning hydrates, hydrate inhibition and MEG recovery processes in offshore rigs, as well as comparatively evaluating three MRU technologies in terms of energy consumption and exergy efficiency.

Furthermore, key aspects related to thermodynamics of glycol systems and thermodynamic efficiency of distillation columns are also discussed, as well as the development of formulae for exergy flow and also pertinent discussion about reference states for MEG so as to achieve an effective exergy analysis. Finally, after exergy analysis is successfully conducted, wherein the most inefficient process components are identified in MEG plants, a sensitivity analysis based on common design criteria is also covered in order to evaluate its impact on overall efficiency.

References

Bikkina C, Radhakrishnan N, Jaiswal S, Harrington R, Charlesworth M (2012) Development of MEG regeneration unit compatible corrosion inhibitor for wet gas systems. Paper presented at SPE Asia Pacific oil & gas conference and exhibition, Perth, Australia, 22–24 October 2012. SPE 160301. doi:10.2118/160301-MS

Boroumandjazi G, Rismanchi B, Saidur R (2013) A review on exergy analysis of industrial sector. Renew Sust Energ Rev 27:198–203. doi:10.1016/j.rser.2013.06.054

Gupta G, Singh SK (2012) Hydrate inhibition - optimization in deep water gas field. Paper presented at SPE oil and gas India conference and exhibition, Mumbai, India, 28–30 March 2012. SPE 153504. doi:10.2118/153504-MS

Haghighi H, Chapoy A, Burgess R, Tohidi B (2009) Experimental and thermodynamic modelling of systems containing water and ethylene glycol: application to flow assurance and gas processing. Fluid Phase Equilib 276(1):24–30. doi:10.1016/j.fluid.2008.10.006

Nazeri M, Tohidi B, Chapoy A (2012) An evaluation of risk of hydrate formation at the top of a pipeline. Paper presented at SPE Asia Pacific oil & gas conference and exhibition, Perth, Australia, 22–24 October 2012. SPE 160404. doi:10.2118/160404-MS

Nazzer CA, Keogh J (2006) Advances in glycol reclamation technology. Paper presented at offshore technology conference, Houston, USA, 1–4 May 2006. OTC 18010. doi:10.4043/18010-MS

Pickering PF, Edmonds B, Moorwood RAS, Szczepanski R, Watson MJ (2001) Evaluating new chemicals and alternatives for mitigating hydrates in oil & gas production.. http://feesa.net/pdf/

Discussion%20Papers/010918%20%20Evaluating%20Hydrate%20Inhibitors%20-%20Rev%20A.pdf. Accessed 06 Jun 2012

Teixeira AM, de Medeiros JL, Araújo OQF (2015) Exergy analysis of monoethylene glycol (MEG) recovery systems. Computer Aided Chemical Engineering, 12th international symposium on process systems engineering 37(1):533–538. doi:10.1016/B978-0-444-63578-5.50084-0

Teixeira AM, Arinelli LO, de Medeiros JL, Araújo OQF (2016) Exergy analysis of monoethylene glycol recovery processes for hydrate inhibition in offshore natural gas fields. J Nat Gas Sci Eng 35(1):798–813. doi:10.1016/j.jngse.2016.09.017

World Ocean Review 3, Maribus gGmbH, Hamburg, Germany (2014). ISBN 978-3-86648-221-0. http://worldoceanreview.com/wp-content/downloads/wor3/WOR3_chapter_1.pdf. Accessed 8 Nov 2016

Chapter 2
Hydrate Formation and Inhibition in Offshore Natural Gas Processing

Abstract Natural gas hydrates are crystalline water-based solids physically resembling ice, with a crystalline structure comprised of water and light hydrocarbon molecules (mainly CH_4). Such solids can be formed above the freezing temperature of water, and, for this reason, represent a major flow assurance concern, especially at high pressures. Gas hydrate structures are characterized by repetitive crystal units composed of asymmetric, spherical-like "cages" of hydrogen-bonded water molecules, each cage typically containing one (or more) guest molecule(s) held in its interior by dispersion forces. A lot of shortcomings might occur if gas hydrates accumulates severely in subsea flowlines. Their remediation is costly and risky and could mean production stoppages, causing economic losses, and posing hazards to the security and integrity of the pipelines. To thermodynamically inhibit hydrate formation in continuous gas pipeline systems, the most common prevention method is to continuously displace the hydrate forming boundary such that the operational temperature and pressure of the system lie on the outside of the hydrate boundary. This is accomplished by continuous injection of a certain flow rate of a THI compound, which must be proportional to the flow rate of water carried by the stream. This chapter covers the main aspects of hydrates and their structures, hydrate remediation and the mechanism of thermodynamic inhibition of hydrate formation.

Natural gas hydrates are crystalline water-based solids physically resembling ice, with a crystalline structure comprised of water and light hydrocarbon molecules (mainly CH_4). Such solids can be formed above the freezing temperature of water, and, for this reason, represent a major flow assurance concern, especially at high pressures.

Gas hydrate structures are characterized by repetitive crystal units composed of asymmetric, spherical-like "cages" of hydrogen-bonded water molecules, each cage typically containing one (or more) guest molecule(s) held in its interior by dispersion forces.

Common gas hydrate crystalline structures are cubic structure I (sI), cubic structure II (sII), or hexagonal structure H (sH).

Type I cubic structure sI is formed with guest molecules having diameters between 4.2 and 6 Å, such as CH_4, C_2H_6, CO_2, and H_2S, therefore being directly

A. Mendonça Teixeira et al., *Monoethylene Glycol as Hydrate Inhibitor in Offshore Natural Gas Processing*, SpringerBriefs in Petroleum Geoscience & Engineering,
DOI 10.1007/978-3-319-66074-5_2

associated to natural gas hydrates, but the other two structures can also occur in the NG context.

Cubic structure sII is more common with larger hydrocarbon molecules like C_3H_8 and i-C_4H_{10}, while the hexagonal structure sH is associated with multicomponent cages that encapsulates two hydrocarbon molecules like CH_4 with C_4H_{10}, C_5H_{12} or C_6H_{14} (Sloan and Koh 2008). It should be noted that n-butane does form a hydrate, but it is unstable. However, n-butane and larger hydrocarbons can form a stabilized hydrate in the presence of small "coadjutant" gases such as methane or nitrogen, which are held in the cages jointly with the larger molecule (e.g., C_4H_{10}).

Furthermore, although the challenge of gas hydrate formation is predominantly linked to gas production systems, hydrates can also form in oil production systems with associated gas and water in situ. In general, when the multiphase fluid produced at the wellhead flows through submarine pipelines, the fluid temperature falls with time and distance traveled by the fluid. Thus, in most subsea pipelines, the production stream cools to the temperature of the sea before arriving at the processing facilities, making possible the formation of hydrates.

Another case of concern occurs during plant shutdowns, wherein the pipeline fluid cools down to room/seabed temperature at high pressures, unless the system is depressurized. That is, in general, depending on the fluid composition and pressure and temperature conditions, hydrate formation can also occur even in multiphase flow of oil and gas systems (Kanu et al. 2014).

Moreover, another case of concern is at any point where a depressurization is present. For example, after the gas is extracted from the reservoir, it carries an extremely huge pressure from the well, conditions that the pipelines are not able to support. Hence, there must be a gas depressurization prior to the pipeline, and such depressurization entails temperature reduction, which can be conductive to hydrate formation. The greater such depressurization, the greater the temperature drop, and the greater the risk of hydrate formation.

Hence, a main challenge is to ensure flow in pipelines and processing facilities, since a critical factor in water saturated natural gas (NG) pipelines under offshore environment, especially in deepwater environments, is the potential formation of methane hydrates, which can damage equipment, blocking the following spaces upstream the production platform:

- Choke lines and kill lines (pipes for secondary access to well).
- Annular space (space between the production drill and the casing).
- Below the Blow-Out Preventer (BOP).
- The drill string.
- In subsea flowlines transporting the gas from the well to risers.
- In risers.
- Above the BOP or in its casing.

Additionally, there are other places downstream the production platform where hydrates can form:

- Pipe system and platform facilities.
- Subsea pipes for gas transportation.
- Pipes for the products of the platform.
- Underground gas storage systems.

Subsea operating conditions in well-heads and flowlines under deep waters—which commonly involve low temperatures from 0 to 4 °C, liquid formation water, and high pressures—can favor enormously the formation of hydrocarbon gas hydrates.

Additionally, recent cases have been observed where gas hydrates form in gas streams containing water vapor, without free liquid water. Gas hydrate from water vapor falls down as snow-like particles, which may settle to form plugs. Although free liquid water is not essential, it certainly raises the potentiality of hydrate formation very much, among other reasons because the gas–water interface is a good nucleation site for hydrate formation.

Once gas hydrates are detected inside a certain segment of flowline, an adequate remediation must be carried out. Main remediation techniques may include: controlled line depressurization, controlled line heating and injection of THI inhibitors. But it is obvious that a fundamental step is to find out the precise location where the solid hydrate has accumulated. This can be accomplished by pressurizing one end of the line with a known volume and measuring the corresponding pressure increase at several locations.

In the depressurization technique, when depressurizing only a single side, the hydrate plug will come off the wall at certain moment, and if there is a large differential pressure it will be projected at high speed, generating risks and damages, such as pipeline rupture. Depressurization on both sides is difficult to be implemented and, depending on the location of the accumulation of gas hydrate, it may not be possible.

Heating can be as dangerous as depressurization, because under exposure to heat, gas hydrates suddenly release a large localized amount of gas. Under the circumstance that the gas is released in the center of the plug and the rest of the plug is nonporous on both sides, the sudden confined release of gas can cause excessive sudden local pressure which can lead to pipe rupture at that point.

In the case of injection of a THI inhibitor, there is a small effective area of contact between the incoming phase of the inhibitor and the plug. Consequently, with time the front of THI becomes diluted in the dissociated water, weakening its strength of action. Hence, the THI must be continuously renewed by withdrawing the diluted (rich) THI and substituting it with lean THI during the process (Gate, Inc. 2012; Statoil 2012).

Therefore, a lot of shortcomings might occur if gas hydrates accumulates severely in subsea flowlines. Their remediation is costly and risky and could mean production stoppages, causing economic losses, and posing hazards to the security and integrity of the pipelines.

Figure 2.1 depicts a representation of the methane hydrate boundary without the presence of THIs (StatoilHydro 2008). This figure indicates that, at a given

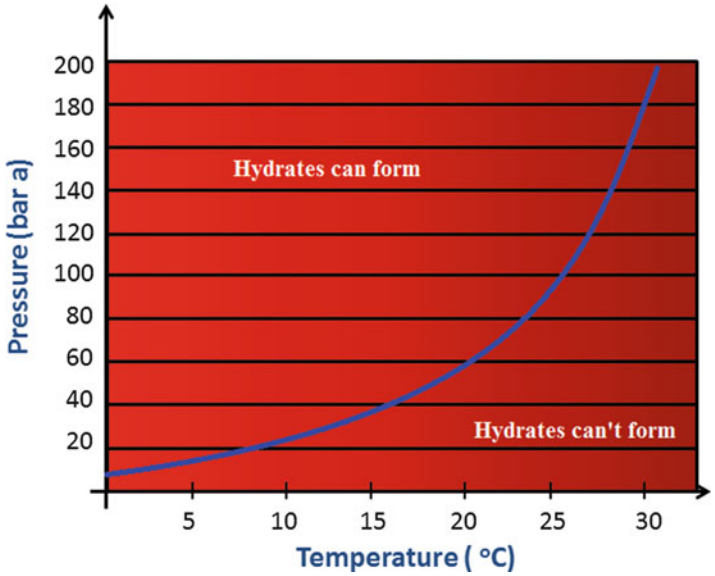

Fig. 2.1 Gas hydrate equilibrium curve of CH_4 + water

temperature, and under presence of water, methane hydrate forms if the pressure is equal or greater than the curve ordinate. Another aspect is that this curve is unbounded, so that methane hydrates are stable even at warm temperatures if the pressure is high enough.

To thermodynamically inhibit hydrate formation in continuous gas pipeline systems, the most common prevention method is to continuously displace the hydrate forming boundary such that the operational temperature and pressure of the system lie on the outside of the hydrate boundary. This is accomplished by continuous injection of a certain flow rate of a THI compound, which must be proportional to the flow rate of water carried by the stream, according to the following procedure:

- Continuous injection of a lean THI at the location in the pipeline system where the warm wet gas is admitted (e.g., well-heads).
- Continuous collection and separation of the rich (hydrated) THI on the other extreme of the pipeline where the gas processing facility is located (e.g., gas processing offshore platform or onshore plant).
- Continuous reprocessing of rich THI to efficiently recover the lean THI (with small losses) to be recycled after makeup to the injection points.

In the illustration of Fig. 2.1, the characteristics of the CH_4 hydrate equilibrium boundary on the plane $P \times T$ are shown under no influence of THIs. As can be seen, typical hydrate boundaries are monotonous curves with everywhere positive inclinations on plane $P \times T$, and in the specific case of CH_4 it is endless—i.e., it does not have a critical point or a sudden end point as occurs with the hydrate boundary of

condensable hydrocarbons like C_2H_6 and C_3H_8, whose hydrate boundary "collides" upward with the VLE (vapor–liquid equilibrium) locus of the hydrocarbon on plane $P \times T$ and cannot trespass this quadruple point temperature (i.e., a four-phase equilibrium, wet gas HC, liquid HC, liquid water, and hydrate) because above it the hydrocarbon is stable as a liquid making the hydrate phase unfeasible. Such quadruple points do not appear in the CH_4 case because methane is supercritical above −82 °C, i.e., its VLE locus does not exist above this temperature. This means that CH_4 hydrates can exist even at warm temperatures like 35 °C, if enough high pressure is available. The domain to the left of the hydrate boundary corresponds to the conditions of temperature and pressure where hydrate can form if water is present in the system.

The addition of Thermodynamic Hydrate Inhibitors (THIs) shifts the gas hydrate boundary to lower temperatures and higher pressures through reduction of the water activity (directly related to the chemical potential of water) in the aqueous liquid phase.

That is, under the presence of sufficient THIs, the gas hydrates are not formed in the flowline, because the system temperature and pressure now correspond to a location on plane $P \times T$ that lies outside the hydrate boundary, where hydrates are not stable.

Thermodynamic Hydrate Inhibitors (THIs) are normally highly hydrophilic species, like:

- Small chain alcohols—methanol and ethanol.
- Glycols—mono ethylene, diethylene, triethylene, and polyethylene glycols (MEG, DEG, TEG, and PEG).
- Strong electrolytes—NaCl and KCl.

Among these THI alternatives, MEG injection has been widely used due to its comparative advantages over other THIs, for instance:

- Low losses to vapor phase.
- Low solubility in condensate phase.
- High depression of water freezing point.
- High depression of hydrate formation temperature.
- Noncorrosiveness (in opposition to strong electrolyte THIs like NaCl).
- Good attenuation of corrosion.

Moreover, MEG is easily recovered and effectively regenerated and recycled, configuring a cost effective choice of THI. MEG is an alcohol with two hydroxyl groups or a diol (Fig. 2.2) and also widely used as automotive and domestic anti-freeze in cold countries. MEG is stable under normal use and storage (Table 2.1). In its pure form, MEG is an odorless, colorless, syrupy liquid compound with a sweet taste. MEG per se has low toxicity, but its metabolism in the human body—when

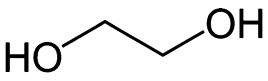

Fig. 2.2 MEG molecular structure

Table 2.1 Physical properties of monoethylene glycol (MEG)

Molar mass	62.07 g/mol
Density (at 20 °C)	1.1135 g/cm^3
Normal melting point	−13.0 °C
Normal boiling point	197.6 °C
Water solubility	Soluble in water in any proportion

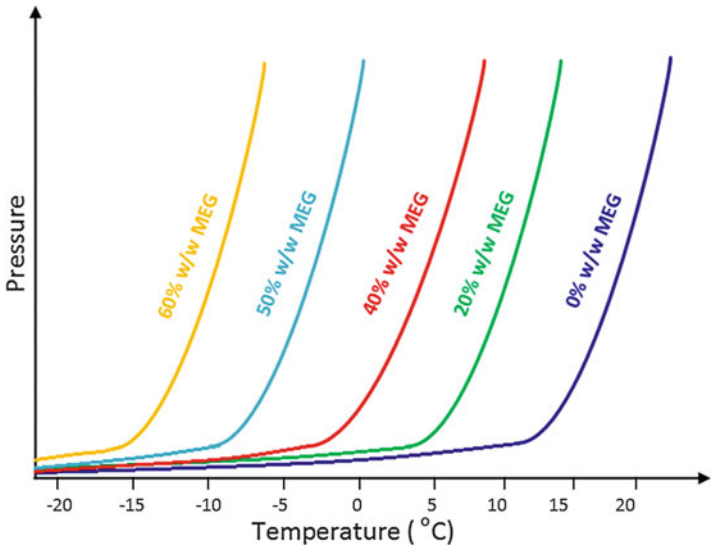

Fig. 2.3 Effect of MEG composition on the hydrate equilibrium curve of liquid water with CH_4

ingested, inhaled or absorbed through skin—produces toxic metabolites which can be lethal beyond certain concentration levels.

MEG, as any good THI, establishes strongly attractive interactions with water in the liquid phase due to hydrogen bonds, reducing the chemical potential of water in this phase. In view of VLE, this also involves the reduction of the chemical potential of water in the vapor phase. The chemical potential of water is reduced due to dilution and also due to the nonideal attraction between MEG and water which drag both these activity coefficients to values below 1. Hence, with the addition of THIs the chemical potential of H_2O in the aqueous liquid is reduced, stabilizing this phase, and shifting the hydrate formation boundary to lower temperatures and higher pressures.

Figure 2.3 depicts a qualitative displacement of the hydrate formation boundary by adding MEG in the liquid water phase (Gupta and Singh 2012). This displacement takes place to the left as the MEG content is increased in the aqueous liquid phase. It is worth noting that the hydrate formation boundary can be shifted even to negative Celsius temperatures.

As a continuous anti-hydrate commercial solution, THIs are injected into processing lines (subsea lines, pipelines, well-heads, etc.) under appropriate proportion with respect to the water content of the stream, breaking hydrogen bonds in gas hydrates (i.e., melting the solid gas hydrates) and establishing competition with the hydrates for water molecules.

References

Gate, Inc. (2012) Hydrates: prediction, mitigation & remediation techniques. GAT2004-GKP-2012.02. http://www.gateinc.com/wp-content/uploads/2012/02/GAT2004-GKP-2012.02-Hydrates-Prediction-Mitigation-Methods-Remediation-Techniques-.pdf. Accessed 19 Oct 2014

Gupta G, Singh SK (2012) Hydrate inhibition - optimization in deep water gas field. Paper presented at SPE oil and gas India conference and exhibition, Mumbai, India, 28–30 March 2012. SPE 153504. doi:10.2118/153504-MS

Kanu A, Al-Hajiri N, Messaoud Y, Ono N (2014) Mitigating hydrates in subsea oil flowlines: consider production flow monitoring & control. Paper presented at international petroleum technology conference, Doha, Qatar, 19 January 2014. IPTC 17492. doi:10.2523/IPTC-17492-MS

Sloan ED, Koh CA (2008) Clathrate hydrates of natural gases, 3rd edn. CRC Press, Taylor & Francis Group, Boca Raton, FL

Statoil (2012) Hydrate plugs – still a major flow assurance challenge. In: Li X (ed) Flow assurance lecture. NTNU, 16 April 2012. http://www.ipt.ntnu.no/~jsg/undervisning/prosessering/gjester/LysarkLi2012.pdf. Accessed 19 Oct 2014

StatoilHydro (2008) Glycol injection and processing.. http://www.ipt.ntnu.no/~jsg/undervisning/naturgass/lysark/LysarkKaasa2008.pdf. Accessed 8 Oct 2013

Chapter 3
MEG Loops in Offshore Natural Gas Fields

Abstract As a thermodynamic hydrate inhibitor (THI), MEG must be injected at certain points of the natural gas production systems to be thermodynamically effective against hydrate formation. The most appropriate points for injection of THIs are the warm wet points in the system like "heads" of production wells (well-heads) upstream the production choke, subsea transmission lines and flowlines that will be subjected to cooling at high pressures. The flow rate of MEG must be dosed proportionally to the expected flow rate of water in the system according to a proportion at least 1:1 in molar basis. After injection, MEG circulates through the production system and emerges at high pressure as Rich MEG (i.e., MEG solution rich in water and possibly having dissolved salts) on the production platform. At this point, after depressurization and separation of the gas and condensate phases, the treatment of Rich MEG stream is necessary in order to perform the recovery and regeneration of lean MEG for reuse, together with the disposal of water and salts. This step, known as MEG recovery (regeneration), is accomplished in MEG Recovery Units (MRUs). The MEG loop is a critical subsystem in the gas production system, because the MEG maintained in a closed circuit can become gradually degraded and contaminated with its continued utilization. This chapter describes MEG loops with MRU either located onshore or offshore, as well as presents some examples of MRUs.

As a THI, MEG must be injected at certain points of the natural gas production systems to be thermodynamically effective against hydrate formation. The most appropriate points for injection of THIs are the warm wet points in the system like "heads" of production wells (well-heads) upstream the production choke, subsea transmission lines and flowlines that will be subjected to cooling at high pressures. The flow rate of MEG must be dosed proportionally to the expected flow rate of water in the system according to a proportion at least 1:1 in molar basis.

After injection, MEG circulates through the production system and emerges at high pressure as Rich MEG (i.e., MEG solution rich in water and possibly having dissolved salts) on the production platform. At this point, after depressurization and separation of the gas and condensate phases, the treatment of Rich MEG stream is necessary in order to perform the recovery and regeneration of lean MEG for reuse,

A. Mendonça Teixeira et al., *Monoethylene Glycol as Hydrate Inhibitor in Offshore Natural Gas Processing*, SpringerBriefs in Petroleum Geoscience & Engineering,
DOI 10.1007/978-3-319-66074-5_3

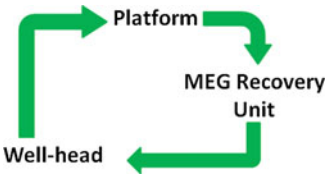

Fig. 3.1 Scheme for closed MEG loop

together with the disposal of water and salts. This step, known as MEG recovery (regeneration), is accomplished in MEG recovery units (MRUs).

MEG recovery, reconcentration, and salt removal are necessary before recirculation through subsea pipelines in order to avoid accumulation of salts and its saturation, which would entail scaling and other concerns. The recovery process generates the Lean MEG stream, a concentrated MEG solution with low water content. Lean MEG is then sent to reinjection in well-heads, thereby closing the MEG operating cycle, as in Fig. 3.1.

The MEG loop is a critical subsystem in the gas production system, because the MEG maintained in a closed circuit can become gradually degraded and contaminated with its continued utilization. This can occur if the impurities are not treated and removed in a controlled manner and periodically. In some cases, MEG make-up is necessary to prevent corrosion in both injection and recovery systems. Dissolved salts in produced water and products used to prevent corrosion of the pipelines are the main responsible for this kind of problems. Figure 3.2 illustrates the situation of fouling of equipment by calcium carbonate deposits.

Basically, offshore MRUs in MEG loops comprise:

- Pretreatment, where after separation from the other phases (for example in a slug-catcher) the Rich MEG stream is preheated and depressurized to remove hydrocarbons.
- MEG Recovery (regeneration), where Rich MEG is transformed into Lean MEG, with disposal of water and salts.
- Make-up of MEG in the stream of Lean MEG, if necessary.
- Storage of Lean MEG.
- Pumping station to send Lean MEG to reinjection.

Figures 3.3 and 3.4 illustrate a few examples of MRU modules for natural gas offshore platforms.

In some alternative cases, the crude natural gas is not processed in a platform, but on an onshore facility. This is advantageous, for example, when the source of the gas is a reserve of associated gas in oil fields. The reason is connected with the fact that offshore natural gas processing involves many high pressure complex operations that require a large percentage of topside area of FPSOs responsible exclusively for gas processing. This, in turn, reduces the area and weight available for processing and stocking oil, the main component of cash flow in the oil industry.

In this case, the MRU can be located onshore, so that there must exist a multiphase pipeline for transportation of the crude wet natural gas to the onshore processing facility. The multiphase flow results from the simultaneous transport of

Fig. 3.2 Scaling on heat exchanger surfaces. (Reproduced with permission of H&C Heat Transfer Solutions)

Fig. 3.3 An offshore MRU in the USA. (Courtesy of Prosernat)

the gas phase, with the MEG aqueous phase and possibly a third hydrocarbon condensate phase, after subsea separation from the oil and liquid water.

After the recovery of MEG by the MRU, another smaller pipeline must be available to return the Lean MEG to the production site. The Lean MEG stream is pumped back by a submarine pipeline to the injection point at the beginning of

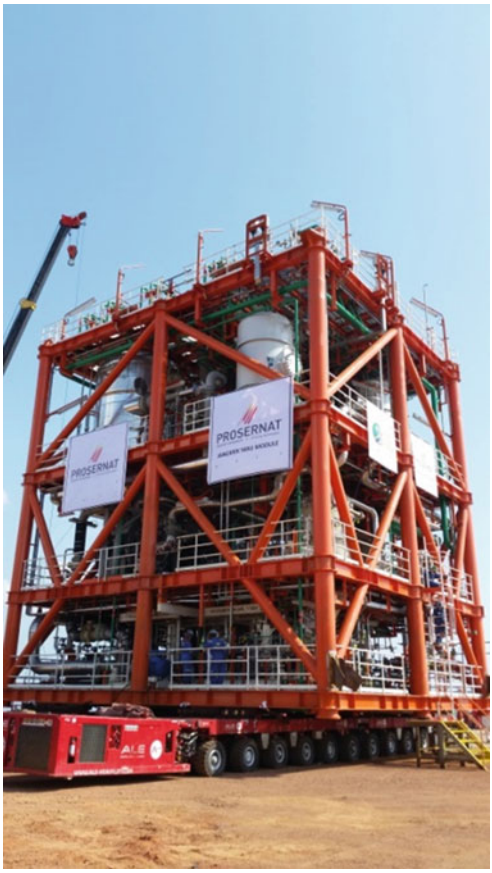

Fig. 3.4 An offshore MRU module of Jangkrik Field, Indonesia. (Courtesy of Prosernat)

the multiphase gas pipeline, thereby closing the MEG loop in this case (Almeida et al. 2016).

Reference

Almeida JSC, de Medeiros JL, Araújo OQF (2016) Analysis of natural gas production in pre-salt via pipelines with MEG and onshore processing. Appl Mech Mater 830(1):85–92. doi:10.4028/www.scientific.net/AMM.830.85

Chapter 4
Thermodynamics of Glycol Systems

Abstract Thermodynamic calculations using the Twu-Sim-Tassone EOS provide accurate glycol–water modeling (including MEG, TEG, and DEG), as well as reliable methods for phase equilibrium, surface tension prediction, and liquid density prediction. Twu, Sim, and Tassone have developed an excess Gibbs free energy function G^E that allows both zero-pressure and infinite-pressure cubic equations of state/A^E (CSEOS/A^E) mixing rules to transition smoothly to the conventional van der Waals one-fluid mixing rules. The alpha function of TST-EOS is generalized as a linear function of acentric factor at a constant reduced temperature, guaranteeing a very accurate prediction of hydrocarbon vapor pressure from the triple point to the critical point. Thus, the EOS can handle nonpolar systems as well as nonideal systems with precise calculation of high pressure and high temperature phase equilibria. This chapter details the Twu–Sim–Tassone equation of state used in this work for simulation of binary systems of monoethylene glycol and water.

Thermodynamic calculations using the Twu–Sim–Tassone EOS (Twu et al. 2002) provide accurate glycol–water modeling (including MEG, TEG, and DEG), as well as reliable methods for phase equilibrium, surface tension prediction, and liquid density prediction (Aspentech 2013).

Twu, Sim, and Tassone have developed an excess Gibbs free energy function G^E that allows both zero-pressure and infinite-pressure cubic equations of state /A^E (CSEOS/A^E) mixing rules to transition smoothly to the conventional van der Waals one-fluid mixing rules. The alpha function of TST-EOS is generalized as a linear function of acentric factor at a constant reduced temperature, granting a very accurate prediction of hydrocarbon vapor pressure from the triple point to the critical point. Thus, the EOS can handle nonpolar systems as well as nonideal systems with precise calculation of high pressure and high temperature phase equilibria.

The TST cubic EOS is shown in Eq. (4.1):

A. Mendonça Teixeira et al., *Monoethylene Glycol as Hydrate Inhibitor in Offshore Natural Gas Processing*, SpringerBriefs in Petroleum Geoscience & Engineering,
DOI 10.1007/978-3-319-66074-5_4

$$P = \frac{RT}{v-b} - \frac{a}{(v+3b)(v-0.5b)} \tag{4.1}$$

where a and b are parameters related to the critical temperature of the component. The values of those parameters at critical temperature are found by setting the first and second derivatives of pressure with respect to volume to zero at critical point:

$$a_c = 0.470507R^2\frac{T_c^2}{P_c} \tag{4.2}$$

$$b_c = 0.740740R\frac{T_c}{P_c} \tag{4.3}$$

$$z_c = 0.296296 \tag{4.4}$$

The parameter $a(T)$ is a function of temperature. The value of $a(T)$ at temperatures other than the critical temperature is calculated using Eq. (4.5):

$$a(T) = \alpha(T)a_c \tag{4.5}$$

where $\alpha(T)$ is a function of reduced temperature $T_r = T/T_c$.

Twu et al. (1991) correlation is applied here, and $\alpha(T)$ is written as:

$$\alpha(T) = T_r^{N(M-1)}e^{L\left(1-T_r^{NM}\right)} \tag{4.6}$$

where L, M, N are parameters unique to each component, determined from the regression of pure component vapor pressure data.

For non-library components, the generalized alpha function is expressed as a function of the reduced temperature and the acentric factor:

$$\alpha(T) = \alpha(T_r, \omega) \tag{4.7}$$

The generalized alpha function proposed for non-library and petroleum fractions is

$$\alpha = \alpha^{(0)} + \omega\left(\alpha^{(1)} - \alpha^{(0)}\right) \tag{4.8}$$

where $\alpha^{(0)}$ is for $\omega = 0$ and $\alpha^{(1)}$ is for $\omega = 1$. From correlations best described in Twu et al. (2002), $\alpha^{(0)}$ and $\alpha^{(1)}$ can be written as:

$$\alpha^{(0)} = T_r^{N^{(0)}\left(M^{(0)}-1\right)}e^{L^{(0)}\left(1-T_r^{N^{(0)}M^{(0)}}\right)} \tag{4.9}$$

$$\alpha^{(1)} = T_r^{N^{(1)}\left(M^{(1)}-1\right)}e^{L^{(1)}\left(1-T_r^{N^{(1)}M^{(1)}}\right)} \tag{4.10}$$

where the following values in Table 4.1 are used according to T_r.

Table 4.1 L, M, N values for generalized alpha function

	$T_r \leq 1$		$T_r > 1$	
	$\alpha^{(0)}$	$\alpha^{(1)}$	$\alpha^{(0)}$	$\alpha^{(1)}$
L	0.196545	0.704001	0.358826	0.0206444
M	0.906437	0.790407	4.23478	1.22942
N	1.26251	2.13086	−0.200000	−8.000000

Further, the zero pressure mixing rules for the a and b parameters of the cubic EOS are written as follows:

$$a^* = b^* \left[\frac{a_{\text{vdw}}{}^*}{b_{\text{vdw}}{}^*} + \frac{1}{C_{v_0}} \left(\frac{A_0^E}{RT} - \frac{A_{0,\text{vdw}}^E}{RT} - \ln\left(\frac{b_{\text{vdw}}}{b} \right) \right) \right] \tag{4.11}$$

$$b^* = \frac{b_{\text{vdw}}^* - a_{\text{vdw}}^*}{1 - \left[\frac{a_{\text{vdw}}^*}{b_{\text{vdw}}^*} + \frac{1}{c_{v_0}} \left(\frac{A_0^E}{RT} - \frac{A_{0,\text{vdw}}^E}{RT} - \ln\left(\frac{b_{\text{vdw}}}{b} \right) \right) \right]} \tag{4.12}$$

where a_{vdw} and b_{vdw} are the EOS a and b parameters which are evaluated from the van der Waals mixing rules. A_0^E and $A_{0,\text{vdw}}^E$ are excess Helmholtz energies at zero pressure. The subscript "vdw" in $A_{0,\text{vdw}}^E$ denotes that the properties are evaluated from the cubic EOS using the van der Waals mixing rule for its a and b parameters. The volume dependency in Eqs. (4.11) and (4.12) is made through C_{v_0}, as a function of reduced liquid volume at zero pressure $v_0{}^* = v_0/b$.

$$C_{v_0} = -\frac{1}{w-u} \ln\left(\frac{v_0^* + w}{v_0^* + u} \right)_{\text{vdw}} \tag{4.13}$$

where $v_{0\text{vdw}}^*$ is the zero pressure liquid volume, calculated by setting pressure equal to zero in the cubic EOS using van der Waals mixing rule for its a and b parameters and selecting the smallest root:

$$v_0^* = \frac{1}{2} \left\{ \left(\frac{a^*}{b^*} - u - w \right) - \left[\left(u + w - \frac{a^*}{b^*} \right)^2 - 4 \left(uw + \frac{a^*}{b^*} \right) \right]^{1/2} \right\} \tag{4.14}$$

Equation (4.14) has a root as long as the inequality Eq. (4.15) holds:

$$\frac{a^*}{b^*} \geq (2 + u + w) + 2\sqrt{(u+1)(w+1)} \tag{4.15}$$

The mixing rule for parameter b in Eq. (4.12) forces the quadratic composition dependence of the second virial coefficient. The conventional linear mixing rule could rather be chosen for the b parameter, i.e., ignoring the second virial coefficient boundary condition.

$$b = \sum_i \sum_j x_i x_j \left[\frac{1}{2}\left(b_i + b_j\right)\right] \tag{4.16}$$

Some sort of extrapolation for v_0^* must be made when Eq. (4.14) has no real root. To dismiss the calculation of v_0^* from the EOS, the zero pressure liquid volume of the van der Waals fluid, $v_{0\text{vdw}}^*$, is considered a constant (r) such that Eq. (4.13) is now written as:

$$C_\text{r} = -\frac{1}{w-u}\ln\left(\frac{r+w}{r+u}\right) \tag{4.17}$$

Hence, C_r replaces C_{v_0} and is no longer a density dependent function. Then, Eqs. (4.11) and (4.12) become:

$$a^* = b^*\left[\frac{a_\text{vdw}}{b_\text{vdw}}^* + \frac{1}{C_\text{r}}\left(\frac{A_0^E}{RT} - \frac{A_{0,\text{vdw}}^E}{RT} - \ln\left(\frac{b_\text{vdw}}{b}\right)\right)\right] \tag{4.18}$$

$$b^* = \frac{b_\text{vdw}^* - a_\text{vdw}^*}{1 - \left[\frac{a_\text{vdw}^*}{b_\text{vdw}^*} + \frac{1}{C_\text{r}}\left(\frac{A_0^E}{RT} - \frac{A_{0,\text{vdw}}^E}{RT} - \ln\left(\frac{b_\text{vdw}}{b}\right)\right)\right]} \tag{4.19}$$

The simplified mixing rules given by Eqs. (4.18) and (4.19) depend only on the selected value of r. Twu et al. (2002) recommend using the universal value of $r = 1.18$ for all systems. Then, $A_{0\text{vdw}}^E$ is derived from the EOS by assuming a fixed reduced liquid molar volume r for a van der Waals fluid at zero pressure:

$$\frac{A_{0\text{vdw}}^E}{RT} = \sum_i x_i \ln\left(\frac{b_i}{b_\text{vdw}}\right) + C_\text{r}\left[\frac{a_{0,\text{vdw}}^*}{b_\text{vdw}^*} - \sum_i x_i \frac{a_i^*}{b_i^*}\right] \tag{4.20}$$

where a_vdw and b_vdw are the EOS a and b parameters, evaluated from the conventional van der Waals mixing rules:

$$a_\text{vdw} = \sum_i \sum_j x_i x_j \sqrt{a_i a_j}\left(1 - k_{ij}\right) \tag{4.21}$$

$$b_\text{vdw} = \sum_i \sum_j x_i x_j \left[\frac{1}{2}\left(b_i + b_j\right)\right] \tag{4.22}$$

The excess Helmholtz free energy is much less pressure-dependent than the excess Gibbs free energy. Therefore, $A_{0\text{vdw}}^E$ can be approximated by the excess Helmholtz free energy of van der Waals fluid at infinite pressure:

$$\frac{A^E_{0\text{vdw}}}{RT} = \frac{A^E_{\infty\text{vdw}}}{RT} = C_1 \left(\frac{{a_{\text{vdw}}}^*}{{b_{\text{vdw}}}^*} - \sum_i x_i \frac{{a_i}^*}{{b_i}^*} \right) \tag{4.23}$$

where:

$$C_1 = -\frac{1}{(w-u)} \ln\left(\frac{1+w}{1+u}\right) = \text{const.} \tag{4.24}$$

For algebraic simplicity, the following development is limited to a binary mixture, obtaining Eq. (4.25) for the excess Helmholtz free energy of a van der Waals fluid, derived from Eq. (4.23).

$$\frac{A^E_{0\text{vdw}}}{RT} = \frac{x_1 x_2 b_1 b_2 \delta_{12}}{(x_1 b_1 + x_2 b_2)} \tag{4.25}$$

where δ_{12} is the characteristic parameter of interaction between molecules 1 and 2:

$$\delta_{12} = -\frac{C_1}{RT}\left[\left(\frac{\sqrt{a_1}}{b_1} - \frac{\sqrt{a_2}}{b_2} \right)^2 + 2k_{12} \frac{\sqrt{a_1}}{b_1} \frac{\sqrt{a_2}}{b_2} \right] \tag{4.26}$$

Extending to a multicomponent mixture, Eqs. (4.25) and (4.26) become:

$$\frac{A^E_{0\text{vdw}}}{RT} = \frac{1}{2} \sum_i \sum_j \left(b\delta_{ij}\right) \phi_i \phi_j \tag{4.27}$$

$$\delta_{ij} = -\frac{C_1}{RT}\left[\left(\frac{\sqrt{a_i}}{b_i} - \frac{\sqrt{a_j}}{b_j} \right)^2 + 2k_{ij} \frac{\sqrt{a_i}}{b_i} \frac{\sqrt{a_j}}{b_j} \right] \tag{4.28}$$

$$\phi_i = \frac{x_i b_i}{b} \tag{4.29}$$

For G^E model, a general multicomponent equation for a liquid activity model is proposed for incorporation in the zero pressure mixing rules as:

$$\frac{G^E}{RT} = \sum_i^n x_i \frac{\sum_j^n x_j \tau_{ji} G_{ji}}{\sum_k^n x_k G_{ki}} \tag{4.30}$$

Equation (4.30) is similar to the well-known NRTL equation, but it is not the same. There is a fundamental difference between them: NRTL assumes that A_{ij}, A_{ji}, and α_{ij} are the model parameters, but the proposed excess Gibbs free energy model assumes τ_{ij} and G_{ij} as the binary interaction parameters. Further, any appropriate

temperature-dependent function can be applied to τ_{ij} and G_{ij}. For example, τ_{ij} and G_{ij} can be calculated as usual from the NRLT parameters A_{ij}, A_{ji}, and α_{ij} in order to obtain the NRTL model:

$$\tau_{ij} = \frac{A_{ji}}{T} \tag{4.31}$$

$$G_{ij} = \exp\left(\alpha_{ij}\tau_{ji}\right) \tag{4.32}$$

Thus, NRTL parameters reported in DECHEMA Chemistry Data Series can be used directly in this model mixing rules. Additionally, if the following expressions in Eqs. (4.33) and (4.34) are used for τ_{ij} and G_{ij} in Eq. (4.30), it retrieves the conventional van der Waals mixing rules.

$$\tau_{ji} = \frac{1}{2}\delta_{ij}b_i \tag{4.33}$$

$$G_{ij} = \frac{b_j}{b_i} \tag{4.34}$$

It is worth noting that by substituting Eqs. (4.33) and (4.34) into Eq. (4.30), Eq. (4.27) is obtained. Hence, the model mixing rules—Eqs. (4.18) and (4.19)—reduce to the classical van der Waals one-fluid mixing rules, i.e., Eq. (4.30) is more generic in form than NRTL and both the NRTL and van der Waals fluid parameters are special cases of TST excess Gibbs free energy function.

References

Aspentech (2013) Midstream solutions with aspenONE® Engineering. https://www.aspentech.com/Midstream_Solutions_Brochure.pdf. Accessed 8 Nov 2016

Twu CH, Sim WD, Tassone V (2002) A versatile liquid activity model for SRK, PR and a new cubic equation-of-state TST. Fluid Phase Equilib 194–197(1):385–399. doi:10.1016/S0378-3812(01)00663-X

Twu CH, Bluck D, Cunningham JR, Coon JE (1991) Fluid Phase Equilib 69:33–50

Chapter 5
MRU Processes

Abstract After injection, MEG flows together with production fluids until they reach the processing facility on an offshore platform or on an onshore plant. The denser aqueous phase—also known as Rich MEG—is sent to the MEG recovery unit (MRU) for removal of water, salts, and other impurities in order to regenerate the stream of reconcentrated MEG—also known as lean MEG—to be returned as anti-hydrate to the injection points in the field. Currently, there are three main technologies for offshore MRUs, namely, traditional process (TP), full-stream process (FS) and slip-stream process (SS). The conventional or traditional MRU process simply atmospherically vaporizes the water contained in the Rich MEG stream through an atmospheric distillation column—ADC—to produce the reconcentrated lean MEG stream as bottoms. The full-stream (FS) process first performs preatmospheric evaporation of water from rich MEG in the ADC column as in the TP process. Then, total evaporation of the preconcentrated MEG occurs in a flash vessel operating under vacuum (FLS). The MEG-water vapor generated in the FLS is fed in a subatmospheric distillation column (SDC) which produces water as distillate and lean MEG as bottoms. The slip-stream process (SS) combines the TP process (ADC) with a salt removal unit using the flash-evaporator concept. The TP facet of the SS processes the entire rich MEG in an ADC. But the FLS only processes a fraction of the effluent (i.e., the slip-fraction) from the ADC, saving energy. Each process will be discussed with detail in this chapter.

As previously discussed in Chap. 3, after injection, MEG flows together with production fluids until they reach the processing facility on an offshore platform or on an onshore plant. The first step is to split the three phases—gas, condensate, and aqueous phase—of the incoming stream in a separator vessel.

The denser aqueous phase—also known as rich MEG—is sent to the MEG recovery unit (MRU) for removal of water, salts and other impurities in order to regenerate the stream of reconcentrated MEG—also known as lean MEG—to be returned as anti-hydrate to the injection points in the field.

Currently, there are three main technologies for offshore MRUs, namely, traditional process (TP), full-stream process (FS), and slip-stream process (SS). Each is discussed with detail in the following sections.

A. Mendonça Teixeira et al., *Monoethylene Glycol as Hydrate Inhibitor in Offshore Natural Gas Processing*, SpringerBriefs in Petroleum Geoscience & Engineering,
DOI 10.1007/978-3-319-66074-5_5

5.1 Traditional Process (TP)

The conventional or traditional MRU process simply atmospherically vaporizes the water contained in the Rich MEG stream through an atmospheric distillation column—ADC—to produce the reconcentrated lean MEG stream as bottoms.

TP usually works well when there is no expressive content of formation water. However, if the effluent natural gas carries formation water, there is a change in the amount of salts and other dissolved minerals in the Rich MEG stream overtime. Such salts are not volatile and accumulate in the MEG loop until saturation eventually occurs, triggering precipitation, scaling, and sedimentation of solids in the Rich MEG processing facilities.

Hence, NaCl particles and other salts (carbonates, oxides, sulfides, etc.) can precipitate and block filters and heat exchangers as they accumulate in the MEG loop, resulting in deterioration of the capacity of MRU, frequent stops, corrosion and high losses of glycol by thermal degradation (Nazzer and Keogh 2006).

The traditional process—TP—is a very simple processing route of Rich MEG, as can be seen in Fig. 5.1, which illustrates the flowchart of Kollsnes processing plant (Sandengen 2012).

The main equipment of the conventional TP MEG regeneration system is a reboiler, heat exchangers and an atmospheric distillation column (ADC). The ADC separates water as top distillate and lean MEG as bottoms. As the TP system does not remove salts, its use on offshore platforms has limitations of application because TP cannot cope with the continuous production of saline formation water originating from production wells.

In face of this, it is clear that the TP is not able to guarantee good performance conditions under continued use and is not a satisfactory option in medium and long term campaigns.

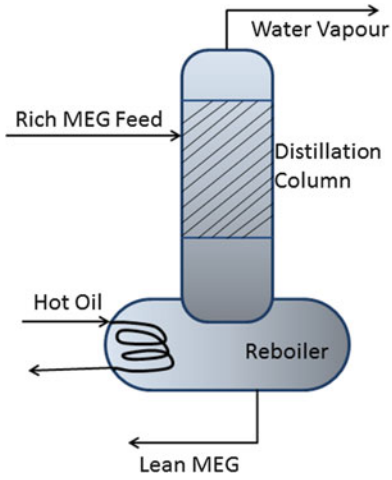

Fig. 5.1 TP MRU of Kollsnes processing plant

5.2 Full-Stream Process (FS)

The full-stream (FS) process first performs preatmospheric evaporation of water from Rich MEG in the ADC column as in the TP process. Then, total evaporation of the preconcentrated MEG occurs in a flash vessel operating under vacuum (reduced pressure) also known as Flash-Evaporator (FLS). The MEG-water vapor generated in the FLS is fed in a subatmospheric distillation column (SDC) which produces water as distillate and lean MEG as bottoms.

In the FLS, MEG and water instantly vaporize by direct contact with a recycle of heated mother liquor highly concentrated in MEG at high flow rate. All the liquid fed to FLS, excluding the dissolved and suspended solids, is vaporized and flows towards the subatmospheric distillation column (SDC) to be separated into pure water and reconcentrated and clean lean MEG.

FLS operates under vacuum to ensure lower operating temperatures, thereby avoiding thermal degradation of MEG, which starts above 162 °C. Salts, especially NaCl, crystallize in the liquid phase and can be separated by centrifugation, for example. FLS has a spiral heat exchanger (SHE) to heat the recycle of mother liquor returning to FLS. The MEG-water vapor generated in FLS goes to SDC, which produces pure water as top distillate and lean MEG as bottoms in the specification required for reinjection.

Figure 5.2 illustrates the flowsheet of the full-stream process (Petrobras 2007), englobing the above-described steps.

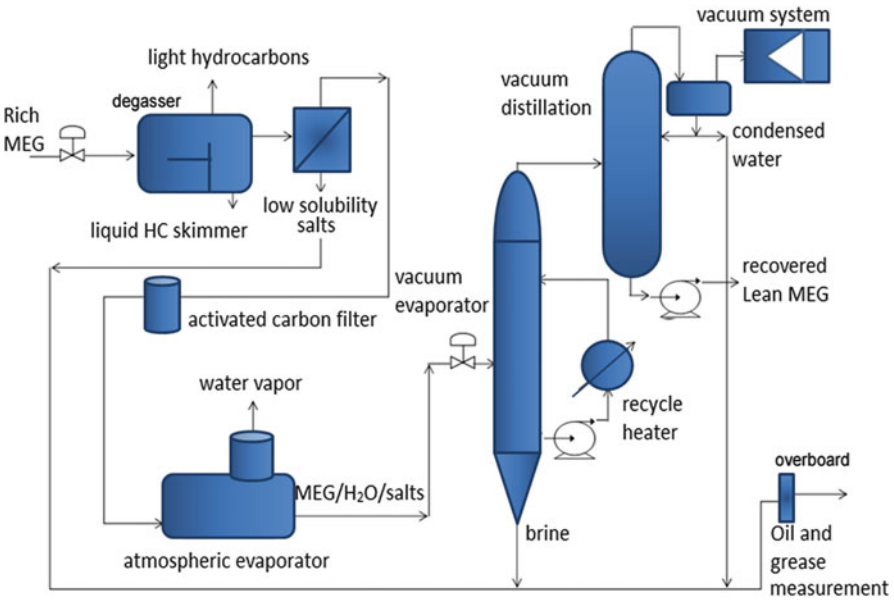

Fig. 5.2 Full-stream (FS) MRU flowsheet

It is worth noting that the exchanger SHE for the recycled mother liquor is a critical item in this technology. The SHE should be designed so as to reliably heat a salty liquid with high flow rate and concentrated in MEG without the risk of fouling, clogging and without allowing suspended particulates to sediment, which could block the flow exposing the recycled liquid to high residence times under high temperatures that might promote thermal degradation.

The SHE contacts the mother liquor with the thermal hot fluid at spiral counterflow. The hot fluid, for instance, can be hot thermal oil, or pressurized hot water (PHW). The high speed provided by the SHE spiral circuit maximizes the heat flow and maintains the salt particles moving so that they do not settle and do not cause hot spots or clogging. Moreover, such velocities also ensure that the recycled liquid is in contact with the hot metal for short times and, for this reason, it is safe to use, for example, hot thermal oil above 280 °C as heating medium without additional risk of MEG degradation.

A shell and tube heat exchanger could also be used in this service. However, such heat exchanger would be much larger than the SHE and there would be a higher tendency of low flow velocities with greater risk of clogging and solid deposition, which would bring serious maintenance problems in long term campaigns. Moreover, even under the circumstance of a special shell and tube exchanger design, guaranteeing high enough average flow velocities, it is difficult to ensure a uniform high speed field through all the shell, pipes, baffles, and channels. In other words, there would be plenty of stagnation points that favor deposition and clogging on the long term. On the other hand, the spiral design of the SHE offers zero instances of stagnation, if correctly operated.

Another possible configuration would be based on multistep exchangers, but this would turn the heat transfer system from countercurrent to parallel flow, thereby requiring a larger heat transfer area (Nazzer and Keogh 2006).

5.3 Slip-Stream Process (SS)

The slip-stream process (SS) combines the TP process (ADC) with a salt removal unit using the flash-evaporator (FLS) concept. The TP facet of the SS processes the entire rich MEG in an ADC. But the FLS only processes a fraction of the effluent (i.e., the slip-fraction) from the ADC, saving energy.

The main advantage of this system is the reuse of inhibitors and pH stabilizers which are totally lost together with the salts from the FLS in the FS version. Another advantage of SS is the reduction in terms of energy consumption when compared with the FS, which results in lower investment (CAPEX) and lower operating costs (OPEX).

The slip-stream arrangement is suitable for wells with low to intermediate water flow rates. The main disadvantage of SS is that it has some potential for accumulation of solid particles and salts in the MEG loop. As these particles are generators of corrosion, precipitated salts from formation water and from completion fluid can

cause damage to the equipment and piping overtime. The total concentration of salts in the lean MEG therefore must be kept below a maximum limit such that there is no precipitation overtime and that is acceptable for subsea processing. For this reason, SS MRU plants are often designed so that the slip-fraction can be manipulated eventually turning the SS plant into a FS MRU, if necessary.

The presence of carbonates and sulfates has been a problem because they reduce the efficiency of MEG recovery (cause increases of density, viscosity and boiling point). As an example, the MRU plant from Ormen-Lange (Norsk Hydro, Norway), which adopts the slip-stream arrangement, is designed so that the precipitation of $CaCO_3$ and $FeCO_3$ occurs in Rich MEG tanks upstream the reboilers. The retention time is high enough in the tanks for precipitation to occur and the temperature around 80 °C increases the settling velocity. The formed sludge is removed in scheduled maintenance and undergoes further treatment. Figure 5.3 illustrates an example of an MEG recovery system using SS arrangement.

In the SS MRU, Rich MEG is firstly pretreated in a separator to remove hydrocarbons, low-soluble salts and corrosion products before water is partially removed through conventional distillation in the ADC.

Then, only a fraction (slip-fraction) of the preconcentrated bottom product from ADC is treated in a vacuum reclamation FLS where high-soluble salts content is controlled. The other fraction of the preconcentrated MEG from ADC remains untreated. The final lean MEG effluent from the SS MRU results from the mixing of the slip-fraction FLS treated bottom product from ADC with the untreated counterpart from ADC.

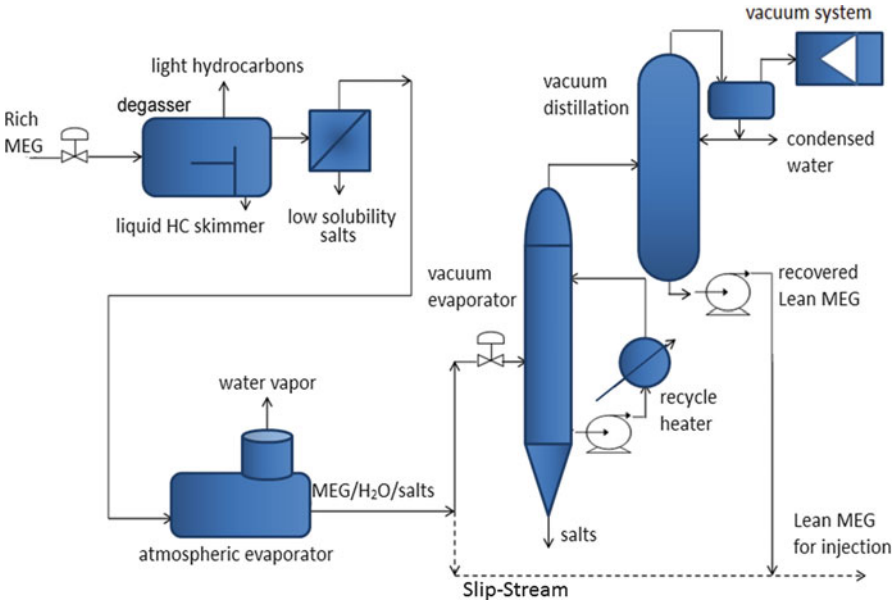

Fig. 5.3 Slip-stream (SS) MRU flowsheet

The slip-stream process is evidently more cost-effective in terms of energy consumption when compared with FS. The underlying reason is that the Rich MEG stream is not fully vaporized in the SS, requiring less energy to heat the material which is actually vaporized. Furthermore, due to lower material flow being treated in the flash-evaporator (FLS) and in the subsequent subatmospheric distillation column (SDC), the dimensions of SS equipment are lower, resulting in a reduced CAPEX and also in a smaller occupied area/module weight, which is a relevant factor in offshore environment.

References

Nazzer CA, Keogh J (2006) Advances in glycol reclamation technology. Paper presented at offshore technology conference, Houston, USA, 1–4 May 2006. OTC 18010. doi:10.4043/18010-MS

Petrobras (2007) Atividade de Produção de Gás e Condensado no Campo de Mexilhão, Bacia de Santos. http://licenciamento.ibama.gov.br/Petroleo/Producao/Producao%20-%20Bacia%20de%20Santos%20%20-%20Campo%20de%20Mexilhao%20-%20%20Petrobras/EIA%20Mexilh%C3%A3o/Cap%C3%ADtulo%20II/02.%20Caracteriza%C3%A7%C3%A3o%20da%20Atividade/II.2.4.2%20K_O_1.pdf. Accessed 8 Nov 2016

Sandengen K (2012) Hydrates and glycol – MEG (Monoethylene Glycol) injection and processing. http://www.ipt.ntnu.no/~jsg/undervisning/naturgass/lysark/LysarkSandengen2010.pdf. Accessed 10 Feb 2014

Chapter 6
Energy Consumption and CO_2 Emission of MRU Processes

Abstract In order to quantitatively evaluate MRU processes in terms of heat and power consumptions, CO_2 atmospheric emissions and exergy performance, traditional, full-stream, and slip-stream processes are first implemented in a professional process simulator, with the same inlet and outlet conditions for a comparative study. Process conditions and relevant parameters are first defined and steady-state flowcharts of MRU processes are installed as process flow diagrams (PFD) in process simulator in order to solve the respective mass and energy balances. Values of electric energy (EE) and heat consumptions of MRU processes are assessed via simulations, as well as all thermodynamic properties of the relevant material, thermal and mechanical energy streams. Heat streams are used to represent heating and cooling effects associated to a contact between two (or more) material streams in a heat exchanger. Hence, some assumptions for the simulations were adopted and they are listed in this chapter. Further, the implementation in simulation environment and the main results, as well as electrical energy (EE) and heat consumptions, required flow rate of utilities and CO_2 emissions for the processes are also presented in this chapter.

In order to quantitatively evaluate MRU processes in terms of heat and power consumptions, CO_2 atmospheric emissions, and exergy performance, TP, FS, and SS are first implemented in a professional process simulator, with the same inlet and outlet conditions for a comparative study.

Process conditions and relevant parameters are first defined and steady-state flowcharts of MRU processes are installed as process flow diagrams (PFD) in process simulator in order to solve the respective mass and energy balances. Values of electric energy (EE) and heat consumptions of MRU processes are assessed via simulations, as well as all thermodynamic properties of the relevant material, thermal and mechanical energy streams. Heat streams are used to represent heating and cooling effects associated to a contact between two (or more) material streams in a heat exchanger.

Hence, some assumptions for the simulations were adopted and they are listed in Sect. 6.1. The next sections illustrate the implementation in simulation environ-

A. Mendonça Teixeira et al., *Monoethylene Glycol as Hydrate Inhibitor in Offshore Natural Gas Processing*, SpringerBriefs in Petroleum Geoscience & Engineering,
DOI 10.1007/978-3-319-66074-5_6

ment, and finally Sect. 6.5 shows the main results, as well as electrical energy (EE) and heat consumptions, required flow rate of utilities, and CO_2 emissions for TP, FS, and SS processes.

6.1 MRU Process Assumptions

- Typical flow rates and conditions in the literature of real MRUs are used to build TP, FS, and SS PFDs (Nazzer and Keogh 2006).
- The operating pressure of MEG boiling systems is set at 0.2 bar A, so that all boiling points lie below 140 °C to avoid thermal degradation of MEG at 162 °C or above.
- NaCl is the main ionic species, representing 1–3% w/w of rich MEG, whereas the other salts—$CaCl_2$, $CaSO_4$ etc.—reach only hundreds of ppm and are irrelevant in terms of thermal effects. Even so, NaCl is not included in the simulation for two reasons: Firstly, NaCl only settles in the FLS after vaporization of MEG and H_2O, which are responsible for the main energy effects associated with phase changes. To confirm this, MRU was simulated with and without NaCl and the differences in terms of heat duties were always found below 1–2% (Teixeira 2014). Secondly, current aqueous solution models are not reliable with strong electrolytes at SVLE (i.e., VLE with NaCl saturation and precipitation) conditions, which would lead to inaccurate thermodynamic properties and consequently affect the accuracy of ExA.
- Rich MEG stream is defined as: 100 t/day, 55% w/w H_2O + 45% w/w MEG at 25 °C, 1 bar.
- Slip-fraction in SS is chosen as 50%.
- Temperature approaches (*TAPP*) in all heat exchangers are set to 5 °C.
- Temperature and pressure of rich and lean MEG have same values on TP, FS, and SS MRUs.
- Thermodynamic calculations use the glycol property package (Twu–Sim–Tassone TST-EOS, as described in Chap. 4) available in the simulation environment (Aspen Hysys v. 8.8).
- Heat consumption is primarily supplied by the waste heat of hot exhaust gas from electric energy generation gas turbines, as explained in the next Sect. 6.1.1. Part of this waste heat is recovered by the HRWH (Heat Recovery Water Heater) and conveyed to the unit operations by the PHW (Pressurized Hot Water) circuit.
- SW (Sea Water) circuit is the ultimate cold sink of the entire heat consumed by MRUs.
- Inlet and outlet temperatures of gas turbine exhausts in HRWH are 600 °C and 300 °C, respectively.

- The temperatures of PHW and ChW (Chilled Water) are 200 °C and 10 °C, respectively.
- Coefficient of CO_2 emission of common turbo-shaft for EE generation by burning natural gas in aviation turbines on offshore rigs are assumed as *56.1 kg* of CO_2 per GJ of EE.
- Initial and final temperatures of SW and CW (Cooling Water) are 20–35 °C and 25–40 °C, respectively.

6.1.1 Power, Heating, and Cooling Resources Available to Offshore MRUs

The adopted MRU technology and process conditions will strongly affect the requirements of heating, cooling, and electric energy (EE) for the MRU operation. Since only MRUs located on offshore platforms are considered here, it is critical to minimize heating, cooling, and EE requirements and also the extent of energy degradation. Moreover, the platform environment molds the available options of cooling, heating and EE resources.

The EE supply on offshore oil and gas rigs is usually provided by burning natural gas in aviation turbines. Gas turbines are widely used for onsite power generation and as mechanical drivers in offshore oil and gas production and processing facilities such as platforms and FPSO—floating production storage and offloading (Araújo et al. 2016).

The temperature of exhaust from gas turbines with power output rating up to 50 MW (both industrial heavy-duty and aero-derivatives) range between 500 and 600 °C (Bianchi et al. 2014; GE Aviation 2003).

In offshore rigs the waste heat from the exhaust gases is partly recovered to increase the temperature of a liquid heating medium, such as mineral oil or pressurized hot water (PHW), while the remaining heat is released with the flue gases to the atmosphere via a stack. The mineral oil or PHW circulates in a closed loop supplying heat to the platform facilities (Nguyen et al. 2013). The most common medium for heat distribution in topside processing facilities is PHW, which is easy to produce in a heat recovery water heater (HRWH) (Araújo et al. 2016), and involves a relatively low safety risk compared to mineral oil or high pressure steam (Parat Halvorsen AS 2008). Direct EE is a common alternative to supply heat on offshore rigs, however up-to-date systems frequently adopt the PHW as a low cost heating solution for reboilers and heaters operating at temperatures below 150 °C (Araújo et al. 2016).

In this work, all necessary MRU heating duties are considered adequately supplied by PHW assuming it is available at 200 °C. FPSO gas turbine power stations are designed with capacity near to 100 MW of EE at full service, not

counting the spare machines. At 100 MW of EE, most vendors guarantee a minimum heat recovery of 75 MW in the HRWH (Araújo et al. 2016). Thus, it is reasonable to assume that the PHW circuit has a maximum capacity of 75 MW of heat supply in typical scenarios, which is perfectly suitable to MRU requirements.

In terms of cooling, the main cooling resource available in offshore rigs is seawater (SW). Again there is a sealed secondary circuit of treated cooling water (CW) which removes heat from the majority of process units discharging it at the coils of the open primary SW circuit (Nguyen et al. 2013). The SW primary circuit is also used to cool the condensers of refrigeration machines that produce chilled water (ChW) at 10 °C.

ChW is necessary for cooling the subcooler at the top of the subatmospheric distillation column (SDC) in order to kill the flow of water vapor to the vacuum pump in FS and SS MRU configurations.

In order to accomplish the cooling services of CW and ChW, the entering temperature of SW is a critical design factor. The temperature of SW depends on the climatic zone considered and the depth where it is collected. In general, the SW in the primary circuit is collected at not particularly high depths and is directly used to cool the secondary CW and ChW circuits, being immediately returned to the sea afterwards. In this work a tropical or subtropical marine scenario is supposed, with SW entering at 20 °C in the admission header. Therefore the final exiting temperature of SW must not be higher than 35 °C in order to avoid environmental issues.

The ChW circuit is a secondary loop cooled by a water chiller using a propane refrigeration cycle. The condenser of this refrigeration cycle is, by its turn, cooled by SW as sketched in Fig. 6.1. Figures 6.2 and 6.3 illustrate the schemes for the circuits of CW and PHW.

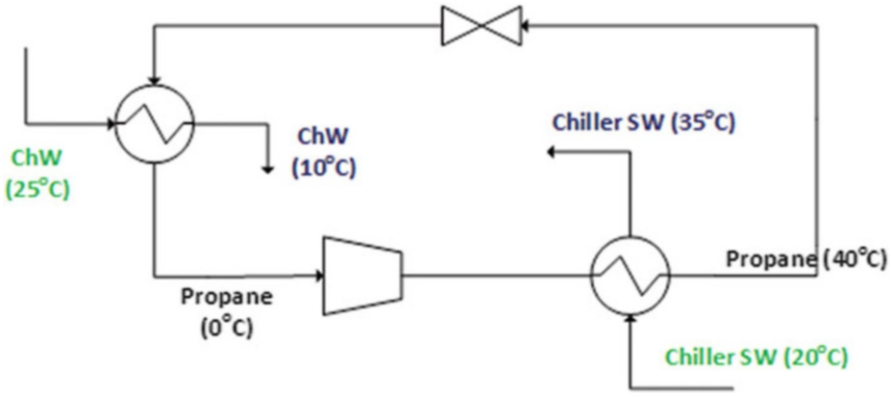

Fig. 6.1 ChW auxiliary loop

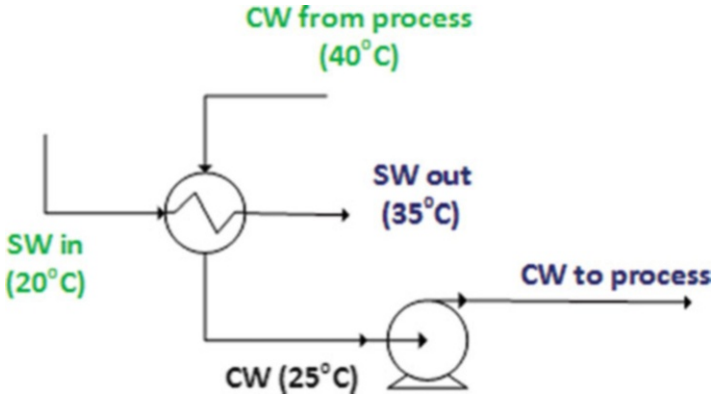

Fig. 6.2 Cooling water regeneration via sea water (SW)

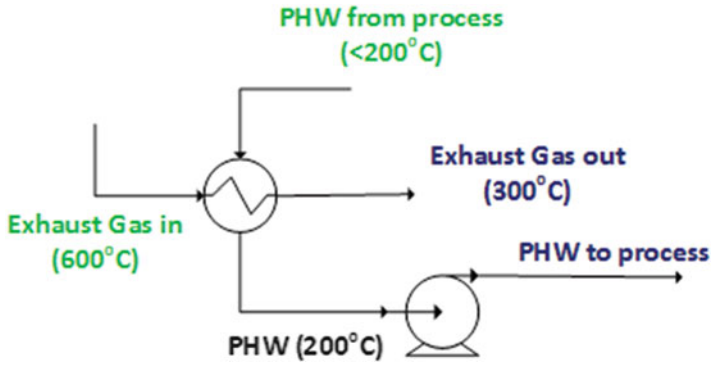

Fig. 6.3 Pressurized hot water (PHW) regeneration via heat recovery from exhaust gas

6.2 TP Implementation

Implemented TP flowsheet is shown in Fig. 6.4, wherein green is used to represent streams entering the flowsheet and dark blue is used to represent streams exiting the flowsheet. Such convention is also used in all flowsheets.

The atmospheric distillation column (ADC) has a heat-integrated condenser, such that the rich MEG feed is preheated in the condenser before entering the column. ADC heat-integrated condenser is followed by a CW finishing condenser. Hence, "rich MEG" is fed into ADC, producing pure water as top product ($\geq$99.99% mol water) and stream "2" as bottoms. Such stream "2" is the lean MEG stream, which passes through pump and heat exchanger to meet temperature and pressure specifications.

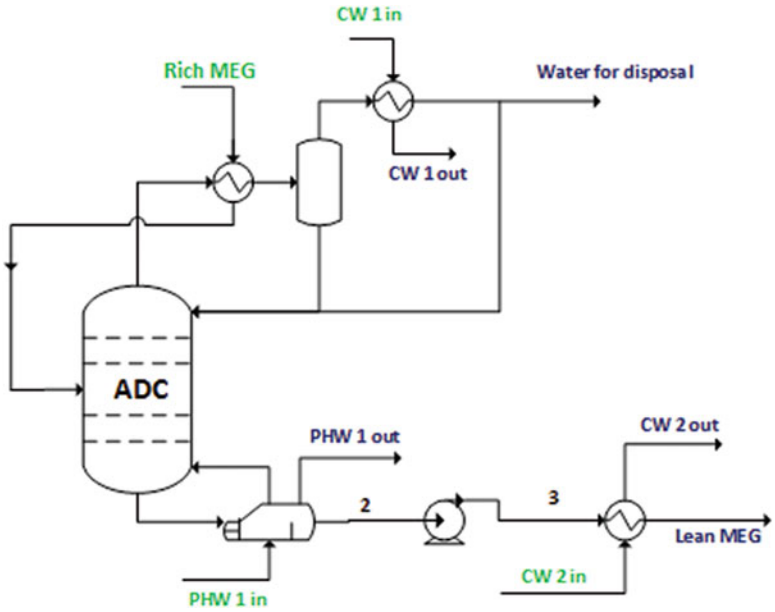

Fig. 6.4 Traditional process (TP) flowsheet

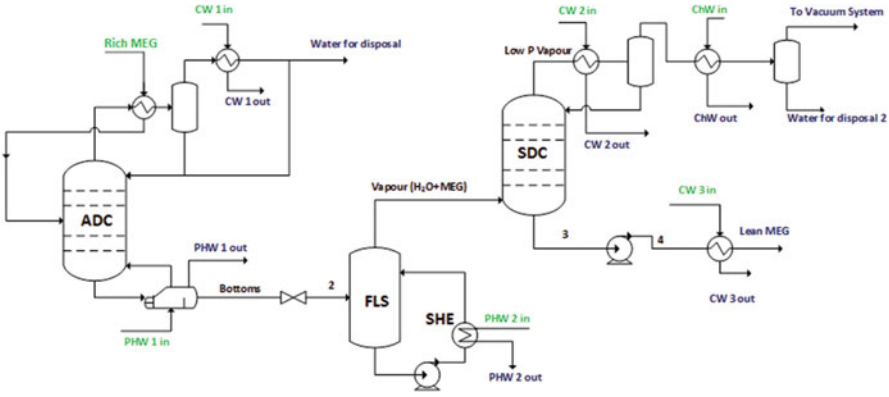

Fig. 6.5 Full-stream process (FS) flowsheet

6.3 FS Implementation

The implemented FS flowsheet is shown in Fig. 6.5. As in the TP case, ADC has a heat-integrated condenser. However, in this case, ADC has the function to only remove part of water present in the rich MEG. ADC bottoms pass through a valve for depressurization to 0.2 bar abs and enter the FLS where it is mixed with the hot liquor from the recycle heater SHE. The hot liquor, highly concentrated in MEG,

has only 20 °C of sensible heat above the dew point in the FLS, but it can vaporize the entire feed by direct contact due to its much larger mass flow rate (liquor–feed proportion of ≈30:1 w/w).

FLS top vapor containing only H_2O and MEG is sent to the sub-atmospheric distillation column (SDC), producing pure water as top distillate and stream "3" as bottoms, which corresponds to lean MEG after passing through the subsequent pump and heat exchanger.

The vacuum system of SDC (vacuum compressor or ejector) must not admit high flow rates of vapor to keep vacuum and save power. To accomplish this, as explained in Sect. 6.1.1, a distillate subcooler is employed, in which chilled water (ChW) at 10 °C is admitted to subcool the water distillate to 15 °C reducing its vapor pressure in order to protect the vacuum suction.

6.4 SS Implementation

The implemented PFD of the SS is shown in Fig. 6.6. As in the previous cases, ADC operates with the same configuration using a heat-integrated condenser. In the SS process the ADC bottom product is divided into two streams:

- The slip-stream, which follows the FS process path towards the FLS-SDC train.
- The slip-stream complement which is left untreated to be mixed with the lean MEG from the SDC bottoms, thereby producing the final lean MEG product.

As in the FS case, SS uses the same vacuum configuration and auxiliary condensers as well.

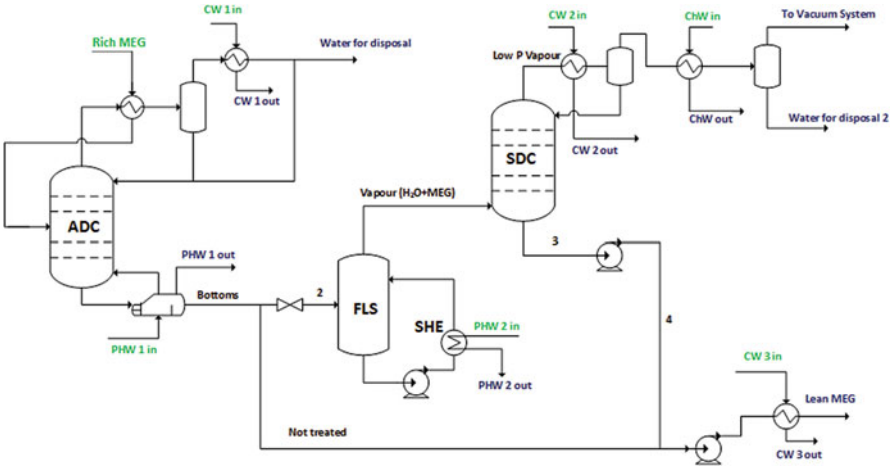

Fig. 6.6 Slip-stream process (SS) flowsheet

6.5 Heat, Power, Utility Consumptions and CO_2 Emissions Results

Mass and energy balances are solved for each MRU process by a professional process simulator, giving thermal duties and mechanical powers for TP, FS, and SS processes. Main heating duties (ADC reboiler and FLS recycle heater) and power consumptions are depicted in Table 6.1, wherein the respective lean MEG compositions and the energy required to achieve them are reported.

TP presents the lowest heat consumption, since it is the simplest process and requires heat only to run the single column ADC for atmospheric distillation of water from the rich MEG.

Among FS and SS, processes which effectively evaporate MEG, SS presents the lowest heat consumption, as only a fraction of rich MEG is actually treated in the vacuum train. On the other hand, FS presents the highest heat consumption, as it vaporizes the whole rich MEG feed, entailing higher energy consumption mainly by the spiral heat exchanger (SHE). Hence, SS occupies an intermediate position, since, in this case, the bottoms from ADC is only partially vaporized and distilled.

The results of consumption of thermal utilities and CO_2 emissions for each MRU are displayed in Table 6.2. CO_2 emissions of MRUs are proportional to the respective power or EE consumptions by using an emission coefficient of *56.1 kg* of CO_2 per GJ of generated electric power in conventional turbo-shafts (Soares 2017).

ChW consumption is higher for FS as the whole MEG from the rich MEG feed is vaporized in the FLS-SDC vacuum train. Consequently, FS presents a higher flow rate of distillated water from the top of SDC, which in turn requires more ChW for subcooling such stream to 15 °C.

The used exhaust gas flow rate is directly related to heat consumption of the MRU process, therefore these figures are proportional.

Table 6.1 Heat and power consumptions of MRU processes

MRU	%w/w MEG of lean MEG	Heat consumption (kW)	Power consumption (kW)
TP	85.83	1734.1	5.1
FS	93.32	2289.8	115.4
SS	85.58	1889.9	52.8

Table 6.2 Consumption of utilities and CO_2 emissions of MRU processes (CO_2 emission proportional to EE consumption)

	ChW (ton/h)	SW (ton/h)	CW (ton/h)	PHW (ton/h)	Exhaust gas (ton/h)	CO_2 emissions (kg/h)
TP	–	93.1	93.2	22.5	19.1	1.0
FS	24.3	132.7	102.1	26.8	24.0	23.3
SS	10.6	105.2	92.0	22.1	19.9	10.7

On the other hand, CO_2 emissions are strictly related to the specific EE consumption of the MRU process in question. They are not related, for example, to the exhaust gas flow rate in Table 6.2, which is supposed available as consequence of the total EE demand of all facilities in the offshore platform.

However, PHW consumption slightly differs from the pattern of heat consumption, as ADC heat duties also differs among the processes. The flow rate of PHW in TP is determined by the heat duty of ADC reboiler and the final temperature reached by PHW, which in turn is based on the temperature approach of 5 °C.

As in TP the temperature of ADC bottoms is higher (~133 °C) than the other ADC bottoms for FS and SS (~117 °C), the temperature variation set for PHW service is lower (from 200 to 138 °C, the temperature of ADC bottoms +5 °C), entailing a greater PHW flow rate to comply with this service. Hence, PHW consumption is larger for TP when compared with SS, despite the higher heat demand of SS. FS has a higher consumption of PHW, when compared to SS, thanks to the greater heat duty in the FLS.

For cooling services, the same pattern of heat consumption is observed. It is worth noting that TP only counts with CW for cooling, whereas FS and SS also use ChW to sub-cool the SDC distillate after a first cooling for condensation with CW.

References

Araújo OQF, Reis AC, de Medeiros JL, do Nascimento JF, Grava WM, Musse AP (2016) Comparative analysis of separation technologies for processing carbon dioxide rich natural gas in ultra-deepwater oil fields. J Clean Prod. doi:10.1016/j.jclepro.2016.06.073

Bianchi M, Branchini L, De Pascale A, Melino F, Peretto A, Valentini E (2014) Thermo-economic evaluation of orc system in off-shore applications. Proceedings of the ASME turbo expo 2014: turbine technical conference and exposition. Paper No. GT2014-25170. doi:10.1115/GT2014-25170

GE Aviation. GE's popular LM6000 now available in gas turbine-generator Set. 15 April 2003. http://www.geaviation.com/press/marine/marine_2003415.html. Accessed 8 Nov 2016

Nazzer CA, Keogh J (2006) Advances in glycol reclamation technology. Paper presented at offshore technology conference, Houston, USA, 1–4 May 2006. OTC 18010. doi:10.4043/18010-MS

Nguyen T-V, Pierobon L, Elmegaard B, Haglind F, Breuhaus P, Voldsund M (2013) Exergetic assessment of energy systems on North Sea oil and gas platforms. Energy 62(1):23–36. doi:10.1016/j.energy.2013.03.011

Parat Halvorsen AS (2008) Offshore heating solutions. http://www.parat.no/media/2993/offshore.pdf. Accessed 8 Nov 2016

Soares CM (2017) Gas turbines in simple cycle & combined cycle applications. https://www.netl.doe.gov/File%20Library/Research/Coal/energy%20systems/turbines/handbook/1-1.pdf. Accessed 15 Apr 2017

Teixeira AM (2014) Exergetic analysis of processes for monoethylene glycol (MEG) recovery in offshore platforms. MSc Dissertation, TPQBq, Escola de Quimica, Federal University of Rio de Janeiro

Chapter 7
Thermodynamic Efficiency of Steady State Operations of MRUs

Abstract Distillation columns and evaporation equipment are the main energy-consuming components utilized by offshore MRUs, besides several heating and cooling operations. One may ask about what would be the range of expected values of thermodynamic efficiencies for the main MRU operations. A first point to be realized beforehand is that thermodynamic efficiency and exergy efficiency are not in general the same thing, but both have a direct relationship and vary in the same direction. When only energy-consuming processes are considered, as in the case of MRUs, the thermodynamic efficiency expresses the ratio between the minimum consumption of equivalent power to accomplish a given task and the actual consumption of equivalent power for the same task. On the other hand, exergy efficiency is based on the fact that the difference between the outlet usable exergy flow rate of streams and the inlet usable exergy flow rate of streams is related to the minimum consumption (maximum production) of power to accomplish the process task under reversible conditions. The definition of exergy efficiency is similar to the thermodynamic efficiency, but its exergy version can give, in general, different results from the classical thermodynamic efficiency, as exergy counterpart is very dependent on the definition of the environment. This chapter initially approaches the thermodynamic efficiency of a binary idealized distillation column solved by the approximate McCabe–Thiele method, then a real commercial multicomponent distillation is assessed in terms of thermodynamic efficiency, being solved via rigorous distillation package of commercial process simulators with typical specification of products.

As seen in previous chapters, distillation columns and evaporation equipment are the main energy-consuming components utilized by offshore MRUs, besides several heating and cooling operations. One may ask about what would be the range of expected values of thermodynamic efficiencies for the main MRU operations.

A first point to be realized beforehand is that thermodynamic efficiency and exergy efficiency are not in general the same thing, but both have a direct relationship and vary in the same direction.

When only energy-consuming processes are considered, as in the case of MRUs, the thermodynamic efficiency—which should also not be confused with the *thermodynamic yield* of power cycles or with the *coefficient of performance* of heat

A. Mendonça Teixeira et al., *Monoethylene Glycol as Hydrate Inhibitor in Offshore Natural Gas Processing*, SpringerBriefs in Petroleum Geoscience & Engineering,
DOI 10.1007/978-3-319-66074-5_7

pump cycles—expresses the ratio between the minimum consumption of equivalent power to accomplish a given task and the actual consumption of equivalent power for the same task. By equivalent power it is meant the actual consumption of pure mechanical power added to the equivalent mechanical power consumption corresponding to all heating and cooling thermal duties.

On the other hand, exergy efficiency is based on the fact that the difference between the outlet usable exergy flow rate of streams ($\dot{B}_{\text{out}}$) and the inlet usable exergy flow rate of streams ($\dot{B}_{\text{in}}$) is related to the minimum consumption (maximum production) of power to accomplish the process task under reversible conditions, i.e., $\dot{W}^{REV} = -\left(\dot{B}_{out} - \dot{B}_{in}\right)$.

In the case of a power-consuming process, like MRUs, the exergy efficiency can be defined in two different ways:

- As the ratio between the minimum power consumption $\left|\dot{W}^{REV}\right| = \left|\dot{B}_{out} - \dot{B}_{in}\right|$ and the actual equivalent power consumption.
- As the ratio between the flow rate of all usable exergy leaving the process ($\dot{B}_{\text{out}} + \dot{B}^{W}_{\text{out}}$)—i.e., excluding the exergy contribution associated to material streams that are effectively discarded into the environment, like gas exhausts and waste water, etc.—and the corresponding flow rate of all usable exergy flows entering the process ($\dot{B}_{\text{in}} + \dot{B}^{W}_{\text{in}}$), where the superscript W refers exclusively to the contribution of non-material streams like pure mechanical energy streams (EE, shaft work, etc.) and the mechanical equivalent value of heat duties.

As can be seen, the first definition of exergy efficiency is similar to the abovementioned thermodynamic efficiency, but its exergy version can give, in general, different results from the classical thermodynamic efficiency. The reason is that the exergy counterpart is very dependent on the definition of RER—the reference environmental reservoir. The RER definition strongly affects the order of magnitude of all exergy flow rates associated to all material streams, and this influences the final value of exergy efficiency, both according to the first or to the second definitions.

To carry out exergy analyses of general chemical processes, the second interpretation of exergy efficiency is usually chosen. In this work, the computation of exergy efficiency of MRUs is conducted in Chap. 9 following exclusively the second definition of exergy efficiency.

The present chapter, on the other hand, has the limited objective of quantitatively approaching the classical thermodynamic efficiency of distillation columns. This intent has two main justifications:

- Firstly, because distillations constitute the main components of MRUs and dominate numerically in the computation of overall efficiency of such processes.
- Secondly, because the evaluation of the thermodynamic efficiency of distillation operations, sweeping ample ranges of reflux ratio values, will make clear the order of magnitude of the efficiencies—either based on classical thermodynamics or on exergy—of such important separation equipment and how it varies according to process conditions. This will also shed some light on the magnitude of efficiencies of MRUs.

This chapter initially approaches the thermodynamic efficiency of a binary idealized distillation column solved by the approximate McCabe–Thiele method, which needs only a hand calculator and simple process data to execute the calculations. Then a real commercial multicomponent distillation is assessed, being solved via rigorous distillation package of commercial process simulators with typical specification of products.

7.1 Thermodynamic Efficiency of Binary Distillation Column

In order to evaluate the magnitude of the thermodynamic efficiency of ordinary distillation columns, consider a simple steady-state binary distillation column at 1 bar operating with hypothetical species "1" and "2." To simplify the nomenclature, all molar fractions refer exclusively to component "1." Thus Z, X_D, and X_B represent the molar fractions of component "1" in the feed stream (F mol/s), in the distillate product (D mol/s), and in the bottoms product (B mol/s), respectively. This binary distillation column with one feed and two product streams is shown in Fig. 7.1. Consider also the following Assumptions:

- Steady-state isobaric atmospheric distillation column at $P = 1$ bar with perfect equilibrium stages (7.1)
- Column with total condenser and total reboiler at $P = 1$ bar with bubble-point effluents (7.2)
- Components "1"and "2" form liquid mixtures at $P = 1$ bar with Ideal Solution behavior (7.3)
- Vapor phase is considered an Ideal Gas at $P = 1$ bar (7.4)
- Feed F mol/s, distillate D mol/s and bottoms B mol/s as saturated liquids at $P = 1$ bar (7.5a)
- Feed flow rate of $F = 100$ mol/s (7.5b)
- Compositions of column external streams: Feed $Z = 0.5$; Distillate $X_D = 0.95$; Bottoms $X_B = 0.05$ (7.6)
- Column is bottom-heated by an isothermal hot reservoir R_H at $T_H = 200\ ^\circ C$ with duty $Q_H > 0$ (7.7)
- Column is top-cooled by an isothermal cold reservoir R_C at $T_C = 50\ ^\circ C$ with duty $Q_C > 0$ (7.8)
- Enthalpy of saturated liquids at $P = 1$ bar is a linear function of the liquid composition: $\bar{H}_L^{Sat}(X) = a + b \cdot X\,(\text{kJ/mol})$ (7.9a)
- Enthalpy of saturated vapors at $P = 1$ bar is a linear function of the vapor composition, with constant distance to the curve of enthalpy of saturated liquids $\bar{H}_V^{Sat}(Y) = a + \lambda + b \cdot Y\,(\text{kJ/mol})$ (7.9b)

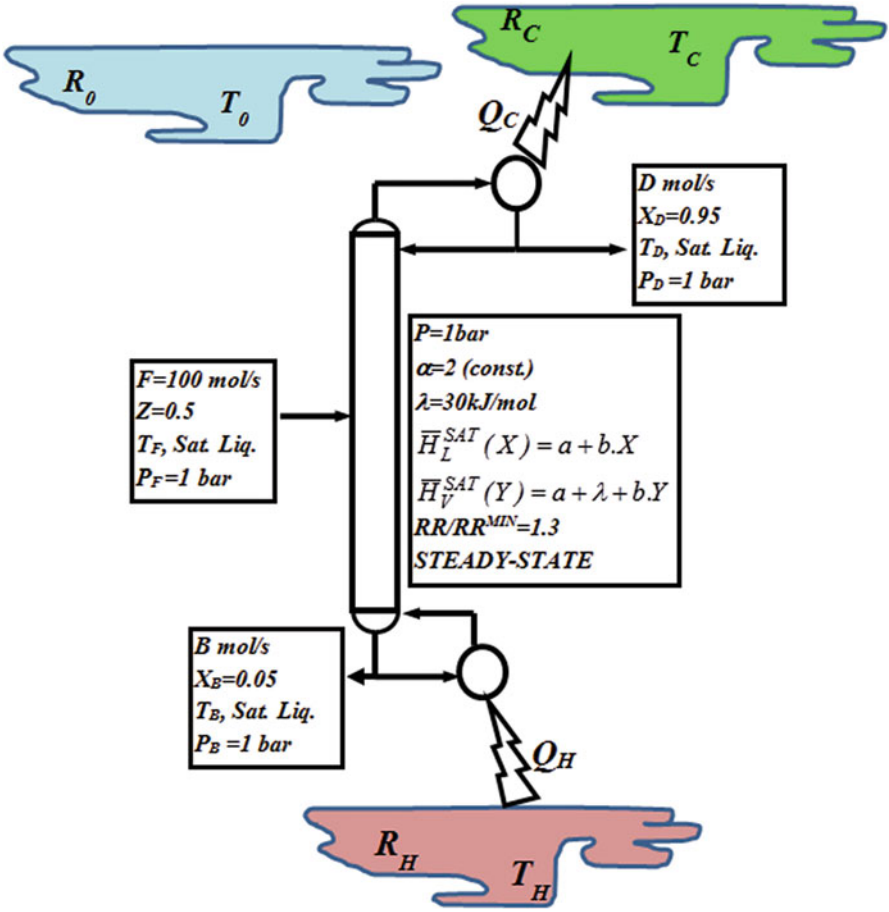

Fig. 7.1 Binary distillation column: feed and product streams as saturated liquids at 1 bar; heating duty Q_H from hot reservoir R_H ($T_H = 200$ °C) to reboiler; cooling duty Q_C from condenser to cold reservoir R_C ($T_C = 50$ °C); reference reservoir R_0 at $T_0 = 25$ °C is idle (not interacting with column)

- Enthalpy of vaporization at $P = 1$ bar is independent of composition with a value of $\lambda = 30$ kJ/mol (7.10)
- Relative volatility at $P = 1$ bar is a constant independent of composition: $\alpha = 2$ (7.11)
- Column reflux ratio (RR) is *30%* above minimum reflux ratio: $\mathrm{RR} = 1.3 \times \mathrm{RR}^{\mathrm{MIN}}$ (7.12)
- Approximately zero head losses along the column, i.e., column is approximately isobaric $P_F \cong P_B \cong P_D \cong 1$ bar (7.13)

The vapor–liquid equilibrium (VLE) relationship, $Y^* = g(X)$, at $P = 1$ bar is obtained by Assumption (7.11) as shown in Eq. (7.14).

$$Y^* = \frac{\alpha \cdot X}{1 - X + \alpha \cdot X} \Rightarrow Y^* = \frac{2X}{1 + X} \qquad \{Y^* = g(X) \tag{7.14}$$

7.1.1 Determination of Steady-State Operation Reflux Ratio and Corresponding Heat Duties

It can be shown that Assumptions (7.9a) and (7.9b) imply that the molar flow rates of liquid and vapor are constant in each column section. This is the well-known constant molar overflow approximation (CMO) that is used in the McCabe–Thiele method. Despite its simplicity, the McCabe–Thiele method can generate approximate designs of binary distillations.

Calling the rectification section as section *0* and the stripping section as section *1*, the molar flow rates (mol/s) of liquid and vapor in these sections are written by CMO according to the formulae from Eqs. (7.15) to (7.18).

$$L_0 = D \cdot \mathrm{RR} \tag{7.15}$$

$$L_1 = D \cdot \mathrm{RR} + F \tag{7.16}$$

$$V_0 = D \cdot (\mathrm{RR} + 1) \tag{7.17}$$

$$V_1 = D \cdot (\mathrm{RR} + 1) \tag{7.18}$$

By solving the column material balances, flow rates D and B are calculated as shown in Eqs. (7.19) and (7.20). From the assumptions (7.9a) and (7.9b), the enthalpy of vaporization λ is constant with the value of 30 kJ/mol by Assumption (7.10). Additionally, with V_0 and V_1 from Eqs. (7.17) and (7.18), the (positive) thermal duties Q_C and Q_H (kW) can be expressed as done in Eqs. (7.21) and (7.22).

$$D = F \cdot \left(\frac{Z - X_B}{X_D - X_B} \right) \Rightarrow D = 50\,\mathrm{mol/s} \tag{7.19}$$

$$B = F \cdot \left(\frac{X_D - Z}{X_D - X_B} \right) \Rightarrow B = 50\,\mathrm{mol/s} \tag{7.20}$$

$$Q_\mathrm{C} = D \cdot (\mathrm{RR} + 1) \cdot \lambda = 1500 \cdot (\mathrm{RR} + 1)\,\mathrm{kW} \tag{7.21}$$

$$Q_\mathrm{H} = D \cdot (\mathrm{RR} + 1) \cdot \lambda = 1500 \cdot (\mathrm{RR} + 1)\,\mathrm{kW} \tag{7.22}$$

In the context of the McCabe–Thiele method, sections *0* and *1* can be solved by a tray-to-tray calculation, from top to bottom, using the VLE relationship in Eq. (7.23) (from Eq. (7.14)) and the Operation Equations of sections *0* and *1* shown in Eqs. (7.24) and (7.25) respectively. In these formulae, X_n and Y_n

represent the liquid and vapor compositions leaving stage n in VLE and X_n and Y_{n+1} represent a crossing pair of compositions (or inter-stage compositions) in those sections.

$$Y_n = g(X_n) \Rightarrow Y_n = \frac{2X_n}{1+X_n} \tag{7.23}$$

$$Y_{n+1} = \left(\frac{L_0}{V_0}\right) \cdot X_n + \left(\frac{D \cdot X_D}{V_0}\right) \Rightarrow Y_{n+1} = \left(\frac{\mathrm{RR}}{\mathrm{RR}+1}\right) \cdot X_n + \left(\frac{X_D}{\mathrm{RR}+1}\right) \tag{7.24}$$

$$\begin{aligned} Y_{n+1} &= \left(\frac{L_1}{V_1}\right) \cdot X_n + \left(\frac{D \cdot X_D - F \cdot Z}{V_1}\right) \\ &\Rightarrow Y_{n+1} = \left(\frac{\mathrm{RR}+F/D}{\mathrm{RR}+1}\right) \cdot X_n + \left(\frac{X_D - Z \cdot F/D}{\mathrm{RR}+1}\right) \end{aligned} \tag{7.25}$$

It is easily shown that the Operating Equations (7.24) and (7.25) intersect in the XY plane at the point (X_{01}, Y_{01}), whose coordinates are given by Eq. (7.26).

$$X_{01} = Z, \quad Y_{01} = \frac{X_D + Z \cdot \mathrm{RR}}{\mathrm{RR}+1} \tag{7.26}$$

At minimum reflux ($\mathrm{RR}^{\mathrm{MIN}}$) a pinch condition is attained at the feed zone, which is represented by the intersection point (X_{01},Y_{01}) in plane XY.

This pinch condition is usually represented as $\left(X_{01}, Y_{01}^{\infty}\right)$ meaning that the intersection point obeys Eq. (7.26) simultaneously with the VLE relationship in Eq. (7.14), as shown in Eq. (7.27). Equation (7.27) then allows the minimum reflux ratio to be determined via Eq. (7.28). With $g(Z) = 2/3$, by Eq. (7.14), the minimal reflux ratio is obtained as $\mathrm{RR}^{\mathrm{MIN}} = 1.7$ for this simple example.

$$X_{01} = Z, \quad Y_{01}^{\infty} = \frac{X_D + Z \cdot \mathrm{RR}^{\mathrm{MIN}}}{\mathrm{RR}^{\mathrm{MIN}}+1} = g(Z) \tag{7.27}$$

$$\frac{X_D + Z \cdot \mathrm{RR}^{\mathrm{MIN}}}{\mathrm{RR}^{\mathrm{MIN}}+1} = g(Z) \Rightarrow \mathrm{RR}^{\mathrm{MIN}} = \frac{X_D - g(Z)}{g(Z) - Z} \overset{g(Z)=2/3}{\rightarrow} \mathrm{RR}^{\mathrm{MIN}} = 1.7 \tag{7.28}$$

The design reflux ratio is obtained via Assumption (7.12) in Eq. (7.29). This determines the design values of the column heat duties via Eqs. (7.21) and (7.22) as shown in Eq. (7.30).

$$\mathrm{RR} = 1.3 \times \mathrm{RR}^{\mathrm{MIN}} \Rightarrow \mathrm{RR} = 2.21 \tag{7.29}$$

$$Q_{\mathrm{H}} = Q_{\mathrm{C}} = 50 \times 3.21 \times 30 = 4815\,\mathrm{kW} \tag{7.30}$$

7.1.2 *Minimum Power Required for Steady-State Separation at Constant* T *and* P

The minimum requirement of power ($\dot{W}^{\mathrm{REV}}$) to produce the steady-state separation in Fig. 7.1 can be obtained with the first and second Laws of Thermodynamics assuming steady-state reversible operation of a reversible machine or open system executing the separation. This open system is shown in Fig. 7.2.

In Fig. 7.1 the respective bubble temperatures T_F, T_D, T_B of feed F and product streams D and B at $P = 1$ bar, are evidently different, but they are not very distant from each other if the relative volatility is 2. For simplicity, it is assumed that these temperatures can be approximated by a certain intermediate value T (i.e., $T_F \cong T_D \cong T_B \cong T$), where T is of the order of ≈80 °C.

Thus, the reversible separation requiring minimum work occurs at constant T and P, where $P_F \cong P_D \cong P_B \cong P = 1$ bar, as shown in Fig. 7.2. The exact nature of the steady-state open system to undertake the separation is not relevant in principle, but it is not a distillation column.

In order to guarantee its constant temperature T this open system is supposed in thermal equilibrium with a heat reservoir R_T at temperature T. As any reservoir, R_T has a very high heat capacity so that its temperature is constant at T independently of the heat exchange Q^{REV} between R_T and the open system.

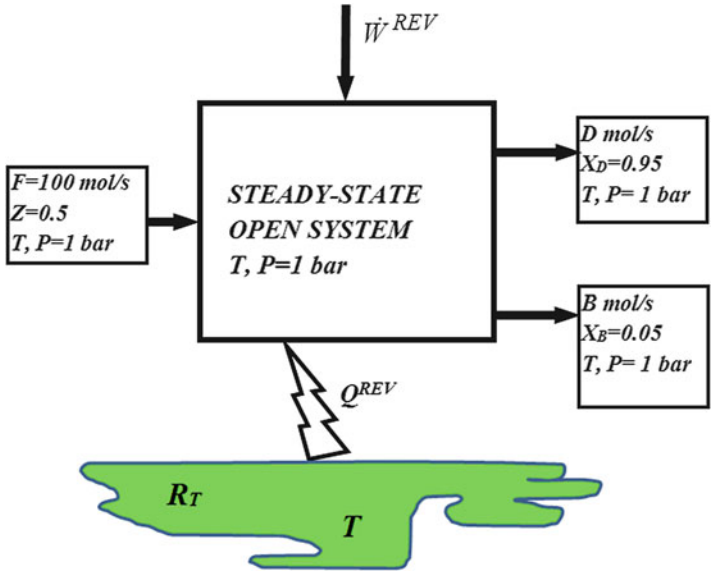

Fig. 7.2 Open system for minimum power separation at constant T and P of feed $F = 100$ mol/s with composition $Z = 0.5$ into product streams D mol/s and B mol/s respectively with compositions $X_D = 0.95$ and $X_B = 0.05$

Both Q^{REV} and $\dot{W}^{\text{REV}}$ are classically defined according to the open system point of view, i.e., Q^{REV} is positive when the system receives heat and $\dot{W}^{\text{REV}}$ is positive (negative) when the system produces (consumes) work.

Applying the First Law of Thermodynamics to the steady-state open system in Fig. 7.2, Eq. (7.31) results, where $\bar{H}_F, \bar{H}_D, \bar{H}_B$ represent the respective molar enthalpies of streams F, D, and B in kJ/mol at (T, P). Assuming reversible operation for $\dot{W}^{\text{REV}}$, the steady-state rate of creation of entropy in the Universe associated to this process is zero as shown in Eq. (7.32), where $\bar{S}_F, \bar{S}_D, \bar{S}_B$ represent the respective molar entropies of streams F, D, and B in kJ/mol K at (T, P). The second term in the left hand side of Eq. (7.32) corresponds to the rate of change of entropy inside the isothermal reservoir R_T as consequence of the heat exchange Q^{REV}originally defined according to the point of view of the open system.

$$F \cdot \bar{H}_F + Q^{\text{REV}} = \dot{W}^{\text{REV}} + D \cdot \bar{H}_D + B \cdot \bar{H}_B \tag{7.31}$$

$$-F \cdot \bar{S}_F - \frac{Q^{\text{REV}}}{T} + D \cdot \bar{S}_D + B \cdot \bar{S}_B = 0 \tag{7.32}$$

Multiplying Eq. (7.32) by T and adding it to Eq. (7.31), results Eq. (7.33) or (7.34) for $\dot{W}^{\text{REV}}$, where $\bar{G}_F, \bar{G}_D, \bar{G}_B$ represent the respective molar Gibbs free energies of streams F, D, and B (kJ/mol) at (T, P).

$$\dot{W}^{\text{REV}} = -\left\{ D \cdot \left(\bar{H}_D - T \cdot \bar{S}_D\right) + B \cdot \left(\bar{H}_B - T \cdot \bar{S}_B\right) - F \cdot \left(\bar{H}_F - T \cdot \bar{S}_F\right) \right\} \tag{7.33}$$

$$\dot{W}^{\text{REV}} = -\left\{ D \cdot \bar{G}_D + B \cdot \bar{G}_B - F \cdot \bar{G}_F \right\} \tag{7.34}$$

Equation (7.34) is a well-known result for the minimum power required (or maximum power produced) for a given steady-state transition of streams under constant (T, P).

Equation (7.34) states that in a steady-state power-consuming operation the minimum requirement of power is the negative of the net rate of variation of Gibbs free energy (kW) in the process, where the rate of Gibbs free energy (kW) assigned to product streams is greater than the rate of Gibbs free energy (kW) assigned to the feed streams.

For steady-state distillation separations, as the one shown in Fig. 7.1, the output flow rate of Gibbs free energy is greater than the respective input rate at constant (T, P). This means that (equivalent) mechanical power has to be spent to support such separation (i.e., $\dot{W}^{\text{REV}} < 0$).

Concerning the separation in Figs. 7.1 and 7.2, all streams F, D, and B are liquids at (T, P) with Ideal Solution behavior. This allows to write Eqs. (7.35a–7.35c) below, where $\mu_1^{\text{L}}(T,P), \mu_2^{\text{L}}(T,P)$ are the chemical potentials of pure liquid species "1" and "2" at (T, P) and $R = 8.314 \times 10^{-3}$ kJ/mol K is the Ideal Gas constant.

$$\bar{G}_F = Z \cdot \mu_1^{\mathrm{L}}(T,P) + (1-Z) \cdot \mu_2^{\mathrm{L}}(T,P) + R \cdot T \cdot \{Z \cdot \ln(Z) + (1-Z) \cdot \ln(1-Z)\} \tag{7.35a}$$

$$\bar{G}_D = X_D \cdot \mu_1^{\mathrm{L}}(T,P) + (1-X_D) \cdot \mu_2^{\mathrm{L}}(T,P) + R \cdot T \cdot \{X_D \cdot \ln(X_D) + (1-X_D) \cdot \ln(1-X_D)\} \tag{7.35b}$$

$$\bar{G}_B = X_B \cdot \mu_1^{\mathrm{L}}(T,P) + (1-X_B) \cdot \mu_2^{\mathrm{L}}(T,P) + R \cdot T \cdot \{X_B \cdot \ln(X_B) + (1-X_B) \cdot \ln(1-X_B)\} \tag{7.35c}$$

Since $D = B = F/2$ by Eqs. (7.19) and (7.20), Eq. (7.36a) can be obtained with Eqs. (7.35a), (7.35b) and (7.35c).

$$\begin{aligned} D \cdot \bar{G}_D + B \cdot \bar{G}_B - F \cdot \bar{G}_F = {} & \{D \cdot X_D + B \cdot X_B - F \cdot Z\} \cdot \mu_1^{\mathrm{L}}(T,P) \\ & + \{D \cdot (1-X_D) + B(1-X_B) - F(1-Z)\} \cdot \mu_2^{\mathrm{L}}(T,P) \\ & + \frac{\mathrm{FRT}}{2} \cdot \{X_D \cdot \ln(X_D) + (1-X_D) \cdot \ln(1-X_D)\} \\ & + \frac{\mathrm{FRT}}{2} \cdot \{X_B \cdot \ln(X_B) + (1-X_B) \cdot \ln(1-X_B)\} \\ & - \mathrm{FRT} \cdot \{Z \cdot \ln(Z) + (1-Z) \cdot \ln(1-Z)\} \end{aligned} \tag{7.36a}$$

The steady-state column material balances, respectively, for components "1" and "2", impose Eqs. (7.36b) and (7.36c). These balances allow Eq. (7.36a) to be finally rewritten according to the form shown in Eq. (7.37).

$$D \cdot X_D + B \cdot X_B - F \cdot Z = 0 \tag{7.36b}$$

$$D \cdot (1-X_D) + B(1-X_B) - F(1-Z) = 0 \tag{7.36c}$$

$$\begin{aligned} D \cdot \bar{G}_D + B \cdot \bar{G}_B - F \cdot \bar{G}_F = {} & \frac{\mathrm{FRT}}{2} \cdot \{X_D \cdot \ln(X_D) + (1-X_D) \cdot \ln(1-X_D)\} \\ & + \frac{\mathrm{FRT}}{2} \cdot \{X_B \cdot \ln(X_B) + (1-X_B) \cdot \ln(1-X_B)\} \\ & - \mathrm{FRT} \cdot \{Z \cdot \ln(Z) + (1-Z) \cdot \ln(1-Z)\} \end{aligned} \tag{7.37}$$

With $X_D = 0.95$, $X_B = 0.05$, $Z = 0.5$, $F = 100$ mol/s and $T \approx 80$ °C (353.15 K), one gets Eq. (7.38) and, then, Eq. (7.39). This last result states that to accomplish the separation in Fig. 7.2 the minimal consumption of power, as stipulated by the second Law, is 145.23 kW.

$$D \cdot \bar{G}_D + B \cdot \bar{G}_B - F \cdot \bar{G}_F = 145.23\,\mathrm{kW} \tag{7.38}$$

$$\dot{W}^{\mathrm{REV}} = -145.23\,\mathrm{kW} \tag{7.39}$$

7.1.3 *Actual Equivalent Power Consumption of a Steady-State Binary Distillation Column via the Method of Carnot Equivalent Cycles*

The actual equivalent power ($\dot{W}$) consumed by the steady-state binary distillation column operating as discussed in Sect. 7.1, producing the separation in Fig. 7.1, is obtained from the absolute values of reboiler and condenser heat duties in Eq. (7.30), $Q_H = Q_C = 4815$ kW. These duties have to be converted to equivalent positive mechanical powers—respectively, $\dot{W}_H > 0$ and $\dot{W}_C > 0$—by means of two reversible Carnot cycles operating, respectively, with the heat reservoirs R_H ($T_H = 200$ °C) and R_C ($T_C = 50$ °C) as hot sinks, coupled to reservoir R_0 ($T_0 = 25$ °C) as cold sink, as shown in Fig. 7.1.

This arrangement, in Fig. 7.3, imposes to reservoirs R_H and R_C the same steady-state transitions that are taking place in the steady-state distillation column. Carnot cycles are chosen because they are the reversible machines with the best thermodynamic yield for conversion of heat into power (and vice versa) given two heat reservoirs at different temperatures.

Thus, the column heating duty $Q_H = 4815$ kW absorbed from reservoir R_H could lead to an equivalent production of power $\dot{W}_H$ by a Carnot engine absorbing Q_H from R_H and rejecting residual heat to reservoir R_0. Analogously, the column cooling duty $Q_C = 4815$ kW, which is discharged into R_C, is equivalent to a consumption of power $\dot{W}_C$ to drive a Carnot heat pump absorbing heat from reservoir R_0 and delivering Q_C to R_C. In other words, the same heat effects exhibited by the distillation column operation, could be used to produce an equivalent net

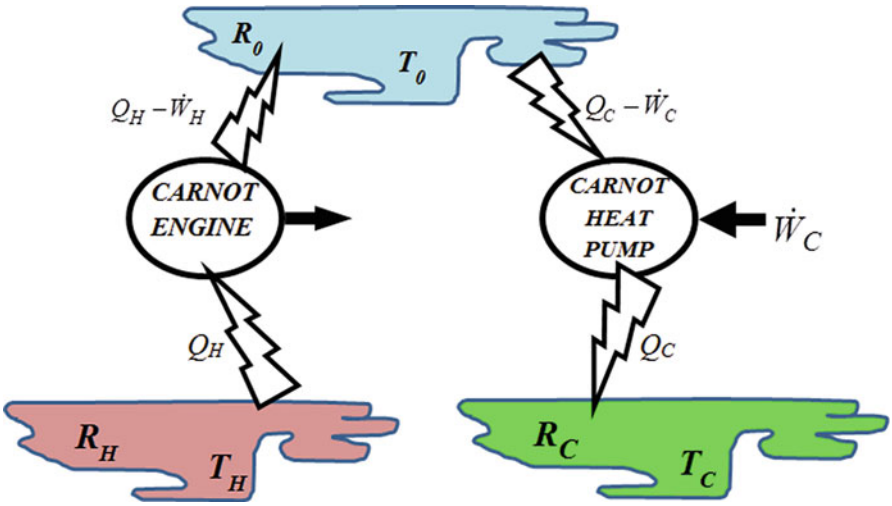

Fig. 7.3 Converting the heating and cooling duties Q_H and Q_C of steady-state distillation column to equivalent production and consumption of powers $\dot{W}_H, \dot{W}_C$ using R_H and R_C as hot sinks and R_0 as cold sink coupled to a Carnot engine and a Carnot heat pump

power effect of $\dot{W}_H - \dot{W}_C$ via Carnot engines coupled as in Fig. 7.3. This net power effect $\dot{W}_H - \dot{W}_C$ is equivalent to the net equivalent power consumption to execute the separation by the distillation column in Fig. 7.1.

The rate of entropy creation associated with the arrangement in Fig. 7.3 is zero because the two Carnot cycles are reversible machines. Thus, Eqs. (7.40a) and (7.40b) represent, respectively, the conservation of entropy associated to the operation of the Carnot engine and the Carnot heat pump. The final formulae in the right side of Eqs. (7.40a) and (7.40b) express the power production and power consumption equivalent to the column heat duties Q_H and Q_C.

With Eqs. (7.40a) and (7.40b), the absolute value of the net equivalent power consumption by the distillation column, $\left|\dot{W}^{EQUIV}\right| = \dot{W}_H - \dot{W}_C$, associated to a steady-state operation under the conditions of Fig. 7.1, is shown in Eq. (7.41). The numerical result is shown in Eq. (7.42) after substituting operation values: $Q_H = 4815\,\text{kW}$, $Q_C = 4815\,\text{kW}$, $T_H = 473.15\,\text{K}$, $T_C = 323.15\,\text{K}$ and $T_0 = 298.15\,\text{K}$.

$$-\frac{Q_H}{T_H} + \frac{Q_H - \dot{W}_H}{T_0} = 0 \Rightarrow \dot{W}_H = \left(1 - \frac{T_0}{T_H}\right) \cdot Q_H \tag{7.40a}$$

$$+\frac{Q_C}{T_C} - \frac{Q_C - \dot{W}_C}{T_0} = 0 \Rightarrow \dot{W}_C = \left(1 - \frac{T_0}{T_C}\right) \cdot Q_C \tag{7.40b}$$

$$\left|\dot{W}^{EQUIV}\right| = \left(1 - \frac{T_0}{T_H}\right) \cdot Q_H - \left(1 - \frac{T_0}{T_C}\right) \cdot Q_C \tag{7.41}$$

$$\left|\dot{W}^{EQUIV}\right| = 1408.38\,\text{kW} \tag{7.42}$$

7.1.4 *Thermodynamic Efficiency of a Steady-State Binary Distillation Column*

The thermodynamic efficiency of the steady-state binary distillation column in Fig. 7.1 is simply calculated with the minimum required power for the separation $\left|\dot{W}^{REV}\right|$ from Eq. (7.39) in Sect. 7.1.2, and the actual equivalent consumption of power $\left|\dot{W}^{EQUIV}\right|$ from Eq. (7.42) in Sect. 7.1.3. This efficiency is given by Eq. (7.43) as only $\eta = 10.31\%$.

$$\eta^{DISTILLATION} = \frac{\left|\dot{W}^{REV}\right|}{\left|\dot{W}^{EQUIV}\right|} * 100 = 10.31\% \tag{7.43}$$

Since the distillation column in the present demonstration operates a single—not too sharp—cut of the feed in terms of two distillation products, the result in

Eq. (7.43) can be generalized as a typical efficiency value for ordinary distillations successfully operating with a single ordinary cut and a narrow margin of reflux ratio above the respective minimum as in Fig. 7.1. This result is a good representative efficiency even in the case of multicomponent distillation columns, provided there is only a single, not too hard, ordinary cut, i.e., the column has one feed and only two product streams which are ordinarily specified in terms of two key components: a light key component and a heavy key component.

If a similar multicomponent distillation column—operating a single ordinary cut with a narrow margin of reflux ratio above the respective minimum—is being modeled via rigorous simulation methods, the obtained thermodynamic efficiency would be of the same order of the value in Eq. (7.43). In other words, the value in Eq. (7.43) is a representative thermodynamic efficiency of a successful distillation column performing a single, not too hard, ordinary cut with a narrow margin of reflux ratio above minimum, despite it has been obtained via a binary distillation solved by a simplified McCabe–Thiele method.

As the separation cut becomes sharper above the level in Fig. 7.1, both $\left|\dot{W}^{\mathrm{REV}}\right|$ and $\left|\dot{W}^{\mathrm{EQUIV}}\right|$ increase with the former a little more rapidly. The result is that the thermodynamic efficiency of the column asymptotically increases above the value in Eq. (7.43). For instance, consider the same feed, pressure, VLE relationship, heat reservoirs, reflux ratio design criteria, and thermodynamic modeling as in Fig. 7.1, but with a sharper cut using new distillate composition at $X_D = 0.999$ and new bottom composition at $X_B = 0.001$. Then, the new values of D, B, $\mathrm{RR}^{\mathrm{MIN}}$, RR, Q_{H}, Q_{C}, $\dot{W}^{\mathrm{REV}}$, $\left|\dot{W}^{\mathrm{EQUIV}}\right|$ and $\eta^{\mathrm{DISTILLATION}}$ will change as shown in Eqs. (7.44a) to (7.44i), evidencing a small increase of thermodynamic efficiency.

$$D = F \cdot \left(\frac{Z - X_B}{X_D - X_B}\right) = 50\,\mathrm{mol/s} \tag{7.44a}$$

$$B = F \cdot \left(\frac{X_D - Z}{X_D - X_B}\right) = 50\,\mathrm{mol/s} \tag{7.44b}$$

$$\mathrm{RR}^{\mathrm{MIN}} = \frac{X_D - g(Z)}{g(Z) - Z} \overset{g(Z)=2/3}{\rightarrow} \mathrm{RR}^{\mathrm{MIN}} = 1.994 \tag{7.44c}$$

$$\mathrm{RR} = 1.3 \times \mathrm{RR}^{\mathrm{MIN}} \Rightarrow \mathrm{RR} = 2.5922 \tag{7.44d}$$

$$Q_{\mathrm{H}} = Q_{\mathrm{C}} = 50 \times 3.5922 \times 30 = 5388.3\,\mathrm{kW} \tag{7.44e}$$

$$\begin{aligned} D \cdot \bar{G}_D + B \cdot \bar{G}_B - F \cdot \bar{G}_F = {} & \frac{\mathrm{FRT}}{2} \cdot \{X_D \cdot \ln(X_D) + (1 - X_D) \cdot \ln(1 - X_D)\} \\ & + \frac{\mathrm{FRT}}{2} \cdot \{X_B \cdot \ln(X_B) + (1 - X_B) \cdot \ln(1 - X_B)\} \\ & - \mathrm{FRT} \cdot \{Z \cdot \ln(Z) + (1 - Z) \cdot \ln(1 - Z)\} \\ = {} & 201.193\,\mathrm{kW} \end{aligned} \tag{7.44f}$$

$$\dot{W}^{\mathrm{REV}} = -201.193\,\mathrm{kW} \tag{7.44g}$$

$$\left|\dot{W}^{\mathrm{EQUIV}}\right| = \left(1 - \frac{T_0}{T_\mathrm{H}}\right) \cdot Q_\mathrm{H} - \left(1 - \frac{T_0}{T_\mathrm{C}}\right) \cdot Q_\mathrm{C} = 1576.1\,\mathrm{kW} \tag{7.44h}$$

$$\eta^{\mathrm{DISTILLATION}} = \frac{\left|\dot{W}^{\mathrm{REV}}\right|}{\left|\dot{W}^{\mathrm{EQUIV}}\right|} \times 100 = 12.77\% \tag{7.44i}$$

The theoretical limit of a cut with pure components ($X_D = 1, X_B = 0$) at RR/RR$^{\mathrm{MIN}} = 1.3$ can also be investigated. One obtains Eqs. (7.45a)–(7.45d):

$$\mathrm{RR}^{\mathrm{MIN}} = 2,\ \mathrm{RR} = 2.6 \tag{7.45a}$$

$$Q_\mathrm{H} = Q_\mathrm{C} = 50 \times 3.6 \times 30 = 5400\,\mathrm{kW} \tag{7.45b}$$

$$\dot{W}^{\mathrm{REV}} = -203.51\,\mathrm{kW}, \left|\dot{W}^{\mathrm{EQUIV}}\right| = 1579.5\,\mathrm{kW} \tag{7.45c}$$

$$\eta^{\mathrm{DISTILLATION}} = \frac{\left|\dot{W}^{\mathrm{REV}}\right|}{\left|\dot{W}^{\mathrm{EQUIV}}\right|} \times 100 = 12.885\% \tag{7.45d}$$

By last one can evaluate the impact of reflux ratio on the efficiency. Consider the theoretical limit of pure components used above giving $\mathrm{RR}^{\mathrm{MIN}} = 2$ and $\dot{W}^{\mathrm{REV}} = -203.51\,\mathrm{kW}$ with $D = B = 50$ mol/s. The reflux ratio affects directly $\dot{W}^{\mathrm{EQUIV}}$ via Eqs. (7.41), (7.21) and (7.22), which were condensed in Eq. (7.46). The final efficiency formula is shown in Eq. (7.47). The graphical behavior of the thermodynamic efficiency of this binary distillation column—with a sharp cut producing pure components—is shown in Fig. 7.4 in terms of the reflux ratio above the minimum value. The best efficiency of 15.4618% corresponds to the minimum reflux ($\mathrm{RR} = \mathrm{RR}^{\mathrm{MIN}}$) operation, falling monotonically towards zero at total reflux operation ($\mathrm{RR} = \infty$).

$$\left|\dot{W}^{\mathrm{EQUIV}}\right| = \left(\frac{T_0}{T_\mathrm{C}} - \frac{T_0}{T_\mathrm{H}}\right) \cdot \left(\left(\frac{\mathrm{RR}}{\mathrm{RR}^{\mathrm{MIN}}}\right) \cdot \mathrm{RR}^{\mathrm{MIN}} + 1\right) \cdot D\lambda \tag{7.46}$$

$$\eta^{\mathrm{DISTILLATION}} = \frac{203.51}{\left(\frac{T_0}{T_\mathrm{C}} - \frac{T_0}{T_\mathrm{H}}\right) \cdot \left(\left(\frac{\mathrm{RR}}{\mathrm{RR}^{\mathrm{MIN}}}\right) \cdot \mathrm{RR}^{\mathrm{MIN}} + 1\right) \cdot D\lambda} \times 100 \tag{7.47}$$

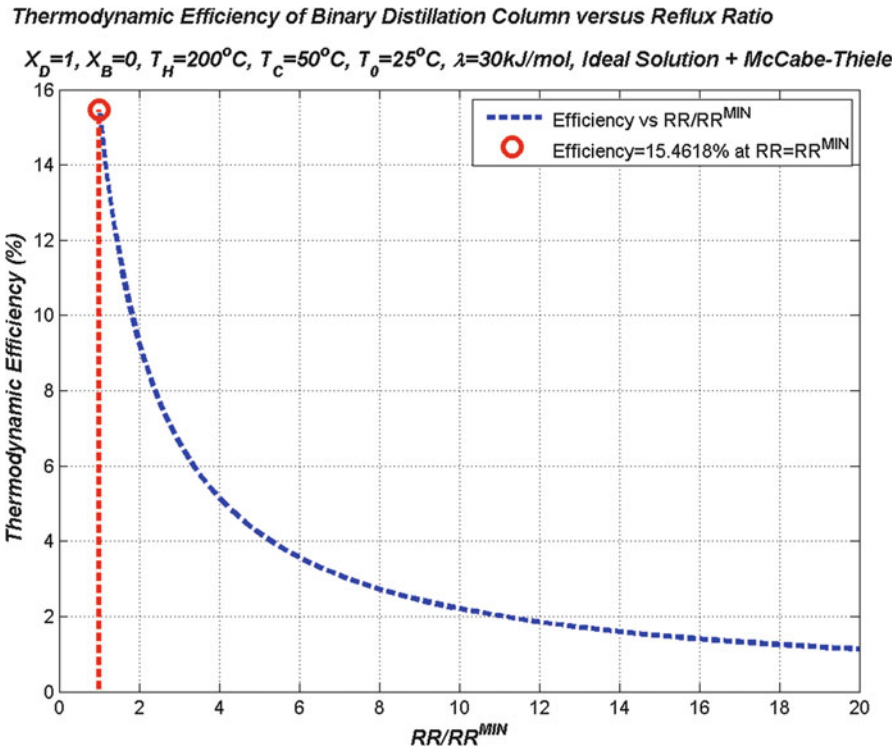

Fig. 7.4 Thermodynamic efficiency of binary distillation column versus reflux ratio

7.2 Multicomponent Distillation Column with Specified Propylene–Propane Sharp Cut

The results of Sect. 7.1 are extended here to a real economically important multicomponent distillation. The objective is to estimate the thermodynamic efficiency of a real hard distillation separation with design to meet commercial targets.

The design method is the Fenske–Underwood–Gilliland method (Henley and Seader 2006). The thermodynamic modeling, property calculations, and operation simulation were performed by a professional process simulator with PR-EOS. All pressures are expressed in absolute values.

The operation is a multicomponent propylene–propane sharp cut distillation in the separation section of a plausible steam-cracker olefins plant. This distillation is especially difficult (hard) due to the small relative volatility propylene/propane which is near 1.1. As a consequence, a high distillation column results. Moreover, this column must operate with very high reflux ratios and very high cooling and heating duties.

The distillation conditions are displayed in Table 7.1 and Fig. 7.5. The light key and heavy key components are C_3H_6 and C_3H_8, respectively. The column uses a

Table 7.1 Data for C_3H_6-C_3H_8 sharp cut distillation

Item	*Feed*	*Distillate*	*Bottoms*
Species	*%mol*	*%Recoveries*	*%Recoveries*
C_2H_6	*0.1%*	*100%*	---
C_3H_6*	*50%*	*99.5%*	*0.5%*
C_3H_8*	*40%*	*0.5%*	*99.5%*
i C_4H_{10}	*7%*	---	*100%*
C_4H_{10}	*2.99%*	---	*100%*
Stream Properties			
Flow Rate (mol/s)	*10000*	*5005*	*4995*
Pressure (bar)	*21.59*	*20.63*	*22.13*
Condition	*Sat. Liquid*	*Sat. Liquid*	*Sat. Liquid*
Temperature (°C)	*59.31*	*50.0*	*69.58*
Enthalpy (kJ/mol)	*-56.1983*	*+7.19807*	*-119.483*
Entropy (kJ/K.mol)	*0.075590*	*0.029204*	*0.111682*

total condenser and a partial kettle reboiler. Head loss of heat exchangers is assumed as 0.5 bar for shell and tubes, excepting the kettle which has negligible shell head loss. The total head loss of the stack of plates is ≈1 bar due to the high number of stages.

Stream temperatures in Table 7.1 were calculated via the bubble-point condition and shown with the respective enthalpies and entropies. Relative volatilities (to C_3H_8) in Table 7.2 for distillate and bottoms were also calculated via bubble-points, whereas the average relative volatilities were given by geometric mean of distillate and bottoms values.

The cold utility is Cooling Water (CW) entering at 35 °C and 4 bar and leaving at 50 °C and 3.5 bar due to the condenser head loss. The condenser discharge pressure is sought to allow cooling by CW with a thermal approach TAPP $\geq$ 15 °C.

The hot utility is Pressurized Hot Water (PHW) entering at 150 °C and 8 bar and leaving at 100 °C and 7.5 bar due to the head loss in the kettle tubes. In the kettle the thermal approach must satisfy TAPP $\geq$ 30 °C.

Despite the small head loss of 0.5 bar of heat exchangers, the thermal transitions of CW and PHW can be approximated by isobaric processes of liquid streams with constant isobaric heat capacities.

In consequence, the enthalpy and entropy changes of CW and PHW can be estimated with good accuracy via Eqs. (7.48a), (7.48b), (7.48c) and (7.48d). The absolute values (>0) of CW and PHW thermal duties follow, respectively, from Eqs. (7.48e) and (7.48f). Table 7.3 summarizes the process data associated with CW and PHW.

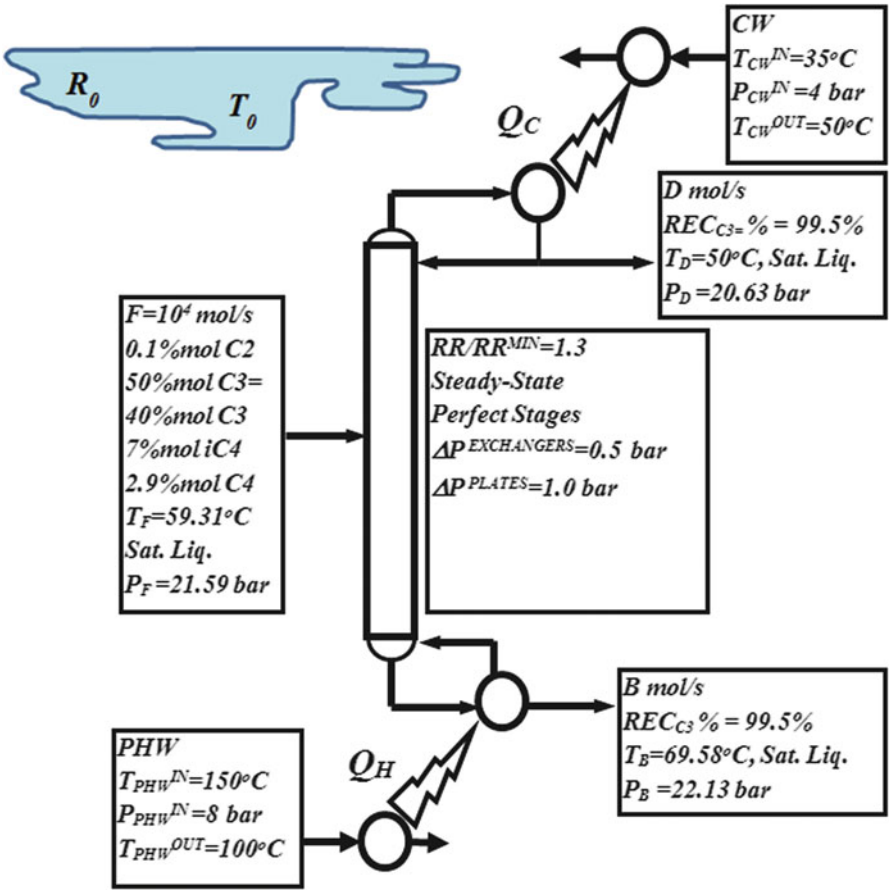

Fig. 7.5 Multicomponent distillation column for C_3H_6-C_3H_8 separation: feed F and products D and B as saturated liquids at 21.59 bar, 20.63 bar and 22.13 bar; heating duty Q_H from PHW (150 °C) to partial reboiler; cooling duty Q_C from total condenser to CW (35 °C); reference reservoir R_0 at $T_0 = 25$ °C is idle

Table 7.2 Relative volatilities (α) for C_3H_6-C_3H_8 distillation

Species	*Feed*	*Distillate*		*Bottoms*		*Average*
	%mol	*%mol*	α	*%mol*	α	α
C_2H_6	0.1%	0.2%	2.20	---	2.043	2.12
C_3H_6*	50%	99.4%	1.07	0.5%	1.12	1.10
C_3H_8*	40%	0.4%	1.0	79.68%	1.0	1.0
$i\,C_4H_{10}$	7%	---	0.486	14.01%	0.6	0.54
C_4H_{10}	2.99%	---	0.423	5.81%	0.5	0.46

[a]Key components

Table 7.3 Properties of water utility streams CW and PHW

Stream	Flow rate (kg/s)	T^{IN} (°C)	P^{IN} (bar)	T^{OUT} (°C)	P^{OUT} (bar)	Mean isobaric heat capacity (kJ/K kg)
CW	q_{CW}	35	4	50	3.5	$\hat{C}_P^{CW} = 4.18$
PHW	q_{PHW}	150	8	100	7.5	$\hat{C}_P^{PHW} = 4.23$

$$\hat{H}_{CW}^{OUT} - \hat{H}_{CW}^{IN} = \hat{C}_P^{CW} \cdot \left(T_{CW}^{OUT} - T_{CW}^{IN}\right) \ (\text{kJ/kg}) \tag{7.48a}$$

$$\hat{S}_{CW}^{OUT} - \hat{S}_{CW}^{IN} = \hat{C}_P^{CW} \cdot \ln\left(\frac{T_{CW}^{OUT}}{T_{CW}^{IN}}\right) \ (\text{kJ/K kg}) \tag{7.48b}$$

$$\hat{H}_{PHW}^{OUT} - \hat{H}_{PHW}^{IN} = \hat{C}_P^{PHW} \cdot \left(T_{PHW}^{OUT} - T_{PHW}^{IN}\right) \ (\text{kJ/kg}) \tag{7.48c}$$

$$\hat{S}_{PHW}^{OUT} - \hat{S}_{PHW}^{IN} = \hat{C}_P^{PHW} \cdot \ln\left(\frac{T_{PHW}^{OUT}}{T_{PHW}^{IN}}\right) \ (\text{kJ/K kg}) \tag{7.48d}$$

$$Q_{CW} = q_{CW} \cdot \hat{C}_P^{CW} \cdot \left(T_{CW}^{OUT} - T_{CW}^{IN}\right) \ (\text{kW}) \tag{7.48e}$$

$$Q_{PHW} = q_{PHW} \cdot \hat{C}_P^{PHW} \cdot \left(T_{PHW}^{IN} - T_{PHW}^{OUT}\right) \ (\text{kW}) \tag{7.48f}$$

7.2.1 *Design of Steady-State Multicomponent Distillation: Determination of Size, Reflux Ratio, Feed Location, and Heat Duties*

The distillation column in Fig. 7.5 and Table 7.1 is designed via the well-known Fenske–Underwood–Gilliland method (Henley and Seader 2006). This is a short-cut method which can give satisfactory results for light hydrocarbon systems like the propylene–propane distillation. The present separation is an example of a partial distribution distillation because some species (C2, iC4, C4) only appear in one of the two column products. Thus, the design strategy adopts the following assumptions:

- Constant relative volatilities given by averaging top and bottoms values as used in Table 7.2.
- Constant molar flow rates of liquid and vapor in each column section (CMO Hypothesis).
- Sharp cut propylene–propane as shown in Table 7.1 with partial distribution of components as in Table 7.2.

Firstly, the column component material balances are solved under partial distribution using the cut recoveries of key components (C_3H_6 and C_3H_8) in Table 7.1. Flow rates D and B and respective compositions are calculated as shown in Tables 7.1 and 7.2. Temperature, enthalpy, and entropy of external streams D, B,

and F are obtained via bubble-point calculations in Table 7.1. The corresponding relative volatilities (relative to C_3H_8) are also given by the bubble-point calculations, and are also displayed in Table 7.2 with the respective average values.

Calling the rectification section in Fig. 7.5 as sec. *0* and the stripping section as sec. *1*, the design internal flow rates (mol/s) of secs. *0* and *1* for liquid and vapor streams are written by CMO according to Eqs. (7.49a)–(7.49d). The absolute value of the total condenser heat duty ($Q_C > 0$) in Fig. 7.5 can be calculated by Eq. (7.49e), whereas the partial reboiler duty ($Q_H > 0$) follows from the column energy balance in Eq. (7.49f) by means of Eq. (7.49g) or Eq. (7.49h). The corresponding flow rates of water utilities CW and PHW are calculated with Q_C, Q_H and Eqs. (7.48e) and (7.48f) as shown in Eqs. (7.49i) and (7.49j).

$$L_0 = D \cdot \mathrm{RR} \tag{7.49a}$$

$$L_1 = D \cdot \mathrm{RR} + F \tag{7.49b}$$

$$V_0 = D(\mathrm{RR} + 1) \tag{7.49c}$$

$$V_1 = D(\mathrm{RR} + 1) \tag{7.49d}$$

$$Q_C = D(\mathrm{RR} + 1)\left(\bar{H}_D^V - \bar{H}_D\right) \ \ (\mathrm{kW}) \tag{7.49e}$$

$$F \cdot \bar{H}_F + Q_H - Q_C = D \cdot \bar{H}_D + B \cdot \bar{H}_B \tag{7.49f}$$

$$Q_H = D \cdot \bar{H}_D + B \cdot \bar{H}_B - F \cdot \bar{H}_F + Q_C \ \ (\mathrm{kW}) \tag{7.49g}$$

$$Q_H = D \cdot \bar{H}_D + B \cdot \bar{H}_B - F \cdot \bar{H}_F + D(\mathrm{RR} + 1)\left(\bar{H}_D^V - \bar{H}_D\right) \ \ (\mathrm{kW}) \tag{7.49h}$$

$$q_{CW} = \frac{Q_C}{\hat{C}_P^{CW} \cdot \left(T_{CW}^{OUT} - T_{CW}^{IN}\right)} \ \ (\mathrm{kg/s}) \tag{7.49i}$$

$$q_{PHW} = \frac{Q_H}{C_P^{PHW} \cdot \left(T_{PHW}^{IN} - T_{PHW}^{OUT}\right)} \ \ (\mathrm{kg/s}) \tag{7.49j}$$

In the context of the Fenske–Underwood–Gilliland method, the Minimum Number of Stages (N^{MIN}) is obtained as $N^{MIN} = 111$ via Fenske Equation Eq. (7.50), where indexes i and j refer respectively to the key components C_3H_6 (light key) and C_3H_8 (heavy key); REC_k and REC'_k represent the top and bottom molar recoveries of components (mol/s) calculated with Table 7.1. This N^{MIN} confirms the non-key REC_k and REC'_k assumed in Table 7.1 via non-key Fenske Equations with column non-key component material balances.

$$N^{MIN} = \frac{\ln\left\{\left(\frac{REC_i}{REC'_i}\right) \times \left(\frac{REC'_j}{REC_j}\right)\right\}}{\ln \alpha_i} = 111 \tag{7.50}$$

The minimum reflux ratio (RR^{MIN}) for this partial distribution case, with only C_3H_6 and C_3H_8 as distributed species, involves finding the unique root θ of the *third* Underwood Equation (7.51a) in the interval [1,α_i] or [1,1.1]. This unique root was found as $\theta = 1.0425593$ by solving Eq. (7.51a) numerically in the interval [1,1.1].

$$\sum_{k=1}^{nc} \frac{\alpha_k Z_k}{\alpha_k - \theta} - \beta = 0 \rightarrow \theta = 1.0425593 \tag{7.51a}$$

At minimum reflux (RR^{MIN}) and partial distribution, it was shown by Underwood (Henley and Seader 2006) that two pinch conditions are attained simultaneously in the rectifying and stripping sections. For these pinches the *first* and the *second* Underwood Equations, Eqs. (7.51b) and (7.51c), must be both satisfied by the unique root $\theta = 1.0425593$ of the *third* Underwood Equation (7.51a), where the superscript ∞ refers to a value at minimum reflux (pinch).

$$\sum_{k=1}^{nc} \frac{\alpha_k \mathrm{REC}_k^{\infty}}{\alpha_k - \theta} - L_0^{\infty} - D^{\infty} = 0 \tag{7.51b}$$

$$\sum_{k=1}^{nc} \frac{\alpha_k \mathrm{REC}_k' {}^{\infty}}{\alpha_k - \theta} + L_1^{\infty} - B^{\infty} = 0 \tag{7.51c}$$

In fact, only one of Eqs. (7.51b) and (7.51c) must be solved because they are not independent relationships as their sum is precisely Eq. (7.51a), which was already solved for $\theta = 1.0425593$. Since the partial distribution top recoveries REC_k^{∞} are all already known in Table 7.1, the distillate flow rate at minimum reflux, D^{∞}, is also known. It has the same value as given in Table 7.1 for the design condition ($D^{\infty} = D = 5005$ mol/s). Thus, Eq. (7.51b) can be trivially solved for L_0^{∞}, giving also the minimum reflux ratio via Eq. (7.49a) as shown below in Eqs. (7.52a) and (7.52b):

$$L_0^{\infty} = \sum_{k=1}^{nc} \frac{\alpha_k \mathrm{REC}_k^{\infty}}{\alpha_k - \theta} - D^{\infty} \Rightarrow L_0^{\infty} = 89,012.36\,\mathrm{mol/s} \tag{7.52a}$$

$$\mathrm{RR}^{\mathrm{MIN}} = \frac{L_0^{\infty}}{D^{\infty}} = 17.8 \tag{7.52b}$$

The design reflux ratio (RR) is obtained by the design reflux condition in Fig. 7.5 as shown in Eq. (7.53). The column heat duties (Q_C, Q_H) and CW and PHW consumptions (q_{CW}, q_{PHW}) at minimum reflux and at the design eflux are calculated via Eqs. (7.49e), (7.49g), (7.49h) and (7.49i) with $\mathrm{RR}^{\mathrm{MIN}}$ and then with RR. The corresponding results are shown in Table 7.4.

$$\mathrm{RR} = 1.3 \times \mathrm{RR}^{\mathrm{MIN}} = 23.14 \tag{7.53}$$

The design of the number of stages of the column (N) is accomplished via the Gilliland-Molokanov correlation (Henley and Seader 2006) with the values of $\mathrm{RR}^{\mathrm{MIN}}$, RR and $\mathrm{N}^{\mathrm{MIN}}$ as shown in Eqs. (7.54a), (7.54b) and (7.54c).

Table 7.4 Propylene–propane multicomponent distillation column. Variables at minimum and design refluxes

Item	Minimum reflux (Underwood method)	Design reflux RR = 1.3 × RR^{MIN}
Column sizing		
Reflux ratio	$RR^{MIN} = 17.8$	RR = 23.14
No. of stages	$N^{\infty} = \infty$	$N = 200$
Feed stage	–	$N_F = 132$
Distillate product (D)		
Flow rate	$D^{\infty} = 5005$ mol/s	$D = 5005$ mol/s
Condition	Sat. liquid	Sat. liquid
Pressure	$P_D = 20.63$ bar	$P_D = 20.63$ bar
Temperature	$T_D = 50$ °C	$T_D = 50$ °C
Enthalpy	$\bar{H}_D = 7.19807\,\mathrm{kJ/mol}$ $\bar{H}_D^V = 19.03611\,\mathrm{kJ/mol}$	$\bar{H}_D = 7.19807\,\mathrm{kJ/mol}$ $\bar{H}_D^V = 19.03611\,\mathrm{kJ/mol}$
Entropy	$\bar{S}_D = 0.029204\,\mathrm{kJ/K\,mol}$	$\bar{S}_D = 0.029204\,\mathrm{kJ/K\,mol}$
Bottoms product (B)		
Flow rate	$B^{\infty} = 4995$ mol/s	$B = 4995$ mol/s
Pressure	$P_B = 22.13$ bar	$P_B = 22.13$ bar
Temperature	$T_B = 69.58$ °C	$T_B = 69.58$ °C
Enthalpy	$\bar{H}_B = -119.483\,\mathrm{kJ/mol}$	$\bar{H}_B = -119.483\,\mathrm{kJ/mol}$
Entropy	$\bar{S}_B = 0.111682\,\mathrm{kJ/K\,mol}$	$\bar{S}_B = 0.111682\,\mathrm{kJ/K\,mol}$
Feed stream (F)		
Flow rate	$F = 10{,}000$ mol/s	$F = 10{,}000$ mol/s
Pressure	$P_F = 21.59$ bar	$P_F = 21.59$ bar
Temperature	$T_F = 59.31$ °C	$T_F = 59.31$ °C
Enthalpy	$\bar{H}_F = -56.1983\,\mathrm{kJ/mol}$	$\bar{H}_F = -56.1983\,\mathrm{kJ/mol}$
Entropy	$\bar{S}_F = 0.075590\,\mathrm{kJ/K\,mol}$	$\bar{S}_F = 0.075590\,\mathrm{kJ/K\,mol}$
Condenser and reboiler		
Condenser duty	$Q_C{}^{\infty} = 1{,}113{,}888.9$ kW	$Q_C = 1{,}430{,}280.7$ kW
Reboiler duty	$Q_H{}^{\infty} = 1{,}113{,}822.5$ kW	$Q_H = 1{,}430{,}214.3$ kW
Cooling water (CW)		
Flow rate	$q_{CW}{}^{\infty} = 17{,}765.4$ kg/s	$q_{CW} = 22{,}811.5$ kg/s
Initial T and P	$T_{CW}^{IN} = 35^{\circ}\mathrm{C}$, $P_{CW}^{IN} = 4\,\mathrm{bar}$	$T_{CW}^{IN} = 35^{\circ}\mathrm{C}$, $P_{CW}^{IN} = 4\,\mathrm{bar}$
Final T and P	$T_{CW}^{OUT} = 50^{\circ}\mathrm{C}$, $P_{CW}^{OUT} = 3.5\,\mathrm{bar}$	$T_{CW}^{OUT} = 50^{\circ}\mathrm{C}$, $P_{CW}^{OUT} = 3.5\,\mathrm{bar}$
Δ Enthalpy	$\Delta\hat{H}_{CW}^{\infty} = 62.7\,\mathrm{kJ/kg}$	$\Delta\hat{H}_{CW} = 62.7\,\mathrm{kJ/kg}$
Δ Entropy	$\Delta\hat{S}_{CW}^{\infty} = 0.198675\,\mathrm{kJ/K\,kg}$	$\Delta\hat{S}_{CW} = 0.198675\,\mathrm{kJ/K\,kg}$
Log-Mean Abs T (Sect.7.2.3)	$T_{CW}^{LM} = 315.59\,\mathrm{K}$	$T_{CW}^{LM} = 315.59\,\mathrm{K}$
Heat capacity (mean)	$\hat{C}_P^{CW} = 4.18\,\mathrm{kJ/K\,kg}$	$\hat{C}_P^{CW} = 4.18\,\mathrm{kJ/K\,kg}$
Pressurized hot water (PHW)		
Flow rate	$q_{PHW}{}^{\infty} = 5266.3$ kg/s	$q_{PHW} = 6762.2$ kg/s
Initial T and P	$T_{PHW}^{IN} = 150^{\circ}\mathrm{C}$, $P_{PHW}^{IN} = 8\,\mathrm{bar}$	$T_{PHW}^{IN} = 150^{\circ}C$, $P_{PHW}^{IN} = 8\,\mathrm{bar}$
Final T and P	$T_{PHW}^{OUT} = 100^{\circ}\mathrm{C}$, $P_{PHW}^{OUT} = 7.5\,\mathrm{bar}$	$T_{PHW}^{OUT} = 100^{\circ}\mathrm{C}$, $P_{PHW}^{OUT} = 7.5\,\mathrm{bar}$

(continued)

Table 7.4 (continued)

Item	Minimum reflux (Underwood method)	Design reflux RR = 1.3 × RR^{MIN}
Δ Enthalpy	$\Delta\hat{H}^{\infty}_{PHW} = -211.5\,kJ/kg$	$\Delta\hat{H}_{PHW} = -211.5\,kJ/kg$
Δ Entropy	$\Delta\hat{S}^{\infty}_{PHW} = -0.531907\,kJ/K\,kg$	$\Delta\hat{S}_{PHW} = -0.531907\,kJ/K\,kg$
Log-Mean Abs T (Sect. 7.2.3)	$T^{LM}_{PHW} = 397.63\,K$	$T^{LM}_{PHW} = 397.63\,K$
Heat capacity (mean)	$\hat{C}_P^{PHW} = 4.23\,kJ/K\,kg$	$\hat{C}_P^{PHW} = 4.23\,kJ/K\,kg$

$$\Omega = \frac{RR - RR^{MIN}}{RR + 1} = 0.22121 \tag{7.54a}$$

$$\Xi = 1 - \exp\left\{\left(\frac{1 + 54.4 \times \Omega}{11 + 117.2 \times \Omega}\right) \cdot \left(\frac{\Omega - 1}{\sqrt{\Omega}}\right)\right\} = 0.4426 \tag{7.54b}$$

$$N = \frac{N^{MIN} + \Xi}{1 - \Xi} = 199.93 \Rightarrow N = 200 \tag{7.54c}$$

The optimum feed location is estimated via Kirkbride correlation with N, REC'_{C3H6}, REC_{C3H8}, D, B, Z_{C3H6}, Z_{C3H8} gathered from Table 7.1 as shown in Eqs. (7.55a) and (7.55b). In these formulae N_R and N_S represent numbers of stages, respectively, above and below the feed. In this case the optimum feed location is estimated with $N_R = 102$ and $N_S = 98$. Nevertheless, by simulating the column design with the Kirkbride location $N_R = 102$ it was found that the cut specifications in Table 7.1 ($REC'_{C3H6}\% = 0.5\%$, $REC_{C3H8}\% = 0.5\%$) could not be met. In other words, the optimum feed location had to be found by trial and error leading this time to $N_R = 131$, i.e., the best feed stage actually corresponds to stage 132.

$$\frac{N_R}{N_S} = \left\{\frac{Z_{C3H8}}{Z_{C3H6}} \times \left(\frac{REC'_{C3H6}}{REC_{C3H8}}\right)^2 \times \frac{D}{B}\right\}^{0.206} \tag{7.55a}$$

$$N_R + N_S = N \tag{7.55b}$$

The final consolidation of minimum reflux variables and design variables for the propylene–propane distillation column is shown in Table 7.4.

7.2.2 *Minimum Power Required for Steady-State Propylene–Propane Separation*

The minimum requirement of power ($\dot{W}^{REV}$) to produce the steady-state propylene–propane separation in Fig. 7.5 can be obtained with the First and Second Laws of Thermodynamics assuming steady-state reversible operation of a machine or open

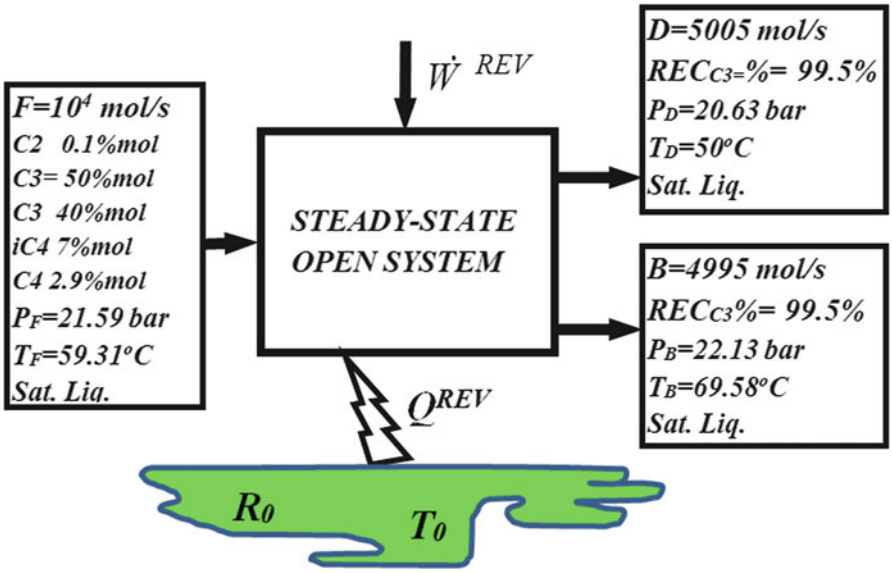

Fig. 7.6 Open system for minimum power separation of the propylene–propane feed $F = 10^4$ mol/s into product streams $D = 5005$ mol/s with 99.5% of propylene recovery and $B = 4995$ mol/s with 99.5% of propane recovery

system executing the separation with the same external streams, states and targets as defined in Fig. 7.5 and Table 7.1. This open system is shown in Fig. 7.6. The open system is supposed subjected to thermal interaction with a heat reservoir R_0 at temperature T_0.

The exact nature of the steady-state open system to undertake the separation is not relevant in principle, but it is certainly not a distillation column. As any reservoir, R_0 has a very high heat capacity so that its temperature is constant at T_0 independently of the heat exchange Q^{REV} between R_0 and the open system. Q^{REV} and $\dot{W}^{\text{REV}}$ are classically defined according to the open system point of view, i.e., Q^{REV} is positive when the system receives heat and $\dot{W}^{\text{REV}}$ is positive when the system produces power (i.e., negative if the system receives power).

Applying the First Law of Thermodynamics to the steady-state open system in Fig. 7.6, Eq. (7.56) results, where $\bar{H}_F, \bar{H}_D, \bar{H}_B$ represent the respective molar enthalpies of streams F, D, and B in kJ/mol. Assuming reversible operation for $\dot{W}^{\text{REV}}$, the steady-state rate of creation of entropy in the Universe associated to this process is zero as shown in Eq. (7.57), where $\bar{S}_F, \bar{S}_D, \bar{S}_B$ represent the respective molar entropies of streams F, D, and B in kJ/K mol. The second term in the left hand side of Eq. (7.57) corresponds to the rate of change of entropy inside the isothermal reservoir R_0 as consequence of the heat exchange Q^{REV} originally defined according to the point of view of the open system.

$$F \cdot \bar{H}_F + Q^{\text{REV}} = \dot{W}^{\text{REV}} + D \cdot \bar{H}_D + B \cdot \bar{H}_B \tag{7.56}$$

$$-F \cdot \bar{S}_F - \frac{Q^{\text{REV}}}{T_0} + D \cdot \bar{S}_D + B \cdot \bar{S}_B = 0 \tag{7.57}$$

Multiplying Eq. (7.57) by T_0 and adding it to Eq. (7.56), results Eq. (7.58) for $\dot{W}^{\text{REV}}$.

$$\dot{W}^{\text{REV}} = -\left\{ \begin{array}{c} D \cdot \left(\bar{H}_D - T_0 \cdot \bar{S}_D\right) + B \cdot \left(\bar{H}_B - T_0 \cdot \bar{S}_B\right) \\ -F \cdot \left(\bar{H}_F - T_0 \cdot \bar{S}_F\right) \end{array} \right\} \tag{7.58}$$

Equation (7.58) is a well-known result for the minimum power required (or maximum power produced) for a given steady-state transition of streams subjected to thermal interaction only with a heat reservoir at T_0. Equation (7.58) states that in a steady-state power-consuming operation the minimum requirement of power is the negative of the net rate (kW) of variation of the property $\bar{H} - T_0 \cdot \bar{S}$ also known as Availability, where the rate of Availability (kW) assigned to product streams is greater than the rate of Availability (kW) assigned to feed streams.

For steady-state distillation separations, as the propylene–propane separation in Fig. 7.5, the output flow rate of Availability is greater than the respective input rate. This means that mechanical power has to be spent to support such separation ($\dot{W}^{\text{REV}} < 0$). Concerning the separation in Figs. 7.5 and 7.6, all streams F, D, and B are saturated liquids at their respective pressures with thermodynamic behavior predicted by PR-EOS.

The temperature of the heat reservoir R_0, T_0, strongly affects the results. Assuming R_0 as the standard atmosphere with temperature $T_0 = 298.15$ K (25 °C), the minimum requirement of power for the propylene–propane separation, according to the targets in Fig. 7.5 and Table 7.1, is calculated with Eq. (7.58) and with the data in Table 7.4 or Table 7.1, giving the results shown in Eqs. (7.59a) and (7.59b).

$$\dot{W}^{\text{REV}} = -16,660.49\,\text{kW} \tag{7.59a}$$

Or, in terms of absolute power value:

$$\left|\dot{W}^{\text{REV}}\right| = 16,660.49\,\text{kW} \tag{7.59b}$$

In other words, the Second Law of Thermodynamics prescribes a minimum requirement of 16,660.49 kW to split the feed of propylene–propane in Table 7.1 following the recoveries in Fig. 7.5 and Table 7.1.

7.2.3 *Actual Equivalent Power Consumption of Steady-State Propylene–Propane Distillation Column via the Method of Carnot Equivalent Cycles*

The actual equivalent power ($\dot{W}$) consumed by the steady-state propylene–propane distillation column in Fig. 7.5, operating as shown in Table 7.1, is obtained from the absolute values of reboiler (Q_H = 1,430,214.3 kW) and condenser (Q_C = 1,430,280.7 kW) heat duties in Table 7.4 with the associated thermal transitions that they cause to the streams CW and PHW. For CW, a flow rate of q_{CW} = 22,811.5 kg/s was used with thermal changes of $\Delta\hat{H}_{CW} = 62.7\,\text{kJ/kg}$ and $\Delta\hat{S}_{CW} = 0.198675\,\text{kJ/K kg}$, whereas for PHW a flow rate of q_{PHW} = 6762.2 kg/s was used with thermal changes of $\Delta\hat{H}_{PHW} = -211.5\,\text{kJ/kg}$ and $\Delta\hat{S}_{CW} = -0.531907\,\text{kJ/K kg}$.

These CW and PHW transitions have to be converted to equivalent positive mechanical powers—respectively, $\dot{W}_H > 0$and $\dot{W}_C > 0$—by means of two reversible Carnot engines operating, respectively, absorbing heat from PHW ($T^{IN}_{PHW} = 150^\circ\text{C} \rightarrow T^{OUT}_{PHW} = 100^\circ\text{C}$) and pumping heat to CW ($T^{IN}_{CW} = 35^\circ\text{C} \rightarrow T^{OUT}_{CW} = 50^\circ\text{C}$), both streams viewed as differential hot sinks with finite heat capacities—i.e., their transition is not isothermal as occurs in a heat reservoir—coupled to a cold reservoir R_0 ($T_0 = 25\,^\circ\text{C}$) as cold sink (Fig. 7.7).

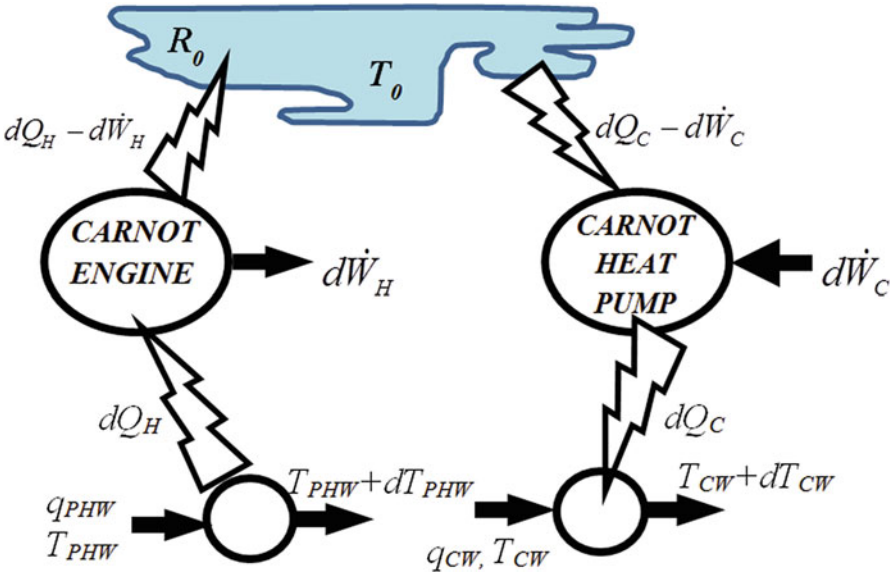

Fig. 7.7 Converting the differential heating and cooling duties dQ_H and dQ_C of streams CW and PHW in the steady-state propylene–propane distillation column to equivalent production and consumption of differential powers $d\dot{W}_H$,$d\dot{W}_C$ using R_0 as cold sink coupled to Carnot engine and Carnot heat pump

This arrangement in Fig. 7.7 imposes to water streams CW and PHW the same steady-state transitions that are taking place in the steady-state propylene–propane distillation column.

Carnot engines are chosen because they are the reversible machines with the best thermodynamic yield for conversion of heat into power (and vice versa) given two heat reservoirs at different temperatures. The only difference here is that the present Carnot engines must operate in a differential way—which is subsequently integrated—because CW and PHW have finite heat capacities, i.e., the Carnot yield changes as the temperature of CW and PHW changes.

Thus, the column heating duty Q_{H} absorbed from non-isothermal stream PHW could lead to an equivalent production of power $\dot{W}_{\mathrm{H}}$ by a Carnot engine absorbing Q_{H} from PHW and rejecting residual heat to reservoir R_0. Analogously, the column cooling duty Q_{C}, which is discharged into the non-isothermal stream CW, is equivalent to a consumption of power $\dot{W}_{\mathrm{C}}$ to drive a Carnot heat pump absorbing heat from reservoir R_0 and delivering Q_{C} to CW. In other words, the same CW and PHW heat effects exhibited by the propylene–propane distillation column operation could be used to produce an equivalent net power effect $\dot{W}_{\mathrm{H}} - \dot{W}_{\mathrm{C}}$ via Carnot engines coupled as in Fig. 7.7. This net power effect $\dot{W}_{\mathrm{H}} - \dot{W}_{\mathrm{C}}$ corresponds to the net equivalent power consumption to execute the propylene–propane separation by the distillation column in Fig. 7.5.

The rate of entropy creation associated with the arrangement in Fig. 7.7 is zero because the two Carnot engines are reversible machines. Thus, Eq. (7.60a) expresses the element of rate of entropy creation in kW/K associated with the absorption of heat from PHW causing an element of cooling $\mathrm{d}T_{\mathrm{PHW}} < 0$ and producing a positive element of power $\mathrm{d}\dot{W}_{\mathrm{H}} > 0$ (in kW). By rearranging Eq. (7.60a), it can be put in the explicit differential form Eq. (7.60b). Equation (7.60b) is then integrated from $T_{\mathrm{PHW}}^{\mathrm{IN}}$ to $T_{\mathrm{PHW}}^{\mathrm{OUT}}$ giving the total production of power $\dot{W}_{\mathrm{H}} > 0$ associated with the cooling of a flow rate q_{PHW} of PHW from $T_{\mathrm{PHW}}^{\mathrm{IN}}$ to $T_{\mathrm{PHW}}^{\mathrm{OUT}}$ as seen in Eqs. (7.60c) and (7.60d). By substitution of $q_{\mathrm{PHW}} = 6762.2\,\mathrm{kg/s}$, $\hat{C}_P^{\mathrm{PHW}} = 4.23\,\mathrm{kJ/K\,mol}$, $T_{\mathrm{PHW}}^{\mathrm{IN}} = 423.15\,\mathrm{K}$, $T_{\mathrm{PHW}}^{\mathrm{OUT}} = 373.15\,\mathrm{K}$, $T_0 = 298.15\,\mathrm{K}$, the integral value of $\dot{W}_{\mathrm{H}}$ is found equal to 357,801.83 kW as in Eq. (7.60e).

$$\frac{q_{\mathrm{PHW}} \cdot \hat{C}_P^{\mathrm{PHW}} \cdot \mathrm{d}T_{\mathrm{PHW}}}{T_{\mathrm{PHW}}} + \frac{-q_{\mathrm{PHW}} \cdot \hat{C}_P^{\mathrm{PHW}} \cdot \mathrm{d}T_{\mathrm{PHW}} - \mathrm{d}\dot{W}_{\mathrm{H}}}{T_0} = 0 \tag{7.60a}$$

$$\mathrm{d}\dot{W}_{\mathrm{H}} = q_{\mathrm{PHW}} \cdot \hat{C}_P^{\mathrm{PHW}} \cdot \left\{ \frac{T_0 \cdot}{T_{\mathrm{PHW}}} - 1 \right\} \cdot \mathrm{d}T_{\mathrm{PHW}} \tag{7.60b}$$

$$\dot{W}_{\mathrm{H}} = q_{\mathrm{PHW}} \cdot \hat{C}_P^{\mathrm{PHW}} \cdot \int_{T_{\mathrm{PHW}}^{\mathrm{IN}}}^{T_{\mathrm{PHW}}^{\mathrm{OUT}}} \left\{ \frac{T_0 \cdot}{T_{\mathrm{PHW}}} - 1 \right\} \cdot \mathrm{d}T_{\mathrm{PHW}} \tag{7.60c}$$

$$\dot{W}_{\mathrm{H}} = q_{\mathrm{PHW}} \cdot \hat{C}_P^{\mathrm{PHW}} \cdot \left\{ T_{\mathrm{PHW}}^{\mathrm{IN}} - T_{\mathrm{PHW}}^{\mathrm{OUT}} - T_0 \cdot \ln \left(\frac{T_{\mathrm{PHW}}^{\mathrm{IN}}}{T_{\mathrm{PHW}}^{\mathrm{OUT}}} \right) \right\} \tag{7.60d}$$

$$\dot{W}_{\mathrm{H}} = 357,801.83\,\mathrm{kW} \tag{7.60e}$$

The same reasoning leads to $\dot{W}_{\mathrm{C}} > 0$ equivalent to the heating of a flow rate q_{CW} of CW from $T_{\mathrm{CW}}^{\mathrm{IN}}$ to $T_{\mathrm{CW}}^{\mathrm{OUT}}$. Equation (7.61a) is the element of rate of entropy creation (kW/K) associated to the heat transfer to CW with an element of heating $\mathrm{d}T_{\mathrm{CW}} > 0$ and consumption of a positive element of power $\mathrm{d}\dot{W}_{\mathrm{C}} > 0$ (kW). Rearranging Eq. (7.61a), results the explicit differential Eq. (7.61b). Equation (7.61b) is integrated from $T_{\mathrm{CW}}^{\mathrm{IN}}$ to $T_{\mathrm{CW}}^{\mathrm{OUT}}$ giving the consumption of power $\dot{W}_{\mathrm{C}} > 0$ associated with the heating of a flow rate q_{CW} of CW from $T_{\mathrm{CW}}^{\mathrm{IN}}$ to $T_{\mathrm{CW}}^{\mathrm{OUT}}$ in Eqs. (7.61c) and (7.61d). By substitution of $q_{\mathrm{CW}} = 22,811.5\,\mathrm{kg/s}$, $\hat{C}_{\mathrm{P}}^{\mathrm{CW}} = 4.18\,\mathrm{kJ/K\,mol}$, $T_{\mathrm{CW}}^{\mathrm{IN}} = 308.15\,\mathrm{K}$, $T_{\mathrm{CW}}^{\mathrm{OUT}} = 323.15\,\mathrm{K}$, $T_0 = 298.15\,\mathrm{K}$, the integral value of $\dot{W}_{\mathrm{C}}$ is found equal to 79,042.10 kW as in Eq. (7.61e).

$$\frac{q_{\mathrm{CW}} \cdot \hat{C}_P^{\mathrm{CW}} \cdot \mathrm{d}T_{\mathrm{CW}}}{T_{\mathrm{CW}}} - \frac{q_{\mathrm{CW}} \cdot \hat{C}_P^{\mathrm{CW}} \cdot \mathrm{d}T_{\mathrm{CW}} - \mathrm{d}\dot{W}_{\mathrm{C}}}{T_0} = 0 \tag{7.61a}$$

$$\mathrm{d}\dot{W}_{\mathrm{C}} = q_{\mathrm{CW}} \cdot \hat{C}_P^{\mathrm{CW}} \left\{ 1 - \frac{T_0}{T_{\mathrm{CW}}} \right\} \cdot \mathrm{d}T_{\mathrm{CW}} \tag{7.61b}$$

$$\dot{W}_{\mathrm{C}} = q_{\mathrm{CW}} \cdot \hat{C}_P^{\mathrm{CW}} \int_{T_{\mathrm{CW}}^{\mathrm{IN}}}^{T_{\mathrm{CW}}^{\mathrm{OUT}}} \left\{ 1 - \frac{T_0}{T_{\mathrm{CW}}} \right\} \cdot \mathrm{d}T_{\mathrm{CW}} \tag{7.61c}$$

$$\dot{W}_{\mathrm{C}} = q_{\mathrm{CW}} \cdot \hat{C}_P^{\mathrm{CW}} \cdot \left\{ T_{\mathrm{CW}}^{\mathrm{OUT}} - T_{\mathrm{CW}}^{\mathrm{IN}} - T_0 \cdot \ln\left(\frac{T_{\mathrm{CW}}^{\mathrm{OUT}}}{T_{\mathrm{CW}}^{\mathrm{IN}}} \right) \right\} \tag{7.61d}$$

$$\dot{W}_{\mathrm{C}} = 79,042.10\,\mathrm{kW} \tag{7.61e}$$

With Eqs. (7.60d) and (7.61d), the formula for the absolute value of the net equivalent power consumption by the propylene–propane distillation column, $\left|\dot{W}^{\mathrm{EQUIV}}\right| = \dot{W}_{\mathrm{H}} - \dot{W}_{\mathrm{C}}$, associated to steady-state operation under the conditions of Fig. 7.5, is shown in Eq. (7.62a). Equation (7.62b) displays the numerical result after substitution of $q_{\mathrm{PHW}} = 6762.2\,\mathrm{kg/s}$, $\hat{C}_P^{\mathrm{PHW}} = 4.23\,\mathrm{kJ/K\,mol}$, $T_{\mathrm{PHW}}^{\mathrm{IN}} = 423.15\,\mathrm{K}$, $T_{\mathrm{PHW}}^{\mathrm{OUT}} = 373.15\,\mathrm{K}$, $T_0 = 298.15\,\mathrm{K}$, $q_{\mathrm{CW}} = 22,811.5\,\mathrm{kg/s}$, $\hat{C}_P^{\mathrm{CW}} = 4.18\,\mathrm{kJ/K\,mol}$, $T_{\mathrm{CW}}^{\mathrm{IN}} = 308.15\,\mathrm{K}$, $T_{\mathrm{CW}}^{\mathrm{OUT}} = 323.15\,\mathrm{K}$.

$$\begin{aligned} \left|\dot{W}^{\mathrm{EQUIV}}\right| = {} & q_{\mathrm{PHW}} \cdot \hat{C}_P^{\mathrm{PHW}} \cdot \left\{ T_{\mathrm{PHW}}^{\mathrm{IN}} - T_{\mathrm{PHW}}^{\mathrm{OUT}} - T_0 \cdot \ln\left(\frac{T_{\mathrm{PHW}}^{\mathrm{IN}}}{T_{\mathrm{PHW}}^{\mathrm{OUT}}} \right) \right\} \\ & - q_{\mathrm{CW}} \cdot \hat{C}_P^{\mathrm{CW}} \cdot \left\{ T_{\mathrm{CW}}^{\mathrm{OUT}} - T_{\mathrm{CW}}^{\mathrm{IN}} - T_0 \cdot \ln\left(\frac{T_{\mathrm{CW}}^{\mathrm{OUT}}}{T_{\mathrm{CW}}^{\mathrm{IN}}} \right) \right\} \end{aligned} \tag{7.62a}$$

$$\left|\dot{W}^{\mathrm{EQUIV}}\right| = 278,759.7\,\mathrm{kW} \tag{7.62b}$$

Equation (7.62a) can be put in a convenient form in terms of the column absolute heat duties $Q_{\mathrm{H}} = q_{\mathrm{PHW}} \cdot \hat{C}_P^{\mathrm{PHW}} \cdot \left(T_{\mathrm{PHW}}^{\mathrm{IN}} - T_{\mathrm{PHW}}^{\mathrm{OUT}}\right)$ and $Q_{\mathrm{C}} = q_{\mathrm{CW}} \cdot \hat{C}_P^{\mathrm{CW}} \cdot \left(T_{\mathrm{CW}}^{\mathrm{OUT}} - T_{\mathrm{CW}}^{\mathrm{IN}}\right)$. This form resembles Eq. (7.41) with the reservoir temperatures replaced by the log-mean *absolute* temperatures $T_{\mathrm{PHW}}^{\mathrm{LM}}$, $T_{\mathrm{CW}}^{\mathrm{LM}}$ of streams PHW and CW as shown in Eqs. (7.63a), (7.63b) and (7.63c). Under the present conditions, $T_{\mathrm{PHW}}^{\mathrm{LM}} = 397.63\,\mathrm{K}$ and $T_{\mathrm{CW}}^{\mathrm{LM}} = 315.59\,\mathrm{K}$.

$$\left|\dot{W}^{\mathrm{EQUIV}}\right| = Q_{\mathrm{H}}\left\{1 - \frac{T_0}{T_{\mathrm{PHW}}^{\mathrm{LM}}}\right\} - Q_{\mathrm{C}}\left\{1 - \frac{T_0}{T_{\mathrm{CW}}^{\mathrm{LM}}}\right\} \tag{7.63a}$$

$$T_{\mathrm{PHW}}^{\mathrm{LM}} = \frac{T_{\mathrm{PHW}}^{\mathrm{IN}} - T_{\mathrm{PHW}}^{\mathrm{OUT}}}{\ln\left(\frac{T_{\mathrm{PHW}}^{\mathrm{IN}}}{T_{\mathrm{PHW}}^{\mathrm{OUT}}}\right)} \tag{7.63b}$$

$$T_{\mathrm{CW}}^{\mathrm{LM}} = \frac{T_{\mathrm{CW}}^{\mathrm{IN}} - T_{\mathrm{CW}}^{\mathrm{OUT}}}{\ln\left(\frac{T_{\mathrm{CW}}^{\mathrm{IN}}}{T_{\mathrm{CW}}^{\mathrm{OUT}}}\right)} \tag{7.63c}$$

Equation (7.63a) can be modified one step further by inserting the expressions for Q_{C} and Q_{H} in terms of the reflux ratio RR as written in Eqs. (7.49e) and (7.49h), which were developed for the propylene–propane multicomponent distillation. The form that initially results is Eq. (7.63d).

$$Q_{\mathrm{C}} = D(\mathrm{RR}+1)\left(\bar{H}_D^{\mathrm{V}} - \bar{H}_D\right) \tag{7.49e}$$

$$Q_{\mathrm{H}} = D \cdot \bar{H}_D + B \cdot \bar{H}_B - F \cdot \bar{H}_F + D(\mathrm{RR}+1)\left(\bar{H}_D^{\mathrm{V}} - \bar{H}_D\right) \tag{7.49h}$$

$$\begin{aligned}\left|\dot{W}^{\mathrm{EQUIV}}\right| = {} & \left(D\bar{H}_D + B\bar{H}_B - F\bar{H}_F + D(\mathrm{RR}+1)\left(\bar{H}_D^{\mathrm{V}} - \bar{H}_D\right)\right) \cdot \left(1 - \frac{T_0}{T_{\mathrm{PHW}}^{\mathrm{LM}}}\right) \\ & - D(\mathrm{RR}+1)\left(\bar{H}_D^{\mathrm{V}} - \bar{H}_D\right) \cdot \left(1 - \frac{T_0}{T_{\mathrm{CW}}^{\mathrm{LM}}}\right)\end{aligned} \tag{7.63d}$$

Equation (7.63d) can be rearranged, one more time, leading to the curious and generic formula in Eq. (7.63e). This formula is a very didactical expression for $\left|\dot{W}^{\mathrm{EQUIV}}\right|$, because it is clearly a generalization of Eq. (7.46)—which was originally developed for the idealized McCabe–Thiele binary distillation column in Sect. 7.1—but has a structure that remarkably resembles the structure of Eq. (7.46), where:

- Cold and hot reservoir temperatures T_{C} and T_{H} were, respectively, replaced by the analogous log-mean *absolute* temperatures of streams CW and PHW, namely, $T_{\mathrm{CW}}^{\mathrm{LM}}$, $T_{\mathrm{PHW}}^{\mathrm{LM}}$.

- The first term in Eq. (7.63e) accounts for the enthalpy gap between products and feed, which is naturally inexistent or zero in the McCabe–Thiele context with D, B, and F as bubble-point liquids.

$$\left|\dot{W}^{\mathrm{EQUIV}}\right|_{\substack{\text{McCabe-Thiele}\\ \text{Distillation}}} = \left(\frac{T_0}{T_{\mathrm{C}}} - \frac{T_0}{T_{\mathrm{H}}}\right) \cdot \left(\left(\frac{\mathrm{RR}}{\mathrm{RR}^{\mathrm{MIN}}}\right) \cdot \mathrm{RR}^{\mathrm{MIN}} + 1\right) \cdot D\lambda \tag{7.46}$$

$$\begin{aligned}\left|\dot{W}^{\mathrm{EQUIV}}\right| = {} & \left(D\bar{H}_D + B\bar{H}_B - F\bar{H}_F\right) \cdot \left(1 - \frac{T_0}{T_{\mathrm{PHW}}^{\mathrm{LM}}}\right) \\ & + \left(\frac{T_0}{T_{\mathrm{CW}}^{\mathrm{LM}}} - \frac{T_0}{T_{\mathrm{PHW}}^{\mathrm{LM}}}\right) \cdot \left(\left(\frac{\mathrm{RR}}{\mathrm{RR}^{\mathrm{MIN}}}\right) \cdot \mathrm{RR}^{\mathrm{MIN}} + 1\right) \cdot D \cdot \left(\bar{H}_D^{\mathrm{V}} - \bar{H}_D\right)\end{aligned} \tag{7.63e}$$

7.2.4 *Thermodynamic Efficiency of a Steady-State Propylene–Propane Distillation Column*

The thermodynamic efficiency of the steady-state propylene–propane distillation column in Fig. 7.5, operating according to Table 7.4, is simply calculated with the minimum required power for the separation $\left|\dot{W}^{\mathrm{REV}}\right|$ from Eq. (7.59b) in Sect. 7.2.2, and the actual equivalent consumption of power $\left|\dot{W}^{\mathrm{EQUIV}}\right|$ from Eq. (7.62b) in Sect. 7.2.3. This efficiency is given by Eq. (7.64) as only $\eta = 5.977\%$.

$$\eta^{\mathrm{DISTILLATION}} = \frac{\left|\dot{W}^{\mathrm{REV}}\right|}{\left|\dot{W}^{\mathrm{EQUIV}}\right|} \times 100 = 5.977\% \tag{7.64}$$

The thermodynamic efficiency of the propylene–propane distillation column is considerably lower than the efficiency of the idealized binary distillation separation in Sect. 7.1. The reason lies on the very hard nature of the propylene–propane separation via distillation, whose relative volatility is only 1.1 at 21 bar, entailing a very high reflux ratio ($\mathrm{RR}^{\mathrm{MIN}} = 17.8$, $\mathrm{RR} = 23.14$, in Table 7.4) and very high consumptions of cooling duty and heating duty per unit of processed feed.

The propylene–propane distillation column in the present demonstration operates a single sharp cut of the feed in terms of two specified distillation products: a top distillate product D rich in propylene and a bottom liquid product B rich in propane and heavier species. This is a very common situation in the context of real commercial distillations. This fact allows us to conclude that the result in Eq. (7.64) can be generalized as a typical efficiency value for *difficult distillations* successfully operating with a single sharp commercial cut and a narrow margin of reflux ratio above the respective minimum as in Fig. 7.5. In other words, this result is a good

representative efficiency of commercial multicomponent hard distillations, provided there is only a single sharp cut, i.e., the column has one feed and only two product streams which are specified in terms of stringent recoveries of two key components: a light key component and a heavy key component.

As the separation cut becomes still sharper, above the level of 99.5% in Fig. 7.5, both $\left|\dot{W}^{\mathrm{REV}}\right|$and $\left|\dot{W}^{\mathrm{EQUIV}}\right|$ increase with the former a little more rapidly. The result is that the thermodynamic efficiency of the column increases monotonously slowly above the value in Eq. (7.64) with the increase of the sharpness of the split.

By last, one can also evaluate the impact of reflux ratio on the column efficiency. Consider the theoretical minimum reflux limit for the separation propylene–propane in Table 7.4 with $\mathrm{RR}^{\mathrm{MIN}} = 17.8$. For this separation the minimum power requirement according to the Second Law of Thermodynamics is $\left|\dot{W}^{\mathrm{REV}}\right| = 16,660.49\,\mathrm{kW}$ by Eq. (7.59b). On the other hand, the reflux ratio RR affects directly $\left|\dot{W}^{\mathrm{EQUIV}}\right|$ via Eqs. (7.62a), (7.63a), and (7.63d), which were condensed in Eq. (7.63e).

The thermodynamic efficiency formula for sharp cut propylene–propane multicomponent distillation (Table 7.1) is shown in Eq. (7.65a), which is brought to the reflux ratio dependent form in Eq. (7.65b) after substituting $\left|\dot{W}^{\mathrm{EQUIV}}(\mathrm{RR})\right|$ with Eq. (7.63e) and replacing $\left|\dot{W}^{\mathrm{REV}}\right|$ by 16,660.49 kW.

$$\eta^{\mathrm{DISTILLATION}} = \frac{\left|\dot{W}^{\mathrm{REV}}\right|}{\left|\dot{W}^{\mathrm{EQUIV}}(\mathrm{RR})\right|} * 100 \tag{7.65a}$$

$$\eta^{\mathrm{DISTILLATION}} = \frac{16,660.49}{\left\{\begin{array}{l}\left(D\bar{H}_D + B\bar{H}_B - F\bar{H}_F\right)\cdot\left(1 - \dfrac{T_0}{T^{\mathrm{LM}}_{\mathrm{PHW}}}\right) \\ +\left(\dfrac{T_0}{T^{\mathrm{LM}}_{\mathrm{CW}}} - \dfrac{T_0}{T^{\mathrm{LM}}_{\mathrm{PHW}}}\right)\cdot\left(\left(\dfrac{\mathrm{RR}}{\mathrm{RR}^{\mathrm{MIN}}}\right)\cdot \mathrm{RR}^{\mathrm{MIN}} + 1\right)\cdot D\cdot\left(\bar{H}^{\mathrm{V}}_D - \bar{H}_D\right)\end{array}\right\}} \times 100 \tag{7.65b}$$

The graphical behavior of the thermodynamic efficiency predicted with Eq. (7.65b) for the propylene–propane multicomponent distillation—with the sharp cut defined in Table 7.1—is shown in Fig. 7.8 in terms of the reflux ratio above the minimum value, where several property values in Table 7.4 were used in these calculations. The best efficiency of 7.6629% corresponds to the minimum reflux ($\mathrm{RR} = \mathrm{RR}^{\mathrm{MIN}} = 17.8$) operation, falling monotonically towards zero at total reflux operation ($\mathrm{RR} = \infty$).

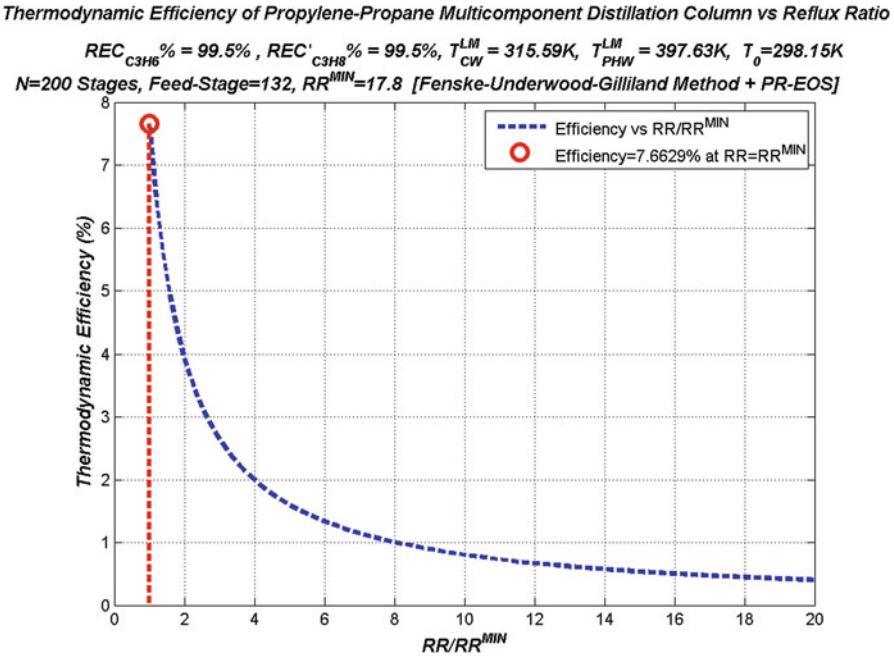

Fig. 7.8 Thermodynamic efficiency of propylene–propane multicomponent distillation column versus reflux ratio

7.3 Thermodynamic Efficiency of a Steady-State Process with Several Power-Consuming Operations

For a process composed exclusively by several steady-state equivalent power-consuming operations—as a typical offshore MEG Recovery Unit or MRU—the overall thermodynamic efficiency of the process can be written with the efficiencies of the constituent operations at a given steady-state condition where the state of all streams are defined.

Representing by η_k and $\left|\dot{W}_k^{\text{EQUIV}}\right|$ the efficiency and equivalent power consumption of operation k ($k = 1...N_{\text{OP}}$) in the steady-state operational point, which were calculated as shown in Sects. 7.1.3, 7.1.4, 7.2.3, and 7.2.4, the overall thermodynamic efficiency is obtained by Eq. (7.66), where the numerator and denominator respectively correspond to the minimum and actual power consumptions of the entire process.

$$\eta^{\text{OVERALL}} = \frac{\sum_{k=1}^{N_{\text{OP}}} \eta_k . \left|\dot{W}_k^{\text{EQUIV}}\right|}{\sum_{k=1}^{N_{\text{OP}}} \left|\dot{W}_k^{\text{EQUIV}}\right|} \tag{7.66}$$

Formula (7.66) shows that the overall thermodynamic efficiency of a given steady-state operational condition of the process is a weighted average of the thermodynamic efficiencies of constituent units, where the weights correspond to the actual equivalent power consumption of units. Another consequence of Eq. (7.66) is that the overall thermodynamic efficiency must be greater than or equal to the lowest thermodynamic efficiency of units and also lower than or equal to the highest thermodynamic efficiency of units. It must be recalled that Eq. (7.66) refers specifically to thermodynamic efficiency and not to, for example, exergy efficiency.

Now consider a typical offshore MRU process. It is well known that in offshore MRU processes the dominant sink of equivalent power consumption corresponds to an ordinary distillation column, namely, the Atmospheric Distillation Column or ADC, which is responsible by the main withdrawal of water from the Rich MEG.

Consequently, the ADC is the dominant consumer of heat in a typical MRU because the major share of vaporization service that occurs in the plant is accomplished by ADC.

The offshore ADC has the following usual characteristics (see Chap. 5; Teixeira et al. 2015, 2016):

- ADC is heated by a PHW stream entering at $T_{\mathrm{PHW}}^{\mathrm{IN}} = 200^{\circ}\mathrm{C}$ and leaving at $T_{\mathrm{PHW}}^{\mathrm{OUT}} = 150^{\circ}\mathrm{C}$, with log-mean temperature $T_{\mathrm{PHW}}^{\mathrm{LM}} = 447.69\,\mathrm{K}$.
- ADC is cooled by CW stream entering at $T_{\mathrm{CW}}^{\mathrm{IN}} = 25^{\circ}\mathrm{C}$ and leaving at $T_{\mathrm{CW}}^{\mathrm{OUT}} = 40^{\circ}\mathrm{C}$, with log-mean temperature $T_{\mathrm{CW}}^{\mathrm{LM}} = 305.59\,\mathrm{K}$.

As said above, in MRU systems the operation ADC is the dominant equivalent power term (kW) appearing in Eq. (7.66). The reason is that ADC exists, with similar operational characteristics, in all MRU configurations TP, FS, and SS. Moreover, since the TP configuration is basically an ADC unit (Chap. 5), the relative magnitude of ADC equivalent power consumption can be inferred from Table 7.5 which displays typical heat consumptions of TP, FS, and SS (Teixeira et al. 2016).

In other words, it can be seen in Table 7.5 that the heat consumption of ADC represents, respectively, 100% of the heat consumption of TP; 75.73% of the heat consumption of FS and 91.76% of the heat consumption of SS. Since the conversions of heat consumptions to equivalent power consumptions apply similar Carnot yield coefficients for TP, FS, and SS, the equivalent power consumption of ADC in TP, FS, and SS will also correspond, respectively, and approximately, to 100%, 75.73% and 91.76% of the total equivalent power consumption. These figures prove

Table 7.5 Heat consumption of MRU processes

MRU	%w/w MEG of lean MEG	Heat consumption (kW)
TP	85.83	1734.1
FS	93.32	2289.8
SS	85.58	1889.9

the dominance of ADC in terms of equivalent power consumption in all MRU Schemes TP, FS, and SS.

The equivalent power consumption of ADC can be written, via Eq. (7.63a), in the form shown in Eq. (7.67), where $Q_{\mathrm{H}}^{\mathrm{ADC}}, Q_{\mathrm{C}}^{\mathrm{ADC}}, T_{\mathrm{CW}}^{\mathrm{LM}}, T_{\mathrm{PHW}}^{\mathrm{LM}}$ represent, respectively, the ADC heating and cooling duties (kW), and the log-mean absolute temperatures (K) of CW and PHW in this ADC. As commonly occurs, the heating and cooling duties are of the same order, allowing Eq. (7.67) to be approximately reduced to the form in Eq. (7.68).

$$\left|\dot{W}_{\mathrm{ADC}}^{\mathrm{EQUIV}}\right| = Q_{\mathrm{H}}^{\mathrm{ADC}}\left\{1 - \frac{T_0}{T_{\mathrm{PHW}}^{\mathrm{LM}}}\right\} - Q_{\mathrm{C}}^{\mathrm{ADC}}\left\{1 - \frac{T_0}{T_{\mathrm{CW}}^{\mathrm{LM}}}\right\} \tag{7.67}$$

$$\left|\dot{W}_{\mathrm{ADC}}^{\mathrm{EQUIV}}\right| \cong Q_{\mathrm{H}}^{\mathrm{ADC}}\left\{\frac{T_0}{T_{\mathrm{CW}}^{\mathrm{LM}}} - \frac{T_0}{T_{\mathrm{PHW}}^{\mathrm{LM}}}\right\} \tag{7.68}$$

By examining Eq. (7.66), one can see that it can be recast via a linear approximation around $\left|\dot{W}_k^{\mathrm{EQUIV}}\right| / \left|\dot{W}_{\mathrm{ADC}}^{\mathrm{EQUIV}}\right| = 0, (k \neq \mathrm{ADC})$ by using the dominance of $\left|\dot{W}_{\mathrm{ADC}}^{\mathrm{EQUIV}}\right|$ over the equivalent powers of the other units, which means $\left|\dot{W}_k^{\mathrm{EQUIV}}\right| / \left|\dot{W}_{\mathrm{ADC}}^{\mathrm{EQUIV}}\right| \ll 1, \ (k \neq \mathrm{ADC})$.

The resulting formula for the overall thermodynamic efficiency of the process is the approximant form in Eq. (7.69a). This form responds linearly with $\left|\dot{W}_k^{\mathrm{EQUIV}}\right|$ $(k \neq \mathrm{ADC})$ and is useful for all MRUs provided $\left|\dot{W}_k^{\mathrm{EQUIV}}\right| / \left|\dot{W}_{\mathrm{ADC}}^{\mathrm{EQUIV}}\right| \ll 1, \ (k \neq \mathrm{ADC})$.

$$\begin{aligned}\eta^{\mathrm{OVERALL}} \cong \eta^{\mathrm{ADC}} &\left\{1 - \sum_{k \neq \mathrm{ADC}}^{N_{\mathrm{OP}}} \frac{\left|\dot{W}_k^{\mathrm{EQUIV}}\right|}{\left(\frac{T_0}{T_{\mathrm{CW}}^{\mathrm{LM}}} - \frac{T_0}{T_{\mathrm{PHW}}^{\mathrm{LM}}}\right) \cdot Q_{\mathrm{H}}^{\mathrm{ADC}}}\right\} \\ &+ \sum_{k \neq \mathrm{ADC}}^{N_{\mathrm{OP}}} \eta_k \cdot \frac{\left|\dot{W}_k^{\mathrm{EQUIV}}\right|}{\left(\frac{T_0}{T_{\mathrm{CW}}^{\mathrm{LM}}} - \frac{T_0}{T_{\mathrm{PHW}}^{\mathrm{LM}}}\right) \cdot Q_{\mathrm{H}}^{\mathrm{ADC}}}\end{aligned} \tag{7.69a}$$

If all units in the MRU flowsheet, excepting ADC, have similar efficiencies such that $\eta_k \cong \eta^{\mathrm{OTHER}}, \ (k \neq \mathrm{ADC})$, Eq. (7.69a) can be reduced one step further to Eq. (7.69b), which estimates the overall efficiency as a weighted average of η^{ADC} and η^{OTHER} with weights that totalize 1, and are defined by the ratio of equivalent power consumption of all joint non-ADC units to the equivalent power consumption of ADC alone.

$$\eta^{\mathrm{OVERALL}} \cong \eta^{\mathrm{ADC}} \left\{ 1 - \frac{\sum_{k \neq \mathrm{ADC}}^{N_{\mathrm{OP}}} \left| \dot{W}_k^{\mathrm{EQUIV}} \right|}{\left(\frac{T_0}{T_{\mathrm{CW}}^{\mathrm{LM}}} - \frac{T_0}{T_{\mathrm{PHW}}^{\mathrm{LM}}} \right) \cdot Q_{\mathrm{H}}^{\mathrm{ADC}}} \right\} + \eta^{\mathrm{OTHER}} \left\{ \frac{\sum_{k \neq \mathrm{ADC}}^{N_{\mathrm{OP}}} \left| \dot{W}_k^{\mathrm{EQUIV}} \right|}{\left(\frac{T_0}{T_{\mathrm{CW}}^{\mathrm{LM}}} - \frac{T_0}{T_{\mathrm{PHW}}^{\mathrm{LM}}} \right) \cdot Q_{\mathrm{H}}^{\mathrm{ADC}}} \right\} \tag{7.69b}$$

In order to test Eq. (7.69b), a basis of calculation can be defined assuming that the three most common commercial MRU versions, TP (traditional process), FS (full-stream), and SS (slip-stream) process a Rich MEG feed of 100 t/day, 55% w/w H_2O + 45% w/w MEG at 25 °C, 1 bar. These MRUs, working in such conditions, have heating consumptions as shown in Table 7.5 in Chap. 6.

Since TP is constituted basically by a single ADC (Teixeira et al. 2015), and FS and SS also have similar ADCs with similar targets, besides other units, one can conclude that the heating duty of all ADCs, considering the feed above, is approximately the heat consumption of TP, that is $Q_{\mathrm{H}}^{\mathrm{ADC}} = 1734.1\,\mathrm{kW}$. Consequently, from Table 7.5 it can be seen that all the remaining operations of FS and SS (i.e., ADC exclusive) have heating duty consumptions respectively totaling of the order of 555 kW and 150 kW. These duties are converted to the respective equivalent power consumptions by a typical Carnot yield factor of the order of ≈1/3 according to the method of Carnot equivalent cycles used in Sect. 7.2.3.

This entails that the equivalent power consumptions of the operations of FS and SS, excluding ADC, correspond respectively to 185 kW and 50 kW. Since the Carnot terms in the denominators of Eq. (7.69b) are also of the order of 1/3, one can reduce Eq. (7.69b) to the forms shown in Eqs. (7.70a)–(7.70c), respectively, for processes TP, FS, and SS. In Eqs. (7.70a)–(7.70c) η^{OTHER} refers to the typical efficiency of other existing operations excluding ADC, assuming they have similar performances. These formulae allow to linearly estimate the thermodynamic efficiency of TP, FS, and SS MRUs from the efficiency of ADC and the typical efficiency of the remaining operations.

$$\eta_{\mathrm{TP}}^{\mathrm{OVERALL}} \approx \eta^{\mathrm{ADC}} \tag{7.70a}$$

$$\eta_{\mathrm{FS}}^{\mathrm{OVERALL}} \cong \eta^{\mathrm{ADC}} \cdot \left\{ 1 - \frac{555}{1734.1} \right\} + \eta^{\mathrm{OTHER}} \cdot \left\{ \frac{555}{1734.1} \right\} \tag{7.70b}$$

$$\eta_{\mathrm{SS}}^{\mathrm{OVERALL}} \cong \eta^{\mathrm{ADC}} \cdot \left\{ 1 - \frac{150}{1734.1} \right\} + \eta^{\mathrm{OTHER}} \cdot \left\{ \frac{150}{1734.1} \right\} \tag{7.70c}$$

Or

$$\eta_{\mathrm{TP}}^{\mathrm{OVERALL}} \approx \eta^{\mathrm{ADC}} \tag{7.70a}$$

$$\eta_{\mathrm{FS}}^{\mathrm{OVERALL}} \cong 0.68 \times \eta^{\mathrm{ADC}} + 0.32 \times \eta^{\mathrm{OTHER}} \tag{7.70d}$$

$$\eta_{\mathrm{SS}}^{\mathrm{OVERALL}} \cong 0.913 \times \eta^{\mathrm{ADC}} + 0.087 \times \eta^{\mathrm{OTHER}} \tag{7.70e}$$

For instance, if the other units in the FS flowsheet are less efficient than ADC (and this is likely to be the case), FS as a whole will have an inferior overall thermodynamic efficiency compared to TP. On the other hand, in the case of SS this factor is much less critical to the overall efficiency of the MRU.

References

Henley E, Seader JD (2006) Separation process principles, 2nd edn. Wiley, New York

Teixeira AM, de Medeiros JL, Araújo OQF (2015) Exergy analysis of monoethylene glycol (MEG) recovery systems. Computer aided chemical engineering, 12th international symposium on process systems engineering 37(1):533–538. doi:10.1016/B978-0-444-63578-5.50084-0

Teixeira AM, Arinelli LO, de Medeiros JL, Araújo OQF (2016) Exergy analysis of monoethylene glycol recovery processes for hydrate inhibition in offshore natural gas fields. J Nat Gas Sci Eng 35(1):798–813. doi:10.1016/j.jngse.2016.09.017

Chapter 8
Exergy Analysis of Chemical Processes

Abstract Exergy analysis (ExA) has been gaining relevance in the field of energy efficiency as a powerful tool to assess degradation of energy quality. ExA quantifies the percentage of destroyed exergy via process irreversibilities, as well as the percentage of lost exergy via process deficiencies when handling waste (material and energy) streams. ExA also assesses the primary sinks responsible for exergy destruction and/or exergy losses by process inefficiencies and/or design limitations. Moreover, ExA might also be used as design criteria for optimization of process in order to minimize energy requirements, energy degradation and waste (material and energy) streams. It is believed that a complete picture of the thermodynamic performance of a process is achieved and best evaluated by performing an exergy analysis in place of or in addition to conventional energy analysis. This is due to the fact that ExA can clearly indicate the components or blocks that destroy or lose exergy the most, i.e., the most thermodynamically or materially inefficient components. In this chapter, formulae for exergy flow rate of streams are obtained from application of first and second Laws of Thermodynamics together with conservation equations for the studied system (general steady-state open system and its reference environment).

Exergy Analysis (ExA) has been gaining relevance in the field of energy efficiency as a powerful tool to assess degradation of energy quality. ExA quantifies the percentage of destroyed exergy via process irreversibilities, as well as the percentage of lost exergy via process deficiencies when handling waste (material and energy) streams. ExA also assesses the primary sinks responsible for exergy destruction and/or exergy losses by process inefficiencies and/or design limitations (BoroumandJazi et al. 2013). Moreover, ExA might also be used as design criteria for optimization of process in order to minimize energy requirements, energy degradation and waste (material and energy) streams.

It is believed that a complete picture of the thermodynamic performance of a process is achieved and best evaluated by performing an exergy analysis in place of or in addition to conventional energy analysis. This is due to the fact that ExA can clearly indicate the components or blocks that destroy or lose exergy the most, i.e., the most thermodynamically or materially inefficient components. This is done by drawing a map of how the flow rate of exergy destruction/loss is distributed over the

A. Mendonça Teixeira et al., *Monoethylene Glycol as Hydrate Inhibitor in Offshore Natural Gas Processing*, SpringerBriefs in Petroleum Geoscience & Engineering,
DOI 10.1007/978-3-319-66074-5_8

system of interest. Therefore, the use of ExA can pinpoint the plant components that can be further improved and reveal whether or not, and by how much, it is possible to design more efficient energy and material usage by reducing the inefficiencies in existing systems (Dincer and Zamfirescu 2011).

Exergy is a concept derived from the combination of first and second Laws of Thermodynamics and it can be defined as the maximum amount of work obtainable when a stream is brought into equilibrium with its surroundings represented as a Reference Environmental Reservoir (RER). Therefore, exergy is a property that depends not only on the state of the system streams, but also on the definition of RER. In this sense, the setting of an appropriate definition for RER is vital in order to allow for an effective ExA. However, defining an appropriate RER is not a simple task, but is a necessary one in exergy studies (Dincer and Zamfirescu 2011).

For this reason, besides performing ExA of MRU processes, the present work is also interested in addressing how the allocation of the state of RER species affects the results of ExA of MRUs. The present approach follows closely the material and results presented in Teixeira et al. (2015), and Teixeira et al. (2016).

In the MRU processing context the critical species is evidently MEG, which, as any typical organic compound, exhibits a very high specific exergy if measured with respect to conventional RER configuration, namely, the standard atmosphere saturated in water containing N_2, O_2, CO_2, H_2O, Ar, etc., where MEG coexists in chemical equilibrium. In this framework, a very high specific exergy results for MEG in MRU streams due to the extremely low chemical potential of this ultra-rarefied gaseous MEG in chemical equilibrium with RER species. Consequently, since MEG is not, in general, destroyed in MRU processes, (i.e., it is equally present in the feeds and products of MRUs), there is a very high percentage of conserved exergy in all MRU technologies masking the real inefficiencies of each process and hindering their discrimination according to ExA. The reason is that all MRUs will appear in the results with very high, unrealistic, exergy efficiencies (i.e., above 80% efficiencies) (Teixeira et al. 2016).

Taking this into account, an alternative and more adequate RER formulation was investigated in order to eliminate this masking of exergy efficiencies, which hindered a meaningful comparison of processes. The central point is to choose RER to promote an adequate evaluation of the specific exergy of MEG in order to allow a fair discrimination of MRU processes via ExA.

Hence, the only possible way is to redefine RER so as to reduce the very high specific exergy of MEG relatively to the species in the conventional RER. As MEG is not consumed or created in all MRUs (i.e., there is no chemical reaction with MEG in MRUs), it seems that the best approach is to allow MEG to *exist as an independent RER species* in phase equilibrium with the remaining RER species. To be meaningful, this MEG RER state could only be feasible if defined in an aqueous liquid phase in equilibrium with the atmosphere, which should be saturated with water. In other words, this new RER is two-phase with MEG infinitely diluted in the aqueous liquid (Teixeira et al. 2016). Such RER definition is reasonable for an offshore MRU, since it would represent the atmospheric air in equilibrium with the ocean.

To explore and evaluate these RER choices, in this book we conduct ExA according to two different conceptions of RER:

- Approach #1: The conventional RER with gaseous MEG in chemical equilibrium with air, corresponding to the standard atmosphere saturated with water via VLE with pure liquid H_2O at 25 °C and 1 bar.
- Approach #2: RER is again the standard atmosphere in VLE with liquid water, but now containing MEG at infinite dilution at 25 °C and 1 bar, MEG which is not chemically equilibrated with air species.

Firstly, formulae for exergy flow rate of streams are obtained from application of first and second Laws of Thermodynamics together with conservation equations for the studied system in Sect. 8.1.

8.1 Steady-State Chemical Processes

Exergy flow (in kW) is defined as the maximum power (mechanical work) obtainable when a stream reaches equilibrium with a reference external environment. Therefore a generalized expression for exergy flow rate of streams is developed considering a general steady-state open system and its reference environment.

According to the second Law of Thermodynamics, the Universe is an isolated system with constant mass, volume and energy, which encompasses all conceivable transitions that may physically occur. The entropy of the Universe increases when irreversible transitions occur or remain constant when only reversible transitions take place.

Following this concept, in the present analysis it is also necessary to define an isolated macro-system which could confine all the relevant transitions that may occur. Such macro-system is, indeed, a miniature Universe—since it is isolated and all conceivable transitions are confined inside it—which includes several pertinent reservoirs and the open system of interest (e.g., an MRU). The macro-system for ExA of MRU systems is represented in Fig. 8.1.

This macro-system or mini Universe has a steady-state finite open system—henceforth called the System—interacting with several different reservoirs as seen in Fig. 8.1. The interactions of the System with each reservoir are very specific and are defined by appropriate specific walls existing on the boundaries of the System, as well on the boundaries of the reservoir in question.

The concept of reservoir is important. Reservoirs are infinite systems—hence their representation with such suggestive indefinite contours in Fig. 8.1—that are characterized by one (or more) constant intensive parameter(s) that regulates the exchanges of certain specific extensive properties like volume, thermal energy, mass of species *1*, mass of species *2*, etc. Central points in the concept of reservoir are:

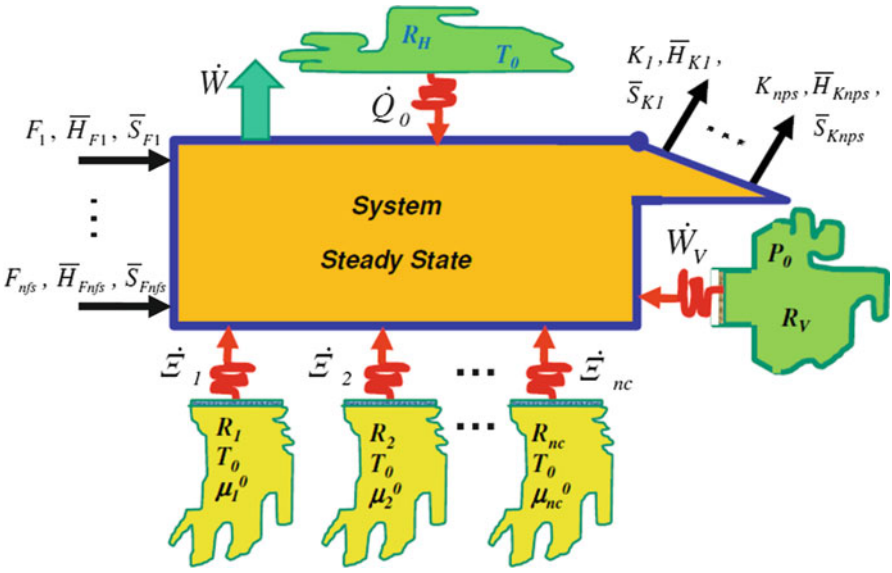

Fig. 8.1 Complex steady-state open system interacting with heat, volume and species reservoirs

- Any finite exchange of the specific exchangeable property(ies) does not alter or disturb the reservoir characteristic intensive parameter(s).
- Reservoirs have appropriate selective walls on their boundaries that allow bidirectional flow exclusively of the exchangeable property (e.g., movable, frictionless, thermally isolated piston to exchange exclusively volume; selective membrane to exchange component *1*, etc.).
- Reservoirs are uniform and always in internal equilibrium (internal reversibility), so that the Fundamental Relationship of the Internal Energy is always integrable for them on any quasi-static transition.

The System is a rigid, steady-state, finite open system with several inlet $\{F_1, F_2, \ldots F_{\text{nfs}}\}$ and outlet $\{K_1, K_2, \ldots, K_{\text{nps}}\}$ streams, where nfs and nps represent, respectively, numbers of feed and product streams.

The System interacts with nc reservoirs of species k $\{R_1, R_2, \ldots, R_{\text{nc}}\}$, where each R_k has a constant volume and state coordinates T_0 and μ_k^0. In all interactions between the System and R_k, only component k is transferred at a certain rate with a simultaneous energy flow $\dot{\Xi}_k$.

The System also interacts with a volume reservoir R_V at constant pressure P_0, where interactions with R_V are adiabatic volume transfers only, with associated work (power) $\dot{W}_V$. Due to its internal reversibility and adiabatic operation, R_V entropy is constant. By last, the System also interacts with a constant volume heat reservoir R_{H} at temperature T_0, through heat transfer $\dot{Q}_0$.

Figure 8.1 illustrates this coupling of System and reservoirs, where the coiled arrows represent transfers between System and reservoirs, such that do not necessarily entail equilibrium between them.

The RER represents a conceptual union of all reservoirs: species, volume, and heat reservoirs R_1, R_2, …, R_{nc}, R_V, R_{H}. Each reservoir is infinite (relatively to System), uniform and supposed in complete (thermo-chemical-mechanical) internal equilibrium. All reservoirs of species (R_k) are supposed in *mutual chemical equilibrium* and at the same temperature T_0.

First, the first Law of Thermodynamics is written in Eq. (8.1) for the open System. Since all reservoirs are at internal equilibrium, *Internal Energy Fundamental Relationships* can be written in rate-based form as shown in Eqs. (8.2)–(8.4). Exchange terms $\dot{Q}_0, \dot{W}, \dot{W}_V, \dot{\Xi}_k$ are defined according to the classical thermodynamic convention following the System viewpoint——that is, work done (received) by the System is positive (negative); heat received (lost) by the System is positive (negative).

The First Law is invoked to relate the exchange terms $\dot{Q}_0, \dot{W}, \dot{W}_V, \dot{\Xi}_k$ with the rate of internal energy of reservoirs as seen in the RHS (Right-Hand Side) of Eqs. (8.2)–(8.4).

$$\sum_{j}^{\mathrm{nps}} K_j \bar{H}_{K_j} = \sum_{j}^{\mathrm{nfs}} F_j \bar{H}_{F_j} + \sum_{k=1}^{\mathrm{nc}} \dot{\Xi}_k + \dot{Q}_0 - \dot{W} - \dot{W}_V \tag{8.1}$$

$$\dot{U}^{(R_{\mathrm{H}})} = T_0 \dot{S}^{(R_{\mathrm{H}})} = -\dot{Q}_0, \quad \dot{V}^{(R_{\mathrm{H}})} = 0 \tag{8.2}$$

$$\dot{U}^{(R_V)} = -P_0 \dot{V}^{(R_V)} = \dot{W}_{\mathrm{V}}, \quad \dot{S}^{(R_V)} = 0 \tag{8.3}$$

$$\dot{U}^{(R_k)} = T_0 \dot{S}^{(R_k)} + \mu_k^0 \dot{N}_k^{(R_k)} = -\dot{\Xi}_{k(k=1..\mathrm{nc})} \tag{8.4}$$

Net rates of creation of volume ($\dot{\Omega}_V$), entropy ($\dot{\Omega}_S$) and species k ($\dot{\Omega}_k$) in the Universe of Fig. 8.1 can be addressed respectively using Eqs. (8.5), (8.6), and (8.7). These relationships must be written for the macro-system in Fig. 8.1, which is defined by the System coupled to reservoirs $R_1, R_2, \ldots, R_{\mathrm{nc}}, R_V, R_{\mathrm{H}}$. Such net rates of creation can be, respectively, expressed as:

$$\dot{\Omega}_V = \dot{V}^{\mathrm{Sys}} + \dot{V}^{(R_V)} + \dot{V}^{(R_{\mathrm{H}})} + \sum_{k=1}^{\mathrm{nc}} \dot{V}^{(R_k)} - \sum_{k}^{\mathrm{nfs}} F_k \bar{V}_{F_k} + \sum_{k}^{\mathrm{nps}} K_k \bar{V}_{K_k} \tag{8.5}$$

$$\dot{\Omega}_S = \dot{S}^{\mathrm{Sys}} + \dot{S}^{(R_{\mathrm{H}})} + \dot{S}^{(R_V)} + \sum_{k=1}^{\mathrm{nc}} \dot{S}^{(R_k)} - \sum_{j}^{\mathrm{nfs}} F_j \bar{S}_{F_j} + \sum_{j}^{\mathrm{nps}} K_j \bar{S}_{K_j} \tag{8.6}$$

$$\dot{\Omega}_k = \dot{N}_k^{\mathrm{Sys}} + \dot{N}_k^{(R_k)} - \sum_{j}^{\mathrm{nfs}} F_j Y_{kF_j} + \sum_{j}^{\mathrm{nps}} K_j Y_{kK_j} \tag{8.7}$$

The steady-state condition of the System implies $\dot{V}^{\mathrm{Sys}}$, $\dot{S}^{\mathrm{Sys}}$, and $\dot{N}_k^{\mathrm{Sys}}$ equal to zero. $\dot{V}^{(R_{\mathrm{H}})}$ and $\dot{V}^{(R_k)}$ are also zero because they refer to constant volume reservoirs.

Similarly, $\dot{S}^{(R_V)}$ is zero because R_V operates at constant entropy. The rate of creation of volume ($\dot{\Omega}_V$) of the Universe is identically zero according to the definition of Universe.

If the System exhibits chemical reactions, the first impression is that species are not conserved in the Universe, i.e., apparently $\dot{\Omega}_k \neq 0$. However, since species reservoirs are *in mutual chemical equilibrium*, the generation/consumption of species k within the System can be compensated by a reverse consumption/generation of species k within reservoir R_k by simply reversibly converting/creating other species in their respective reservoirs without any change in the thermodynamic condition of the Universe. Thus, either with or without chemical reactions in the System, the creation rates of all species in the Universe can be taken as zero ($\dot{\Omega}_k = 0$). With these concepts, it can be shown that the rate of work produced by the System is given by Eq. (8.8a):

$$\begin{aligned} -\dot{W} = & \sum_{j}^{\text{nps}} K_j \left(\bar{H}_{K_j} + P_0 \bar{V}_{K_j} - T_0 \bar{S}_{K_j} - \sum_{k=1}^{\text{nc}} \mu_k^0 Y_{kK_j} \right) \\ & - \sum_{j}^{\text{nfs}} F_j \left(\bar{H}_{F_j} + P_0 \bar{V}_{F_j} - T_0 \bar{S}_{F_j} - \sum_{k=1}^{\text{nc}} \mu_k^0 Y_{kF_j} \right) + T_0 \dot{\Omega}_S \end{aligned} \tag{8.8a}$$

The maximum rate of net work—maximum power—is obtained when the System operates reversibly. In other words, without creation of entropy in the Universe according to the second Law, i.e., $\dot{\Omega}_S = 0$.

In this case, Eq. (8.8a) leads to Eq. (8.8b) which shows that the maximum rate of work production $\dot{W}^{\text{MAX}}$ (or minimum rate of work consumption $\dot{W}^{\text{MIN}}$) is defined by the negative of the difference between the total output flow rate of exergy associated with product streams leaving the System and the total input flow rate of exergy associated with the feed streams entering the System, respectively corresponding to the first and second RHS terms of Eq. (8.8b). In other words, the molar exergies of product stream K_j and of feed stream F_j must be defined, respectively, by:

- $\bar{B}_{K_j} \equiv \bar{H}_{K_j} + P_0 \bar{V}_{K_j} - T_0 \bar{S}_{K_j} - \sum_{k=1}^{\text{nc}} \mu_k^0 Y_{kK_j}$.
- $\bar{B}_{F_j} \equiv \bar{H}_{F_j} + P_0 \bar{V}_{F_j} - T_0 \bar{S}_{F_j} - \sum_{k=1}^{\text{nc}} \mu_k^0 Y_{kF_j}$.

Exergy terms associated to material streams are calculated using only state properties that are expressed as ratios or as "densities," which belong to the respective stream—for example, $\bar{V}, \bar{H}, \bar{S}, Y_k$—multiplied by ("field") parameters P_0, T_0, μ_k^0 that, on the other hand, belong to RER. Each term summed up in the RHS of Eq. (8.8b) represents the ultimate definition of exergy flow rate associated with the respective material stream.

$$-\dot{W}^{\,\mathrm{MAX}} = \sum_{j}^{\mathrm{nps}} K_j \left(\bar{H}_{K_j} + P_0 \bar{V}_{K_j} - T_0 \bar{S}_{K_j} - \sum_{k=1}^{\mathrm{nc}} \mu_k^0 Y_{kK_j} \right) - \sum_{j}^{\mathrm{nfs}} F_j \left(\bar{H}_{F_j} + P_0 \bar{V}_{F_j} - T_0 \bar{S}_{F_j} - \sum_{k=1}^{\mathrm{nc}} \mu_k^0 Y_{kF_j} \right) \tag{8.8b}$$

The difference between Eqs. (8.8a) and (8.8b), leads to the well-known formula for the rate of lost work (lost power) in Eq. (8.8c).

$$\dot{W}^{\,\mathrm{LOST}} = \dot{W}^{\,\mathrm{MAX}} - \dot{W} \; = T_0 \dot{\Omega}_S \tag{8.8c}$$

On the other hand, besides being associated with material flows, exergy can also be associated to pure mechanical energy (power) streams which are contributing terms within $\dot{W}$ and $\dot{W}^{\,\mathrm{MAX}}$.

Therefore, the total inlet and outlet exergy flows can be generalized by adding material and pure mechanical exergy flows as in Eqs. (8.9) and (8.10), where $\dot{B}_{\,\mathrm{in}}$, $\dot{B}_{\,\mathrm{out}}$ are the exergy flow rates associated to all input and output material streams, whereas exergy flows $\dot{B}^{\,W}_{\,\mathrm{in}}, \dot{B}^{\,W}_{\,\mathrm{out}}$ are assigned to all positive pure mechanical power streams (e.g., electric energy streams and/or equivalent mechanical effects associated with heat duties) imported or exported by the System, represented by $\left|\dot{W}_j^{\,\mathrm{imported}}\right|$ and $\left|\dot{W}_k^{\,\mathrm{exported}}\right|$ respectively.

$$\dot{B}_{\,\mathrm{in}} + \dot{B}^{\,W}_{\,\mathrm{in}} = \sum_{j}^{\mathrm{nfs}} F_j \left(\bar{H}_{F_j} + P_0 \bar{V}_{F_j} - T_0 \bar{S}_{F_j} - \sum_{k=1}^{\mathrm{nc}} \mu_k^0 Y_{kF_j} \right) + \sum_{j=1}^{\mathrm{nwi}} \left| \dot{W}_j^{\,\mathrm{imported}} \right| \tag{8.9}$$

$$\dot{B}_{\,\mathrm{out}} + \dot{B}^{\,W}_{\,\mathrm{out}} = \sum_{j}^{\mathrm{nps}} K_j \left(\bar{H}_{K_j} + P_0 \bar{V}_{K_j} - T_0 \bar{S}_{K_j} - \sum_{k=1}^{\mathrm{nc}} \mu_k^0 Y_{kK_j} \right) + \sum_{k=1}^{\mathrm{nwe}} \left| \dot{W}_k^{\,\mathrm{exported}} \right| \tag{8.10}$$

All terms in exergy formulae Eqs. (8.9) and (8.10) can be obtained from process simulations, excepting the RER parameters P_0, T_0, μ_k^0, which depend on the definition of RER outside the flowsheet.

Therefore, in order to investigate which would be the best definition of RER for ExA with MRUs, two RER approaches are considered in the next sections.

Furthermore, for final validation of exergy calculations, two ways of calculating the rate of lost exergy are implemented for each MRU. These two ways can corroborate each other in any application of this methodology because they use different sources of property values. The rate of lost exergy in the Universe can be calculated from:

- The difference between total output and total input flow rates of exergy in Eq. (8.12).
- The rate of lost work in Eq. (8.8c) or Eq. (8.11), where $\dot{\Omega}_S$ is the net rate of creation of entropy in Eq. (8.6), and $\Delta\dot{B}$ arises in the LHS of the difference of Eqs. (8.10) and (8.9).

$$\dot{W}^{\text{LOST}} = T_0\dot{\Omega}_S \tag{8.11}$$

$$\Delta\dot{B} \equiv \left(\dot{B}_{\text{out}} + \dot{B}^{W}_{\text{out}}\right) - \left(\dot{B}_{\text{in}} + \dot{B}^{W}_{\text{in}}\right) \tag{8.12}$$

The exergy efficiency of a process (or unit operation) can be calculated by the ration between the input rate of exergy and the output rate of useful exergy leaving the process (or unit). In this regard, it must be also considered that the rate of loss of exergy in a given process encompasses the true rate of disappearance of exergy plus the rate of exergy that leaves the process as final waste streams as discussed in Chap. 7 (final gas exhausts, final waste water, etc.). The percent exergy efficiency of processes is given in Eq. (8.13) by dividing the LHS's of Eqs. (8.10) and (8.9), where the above mentioned exergy waste terms should not be included in the numerator of Eq. (8.13).

$$\eta\% = \frac{\dot{B}_{\text{out}} + \dot{B}^{W}_{\text{out}}}{\dot{B}_{\text{in}} + \dot{B}^{W}_{\text{in}}} \cdot 100 \tag{8.13}$$

References

Boroumandjazi G, Rismanchi B, Saidur R (2013) A review on exergy analysis of industrial sector. Renew Sust Energ Rev 27(1):198–203. doi:10.1016/j.rser.2013.06.054

Dincer I, Zamfirescu C (2011) Thermodynamic fundamentals. Sustainable energy systems and applications. Springer, New York, pp 1–50. doi:10.1007/978-0-387-95861-3_1

Teixeira AM, de Medeiros JL, Araújo OQF (2015) Exergy analysis of monoethylene glycol (MEG) recovery systems. Computer aided chemical engineering, 12th international symposium on process systems engineering 37(1):533–538. doi:10.1016/B978-0-444-63578-5.50084-0

Teixeira AM, Arinelli LO, de Medeiros JL, Araújo OQF (2016) Exergy analysis of monoethylene glycol recovery processes for hydrate inhibition in offshore natural gas fields. J Nat Gas Sci Eng 35(1):798–813. doi:10.1016/j.jngse.2016.09.017

Chapter 9
Exergy Analysis of MRU Processes in Offshore Platforms

Abstract The theory of exergy analysis (ExA) of the previous chapter is now specifically applied to the three main types of MRU commercially available to offshore oil and gas platforms. The first point to address is the definition of the reference environment reservoir (RER). The RER definition has a great influence on the ExA results, therefore two kinds of RER approaches are considered in this work giving very different exergy efficiencies: RER Approach #1 and RER Approach #2. In this chapter, it is shown that only one of them makes sense to carry out useful ExA of MRUs. RER Approach #2 allows much better discrimination of exergy efficiencies and better identification of exergy sinks in all studied MRUs. RER Approach #1, although consistent and correct, failed to provide discrimination of exergy performances and realistic results, whereas the proposed novel RER Approach #2 is able to provide much more realistic and meaningful exergy efficiency values. Under RER Approach #2 the existing irreversibilities are more easily revealed and, thus, affect with more impact the calculation of exergy efficiencies, better discriminating them.

The theory of exergy analysis (ExA) of the previous chapter is now specifically applied to the three main types of MRU commercially available to offshore oil and gas platforms. The first point to address is the definition of the reference environment reservoir (RER). The RER definition has a great influence on the ExA results, and therefore two kinds of RER approaches are considered in this work giving very different exergy efficiencies: RER Approach #1 and RER Approach #2. It will be shown that only one of them makes sense to carry out useful ExA of MRUs.

9.1 RER Approach #1

RER in Approach #1 is two-phase with gas and liquid portions. It is defined by standard atmospheric air saturated with water at $T_0 = 298.15$ K and $P_0 = 1$ atm in VLE with an infinite body of pure water, where the standard atmosphere has the following dry-basis mol fraction composition in Table 9.1.

A. Mendonça Teixeira et al., *Monoethylene Glycol as Hydrate Inhibitor in Offshore Natural Gas Processing*, SpringerBriefs in Petroleum Geoscience & Engineering,
DOI 10.1007/978-3-319-66074-5_9

Table 9.1 Dry basis composition of atmospheric air

Component	Mole fraction
N_2	0.7808
O_2	0.2095
CO_2	0.0004
Ar	0.0094

In order to obtain the final composition of the RER vapor phase ($Y^0_{N_2}, Y^0_{O_2}, Y^0_{Ar}, Y^0_{CO_2}, Y^0_{H_2O}$), VLE is solved with liquid water as an idle sub-PFD in the professional simulator. However, commercial simulators do not export chemical potentials, so μ_i^0 must be obtained through a three-step semi-manual procedure:

- Enthalpy and entropy of pure species as ideal gases at $T_0 = 298.15$ K and $P_0 = 1$ atm are firstly obtained by defining idle streams of pure N_2, O_2, CO_2 and Ar in the PFD at $T_0 = 298.15$ K and $P_0 = 1$ atm.
- Despite being calculated via EOS, these enthalpy and entropy values are indistinguishable from ideal gas values due to the low pressure and moderate temperature at (T_0, P_0). They are now used to compute $\mu_i^{f,0}(T_0, P_0)$, the chemical potential of pure i at (T_0, P_0), calculated by the simulation PFD with such idle streams of pure i at (T_0, P_0) via Eq. (9.2).
- These values are manually corrected to mixture conditions via Eq. (9.1), valid for ideal gases.
- In all above steps, it is important to ensure thermodynamic consistency by using the same thermodynamic model of the entire simulation (Glycol Thermodynamic Package). Hence, all enthalpies and entropies refer to the same entropy and enthalpy datum values, ensuring consistency for exergy values.

$$\mu_i^0 = \mu_i^{f,0}(T_0, P_0) + RT_0 \ln Y_i^0 \tag{9.1}$$

$$\mu_i^{f,0}(T_0, P_0) = \bar{H}(\text{pure } i, T_0, P_0) - T_0 \bar{S}(\text{pure } i, T_0, P_0) \quad (i = N_2, O_2, Ar, CO_2) \tag{9.2}$$

For the calculation of the chemical potential of water, this procedure must be changed as a pure water stream at T_0 and P_0 will be recognized in liquid state. Thus, an arbitrary idle stream of pure water is created at $T_0 = 298.15$ K and $P = 0.01$ atm, condition which is depressurized enough to be in vapor phase as a stable pure ideal gas. The substitute versions of Eqs. (9.1) and (9.2) for water case correspond to Eqs. (9.3) and (9.4). Properties in Eq. (9.3) come from the idle water gas stream, which are complemented by Eq. (9.4) via the ideal gas chemical potential isothermal change from 0.01 atm to $P_0 = 1$ atm.

$$\mu_i^f(T_0, 0.01\,\text{atm}) = \bar{H}(\text{pure } i, T_0, 0.01\,\text{atm}) - T_0\bar{S}(\text{pure } i, T_0, 0.01\,\text{atm}) \quad (i = \text{H}_2\text{O}) \tag{9.3}$$

$$\mu_i^{f,0}(T_0, P_0) = \mu_i^f(T_0, 0.01\,\text{atm}) + RT_0 \ln\left(\frac{1\,\text{atm}}{0.01\,\text{atm}}\right)(i = \text{H}_2\text{O}) \tag{9.4}$$

Another possible way to calculate $\mu^0_{\text{H}_2\text{O}}$ follows from the value of molar Gibbs energy of pure liquid water at T_0 and P_0 via Eq. (9.5) from an idle stream of liquid water with the same thermodynamic package, since VLE entails water with the same chemical potential in both vapor and liquid phases.

$$\mu^0_{\text{H}_2\text{O}}(T_0, P_0) = \bar{G}\big(T_0, P_0\big)\big|_{\text{Liq.H}_2\text{O}} = \bar{H}(T_0, P_0)|_{\text{Liq.H}_2\text{O}} - T_0\bar{S}(T_0, P_0)|_{\text{Liq.H}_2\text{O}} \tag{9.5}$$

Regarding MEG, as it is not naturally present in the atmosphere, its chemical potential is calculated from the chemical potential of the remaining species present in the atmosphere (N_2, O_2, Ar, CO_2, and H_2O). Hence, it is allocated as a trace component gas in chemical equilibrium with the remaining RER species. From a practical standpoint, the trace presence of MEG is insufficient to affect the gas phase composition and the other chemical potentials.

RER chemical potential of MEG is extremely low as calculated according to a combustion chemical equilibrium among MEG, O_2, CO_2, and H_2O in Eq. (9.6) with standard states of species as (g) state (pure ideal gas, 25 °C, 1 atm). This gives μ^0_{MEG} in Eq. (9.7).

$$\text{C}_2\text{H}_6\text{O}_2(g) + 2.5\text{O}_2(g) \leftrightarrow 2\text{CO}_2(g) + 3\text{H}_2\text{O}(g) \tag{9.6}$$

$$\mu^0_{\text{MEG}} = 2\mu^0_{\text{CO}_2} + 3\mu^0_{\text{H}_2\text{O}} - 2.5\mu^0_{\text{O}_2} \tag{9.7}$$

9.2 RER Approach #2

In Approach #2, RER is again two-phase at $T_0 = 298.15$ K and $P_0 = 1$ atm with H_2O saturated atmospheric air in VLE with liquid H_2O. The difference from Approach #1 lies in the state of MEG: it is allocated *in the liquid phase at infinite dilution without chemical equilibrium with air*.

The vapor phase uses the same dry-basis air composition of RER Approach #1, with final vapor composition obtained by solving the water VLE as before. RER chemical potentials $\mu^0_{\text{N}_2}, \mu^0_{\text{CO}_2}, \mu^0_{\text{Ar}}, \mu^0_{\text{O}_2}, \mu^0_{\text{H}_2\text{O}}$ are calculated as done in the RER Approach #1 with Eqs. (9.1), (9.2), (9.3), and (9.4), with the humid air composition as Y_i^0 values.

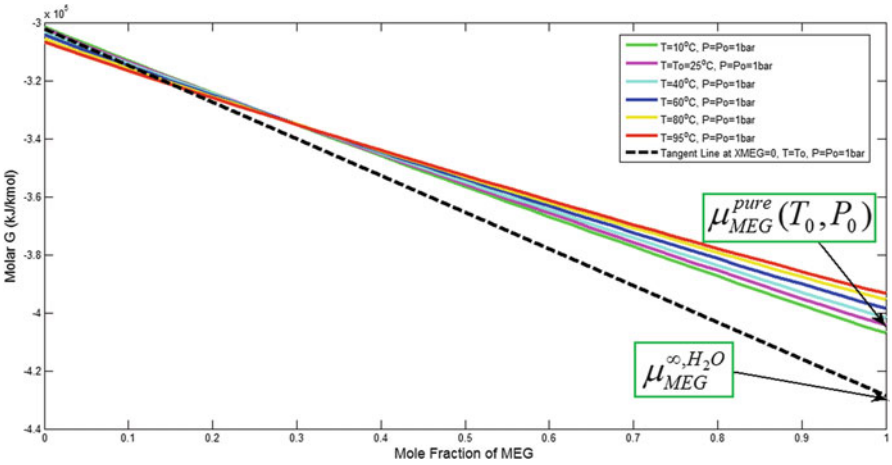

Fig. 9.1 Graphical construction to obtain the chemical potential of MEG infinitely diluted in water

In the case of water, as the liquid phase is essentially pure water, $\mu^0_{H_2O}$ can also be obtained from the molar Gibbs energy of a pure water liquid stream with Eq. (9.8).

In RER Approach #2, the RER chemical potential of MEG, μ^0_{MEG}, is given by the adequate formula of infinite dilution, μ^{∞,H_2O}_{MEG} via Eq. (9.9) (Smith et al. 2001), where X represents the MEG mole fraction in liquid phase.

The derivative term in Eq. (9.9) is obtained via numerical differentiation on the curve $\bar{G}(T_0,P_0,X) = \bar{H}(T_0,P_0,X) - T_0\bar{S}(T_0,P_0,X)$ generated with $\bar{H}(T_0,P_0,X)$, $\bar{S}(T_0,P_0,X)$ values from several composition of H_2O + MEG liquid streams at (T_0, P_0) in the simulation PFD. Graphically, Eq. (9.9) is equivalent to the intersection of the tangent line at $X_{MEG} = 0$ with the line $X_{MEG} = 1$, as illustrated in Figs. 9.1 and 9.2.

Figure 9.1 illustrates this curve for several values of RER temperature (T_0), wherein the tangent line is taken at the temperature of interest $T_0 = 25\,^{\circ}C$. Figure 9.2 is a magnification of Fig. 9.1 in the vicinity of $X_{MEG} = 0$ to provide a better view of the tangent line of $\bar{G}(T_0,P_0,X)$ at $T = T_0$ and $P = P_0$.

$$\mu^0_{H_2O}(T_0,P_0) = \bar{G}(T_0,P_0,X)\big|_{X=0} = \bar{H}(T_0,P_0,X)|_{X=0} - T_0\bar{S}(T_0,P_0,X)|_{X=0} \quad (9.8)$$

$$\mu^{\infty,H_2O}_{MEG}(T_0,P_0) = \bar{G}(T_0,P_0,X)\big|_{X=0} + \frac{d\bar{G}}{dX}(T_0,P_0,X)\bigg|_{X=0} \quad (9.9)$$

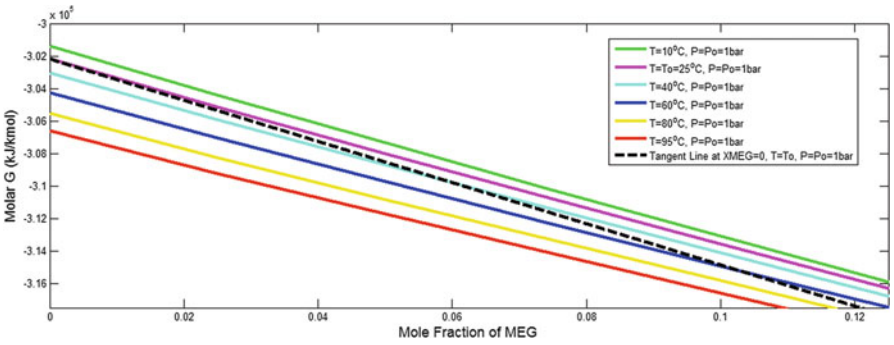

Fig. 9.2 Magnification of Fig. 9.1 in the vicinity of $X_{\mathrm{MEG}} \approx 0$

9.3 Results of Exergy Analysis of MRUs

Values of RER chemical potentials of species for both RER approaches are reported in Table 9.2. Exergy flow rates of streams of all MRUs are calculated accordingly via each RER approach. A primary indicator of consistency is that all exergy flow rates must always have *positive values* expressed in kW, which was correctly accomplished here.

As can be seen in Table 9.2 μ^0_{MEG} differs appreciably for RER Approaches #1 and #2, strongly affecting the numerical values of exergy flow rates. RER Approach #1 provides a very negative μ^0_{MEG} entailing Rich MEG and Lean MEG streams with very high positive values of exergy flow rates and with similar magnitudes as seen in Table 9.3.

On the other hand, under RER Approach #2, exergy flow rates of MEG streams present much lower positive values with dissimilar magnitudes, whose distinction is markedly established as seen in Table 9.4.

According to RER Approach #2, MEG is allocated in liquid phase infinitely diluted in water *without chemical equilibrium with RER species*, thereby representing a state closer to the thermodynamic condition of MEG in the MRU streams. This entails a less negative value for the RER chemical potential of MEG, consequently generating much lower positive values of exergy flow rates associated with MRU streams as seen in Table 9.4. Furthermore, although MEG is now not in the lowest exergy state in RER, this choice of reference is more practical in MRU processing because it is out of question to produce work by oxidizing MEG to CO_2 and H_2O.

Comparing Tables 9.3 and 9.4 it becomes clear that values of exergy flow rates of MEG streams for RER Approach #1 are two orders of magnitude larger than those via RER Approach #2. The underlying reason is that Rich and Lean MEG streams have much more exergy content relatively to RER species in Approach #1 than in Approach #2, as reflected above in the RER chemical potentials of MEG in Table 9.2.

Table 9.2 Chemical potentials of RER species via RER approaches #1 and #2

Species	μ_k^0 RER Approach#1 (kJ/kmol)	μ_k^0 RER Approach #2 (kJ/kmol)
N_2	-5.05×10^4	-5.05×10^4
O_2	-5.39×10^4	-5.39×10^4
Ar	-4.69×10^4	-4.69×10^4
CO_2	-4.60×10^5	-4.60×10^5
H_2O	-3.02×10^5	-3.02×10^5
MEG	-1.71×10^6	-4.43×10^5

Table 9.3 Exergy flow rates of inlet and outlet streams of TP, FS, and SS MRUs with RER Approach #1

TP		FS		SS	
Stream	Exergy flow rate (kW)	Stream	Exergy flow rate (kW)	Stream	Exergy flow rate (kW)
Rich MEG	10,879.8	Rich MEG	10,879.8	Rich MEG	10,879.8
S.W.1 in	13.9	S.W.1 in	10.0	S.W.1 in	11.3
S.W.2 in	0.9	S.W.2 in	5.8	S.W.2 in	2.5
Exhaust gas in	2243.4	S.W.3 in	0.4	S.W.3 in	0.8
Water for disposal	0.2	Exhaust gas 1 in	1713.1	Exhaust gas 1 in	1811.9
S.W.1 out	24.9	Exhaust gas 2 in	1113.7	Exhaust gas 2 in	524.6
S.W.2 out	1.7	Chiller S.W. in	4.9	Chiller S.W. in	2.1
Exhaust gas out	1051.6	Water for disposal	0.1	Water for disposal	0.1
Lean MEG	10,922.5	S.W.1 out	17.9	S.W.1 out	20.3
		S.W.2 out	10.5	S.W.2 out	4.6
		S.W.3 out	0.8	S.W.3 out	1.4
		Exhaust gas 1 out	807.4	Exhaust gas 1 out	806.2
		Exhaust gas 2 out	440.7	Exhaust gas 2 out	226.2
		Chiller S.W. out	8.8	Chiller S.W. out	3.8
		Water for disposal 2	0.1	Water for disposal 2	0.1
		Lean MEG	10,930.3	Lean MEG	10,922.3

The differences between RER Approaches also directly impact exergy efficiencies as seen in Table 9.5.

Exergy efficiencies are calculated as ratios between useful output and input flow rates of exergy (in kW), respectively from Eqs. (8.10) and (8.9), as shown in Eq. (8.13), where the exergy terms of waste streams (gas exhausts, waste water,

Table 9.4 Exergy flow rates of inlet and outlet streams of TP, FS, and SS MRUs with RER Approach #2

TP		FS		SS	
Stream	Exergy flow rate (kW)	Stream	Exergy flow rate (kW)	Stream	Exergy flow rate (kW)
Rich MEG	263.8	Rich MEG	263.8	Rich MEG	263.8
S.W.1 in	13.9	S.W.1 in	10.0	S.W.1 in	11.3
S.W.2 in	0.9	S.W.2 in	5.8	S.W.2 in	2.5
Exhaust gas in	2243.4	S.W.3 in	0.4	S.W.3 in	0.8
Water for disposal	0.1	Exhaust gas 1 in	1713.1	Exhaust gas 1 in	1811.9
S.W.1 out	24.9	Exhaust gas 2 in	1113.7	Exhaust gas 2 in	524.6
S.W.2 out	1.7	Chiller S.W. in	4.9	Chiller S.W. in	2.1
Exhaust gas out	1051.6	Water for disposal	0.1	Water for disposal	0.1
Lean MEG	306.6	S.W.1 out	17.9	S.W.1 out	20.3
		S.W.2 out	10.5	S.W.2 out	4.6
		S.W.3 out	0.8	S.W.3 out	1.4
		Exhaust gas 1 out	807.4	Exhaust gas 1 out	806.2
		Exhaust gas 2 out	440.7	Exhaust gas 2 out	226.2
		Chiller S.W. out	8.8	Chiller S.W. out	3.8
		Water for disposal 2	0.1	Water for disposal 2	0.1
		Lean MEG	314.9	Lean MEG	306.4

Table 9.5 Overall exergy efficiencies (%) of MRU processes via RER Approaches #1 and #2

MRU	RER Approach #1 (%)	RER Approach #2 (%)
Traditional process	83.10	12.13
Full-stream process	78.96	9.76
Slip-stream process	82.21	11.48

etc.) are not considered as useful exergy associated with the output streams. As calculated with Tables 9.3 and 9.4, both approaches provide the same rate of lost exergy (kW).

However, RER Approach #1 leads to MEG streams with very high positive exergy flow rates (≈11,500 kW) of a much greater magnitude than typical exergy losses (≈1600 kW). As MEG is not consumed in the MRUs, total inlet and outlet exergy flows associated with MEG streams have huge magnitudes with only ≈1600 kW of lost exergy. Hence, with RER Approach #1, total exergy flow rates

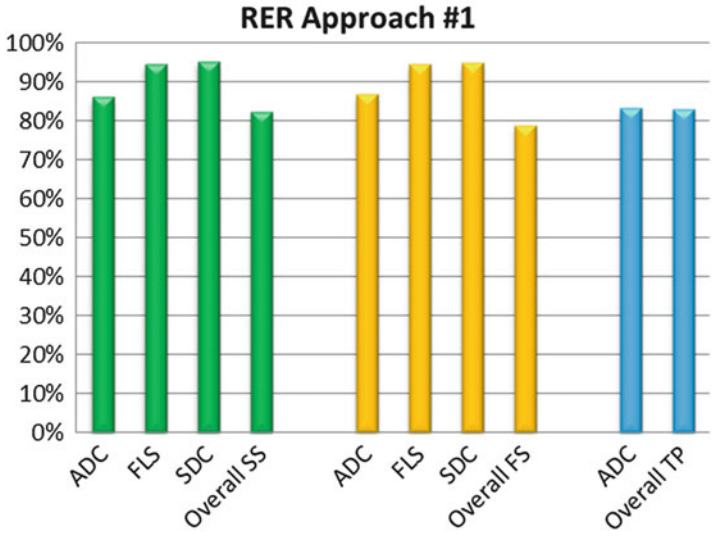

Fig. 9.3 Exergy efficiency of process units of SS, FS, and TP MRUs via RER Approach #1

have a small relative fall and are close in magnitude, entailing exergy efficiencies close to 80%.

On the other hand, RER Approach #2 provides much lower positive values of exergy flow rates associated with MEG streams (≈280–330 kW), and therefore much lower—but much more meaningful—exergy efficiencies are obtained, since the same rate of exergy is lost in both cases. This leads to more realistic efficiencies, which are closer to what is expected for distillation-based processing.

An important aspect about ExA is that it must allow identifying the most inefficient components or blocks in the analyzed process. Then, exergy efficiencies per main equipment were calculated so as to compare the performances of both RER Approaches in this regard. Figures 9.3 and 9.4 depict exergy efficiencies per main processing units.

The main sinks of exergy (i.e., associated with highest rate of destruction of exergy) correspond to the distillations columns: ADC is the biggest sink, whereas FLS is the smallest sink among the main units. However, only RER Approach #2 was able to reveal this kind of detail, while RER Approach #1 provided a much worse discrimination of exergy efficiencies of process units and of the entire PFDs.

Therefore, RER Approach #2 allowed ExA to indicate on which blocks of MRU processes design efforts should be concentrated to minimize energy degradation and improve energy consumption. In this regard, the distillation columns, and particularly ADC in TP, FS, and SS should be considered with more care. Such results are consistent, since the reboiler of ADC represents a great source of irreversibility, which must be compared with the better exergy efficiency of SDC which does not have such reboiler and uses the supply of enthalpy conveyed by the

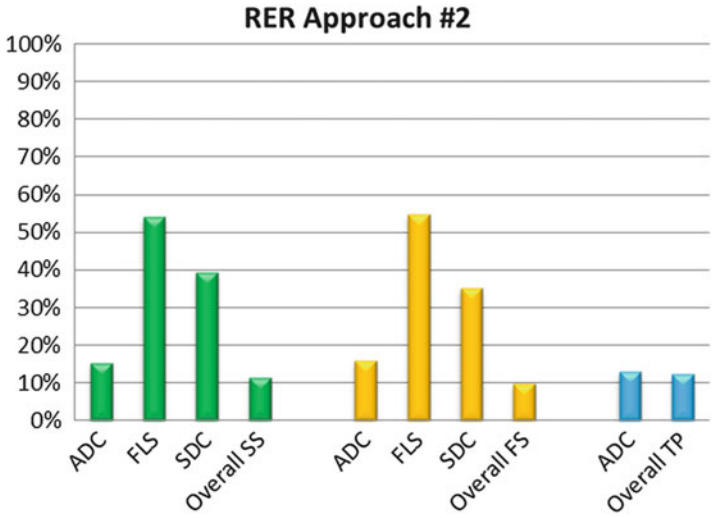

Fig. 9.4 Exergy efficiency of process units of SS, FS, and TP MRUs via RER Approach #2

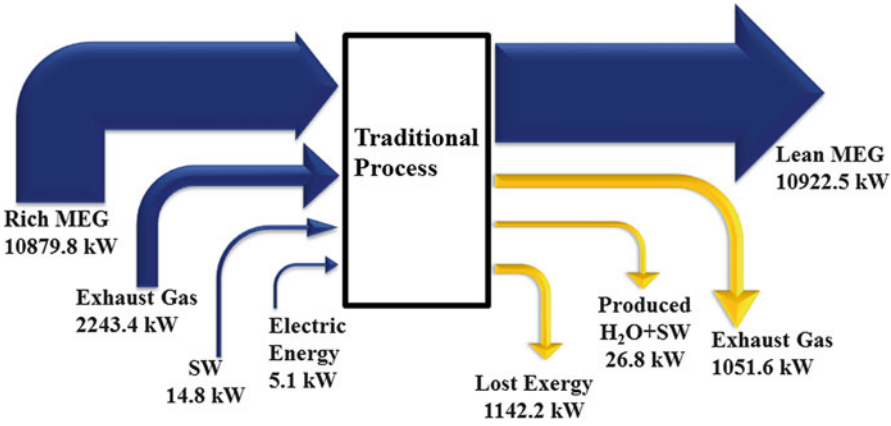

Fig. 9.5 Sankey diagram for traditional process (TP) via RER Approach #1

vapor stream from FLS. Moreover, this is also in accordance with what is expected for ordinary distillation columns as assessed in Chap. 7.

Figures 9.5, 9.6, 9.7, 9.8, 9.9, and 9.10 represent Sankey Diagrams for TP, FS, and SS MRUs under RER Approaches #1 and #2. In such diagrams, the widths of arrows are proportional to the respective exergy flow rates, thereby depicting the distribution of exergy flows of TP, FS, and SS. Very different relative impacts of the rate of lost exergy are markedly observed according to RER Approach #1 and #2.

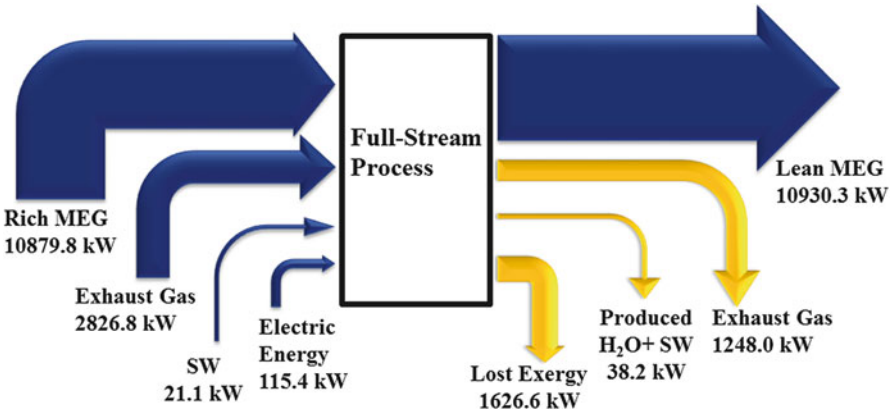

Fig. 9.6 Sankey diagram for full-stream process (FS) via RER Approach #1

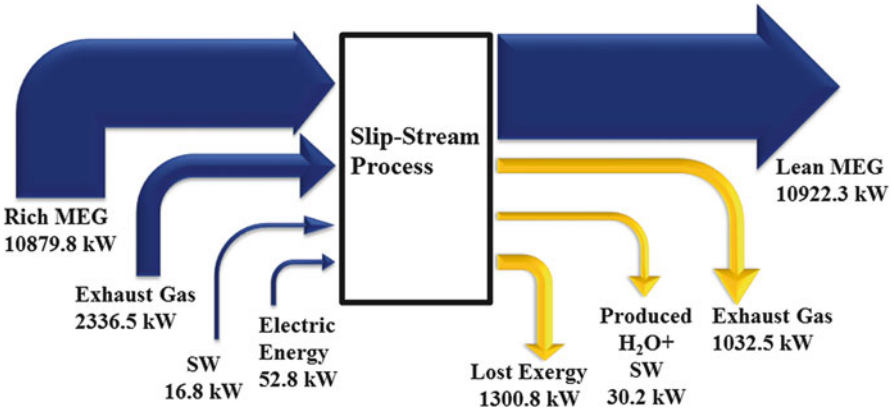

Fig. 9.7 Sankey diagram for slip-stream process (SS) via RER Approach #1

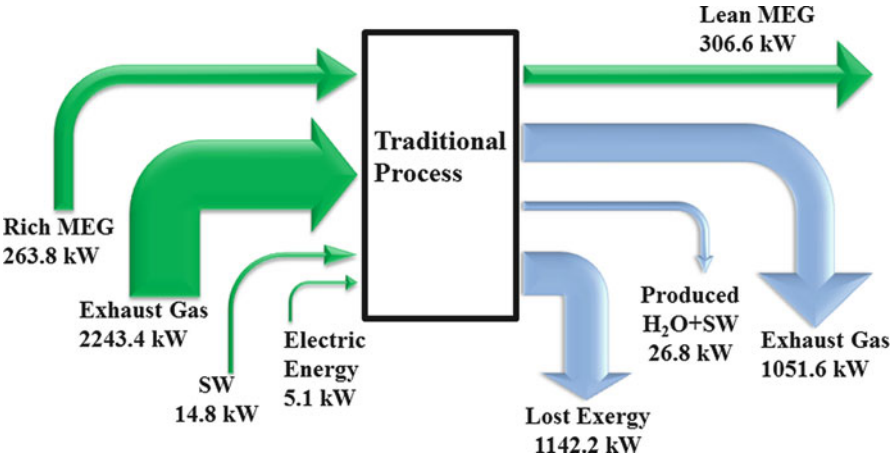

Fig. 9.8 Sankey diagram for traditional process (TP) via RER Approach #2

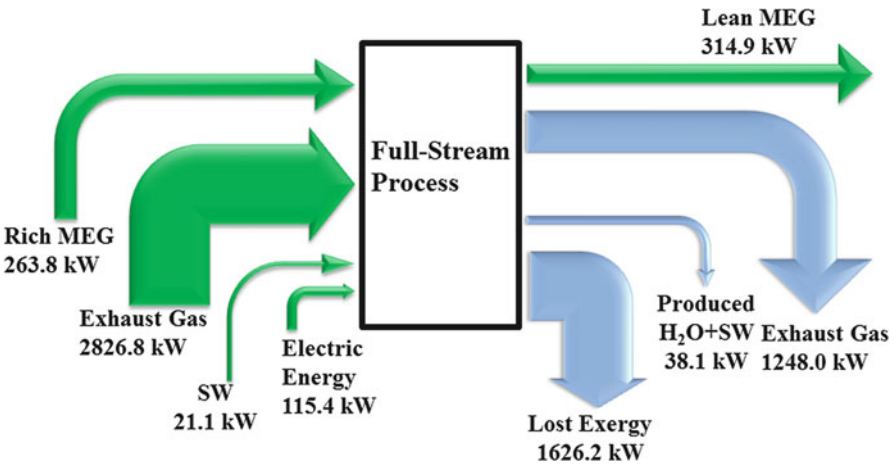

Fig. 9.9 Sankey diagram for full-stream process (FS) via RER Approach #2

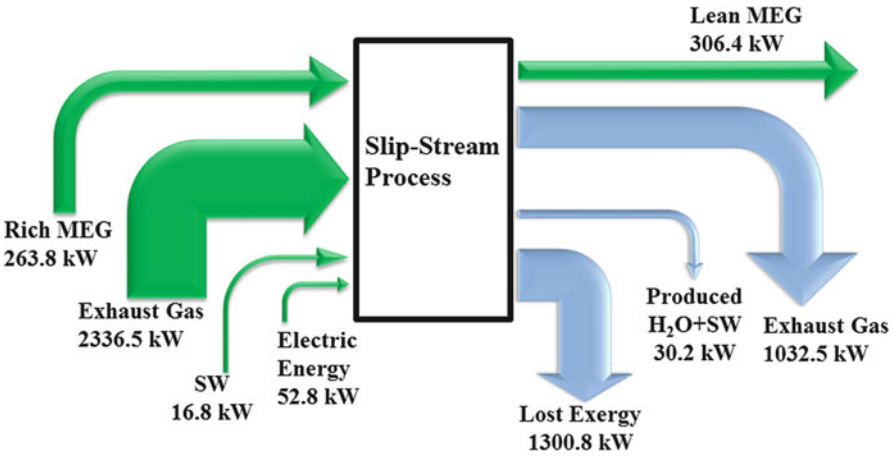

Fig. 9.10 Sankey diagram for slip-stream process (SS) via RER Approach #2

RER Approach #2 allows a more impacting and meaningful role of the rate of lost exergy when compared with the respective main input flow of exergy, namely, the stream of hot exhaust gas.

In other words, ExA with RER Approach #2 (Figs. 9.8, 9.9, and 9.10) reveals that the main input of exergy to drive the transformation of Rich MEG into Lean MEG is just the stream of hot exhaust gas from the gas turbines. RER Approach #2 also indicates that the rate of destroyed exergy amounts about 50–60% of the input exergy conveyed by hot exhaust gas.

Besides the destroyed portion, exergy is also wasted by the output of useless exergy associated to waste streams, such as waste exhaust gas, warm SW and

disposal water. These wasted exergy streams represent approximately 40–50% of the input of exergy with the hot exhaust gas. Therefore, about 90–100% of the main input of exergy (hot exhaust gas) is wasted by irreversible destruction or dispersed into the environment by waste streams.

On the other hand, RER Approach #1 creates an illusory landscape where the main input of exergy to all MRU processes would correspond to the Rich MEG stream, which is portrayed as carrying an exergy flow 4.5 times bigger than the exergy flow of hot exhaust gas. This is a wrong and undesirable message. Rich MEG does not have such a role of resource stream; instead, it is just the raw feed to be upgraded to Lean MEG. The role of "resource stream" must pertain to the hot exhaust gas, which is the real carrier of exergy to drive all MRUs. This feature configures a sensible weak facet of RER Approach #1. In other words, RER Approach #2 is the really useful RER definition for ExA with MRUs.

Despite the different efficiencies calculated via RER Approaches #1 and #2, the results are consistent—but unfair to FS, because the three MRUs do not have isonomic targets—since in both cases TP is the most exergy efficient, while FS is the lesser efficient, with SS occupying an intermediate position.

TP is the simplest MRU, having basically an ADC tower for removing part of the water from Rich MEG. Hence, it has only one primary sink of exergy (ADC) responding by its comparatively lesser exergy loss.

FS and SS also have, from the outset, an ADC with similar targets, but extend the separation beyond the ADC limits. They evaporate partially or totally the fed MEG and sent it to a second distillation operation, the vacuum distillation SDC.

Among FS and SS, FS performs a harder effort by vacuum-distilling a greater material flow and also producing a more concentrated Lean MEG, demanding more heat and more EE to drive vacuum and chiller systems. Such higher heat duties imply higher circulation of PHW, which in turn demands higher heat recovery from hot exhaust gas, as shown in Sect. 6.5. Therefore, FS has to have the highest rate of exergy input with similar rate of output exergy, consequently exhibiting the lowest exergy efficiency.

9.4 Consistency Cross-Check of Exergy Analysis

In order to ensure consistency of exergy calculations, some points must be checked:

- All exergy flow rates of streams must assume positive values and must be higher for streams with greater potential to produce work, e.g., inlet exhaust gas (600 °C) when compared to outlet exhaust gas (300 °C).
- The total exergy flow rate must monotonously decay throughout the processes, since it is always destroyed in spontaneous processes, or lost carried by waste streams, and never created.
- Independent calculations of the rate of lost exergy must be concordant and corroborate each other, as explained next.

Independent calculations of the rate of lost exergy may be carried out so as to ensure exergy consistency, respectively via Eqs. (8.11) and (8.12).

$$\dot{W}^{\,\mathrm{LOST}} = T_0 \dot{\Omega}_S \tag{8.11}$$

$$\Delta \dot{B} \equiv \left(\dot{B}_{\,\mathrm{out}} + \dot{B}^{\,W}_{\,\mathrm{out}}\right) - \left(\dot{B}_{\,\mathrm{in}} + \dot{B}^{\,W}_{\,\mathrm{in}}\right) \tag{8.12}$$

The rate of lost exergy estimated with Eq. (8.12) demands only the exergy flows of MRU streams already displayed in Tables 9.3 and 9.4.

On the other hand, the rate of lost exergy can also be given by the lost work formula in Eq. (8.11), which now demands estimating the rate of creation of entropy in the Universe $\dot{\Omega}_S$ associated with MRU operation.

To estimate $\dot{\Omega}_S$, Eq. (8.6) is used by dropping the first four terms due to steady-state regime and reservoir definition and operation.

$$\dot{\Omega}_S = \dot{S}^{\,\mathrm{Sys}} + \dot{S}^{\,(R_\mathrm{H})} + \dot{S}^{\,(R_V)} + \sum_{k=1}^{\mathrm{nc}} \dot{S}^{\,(R_k)} - \sum_{j}^{\mathrm{nfs}} F_j \bar{S}_{F_j} + \sum_{j}^{\mathrm{nps}} K_j \bar{S}_{K_j} \tag{8.6}$$

The volume reservoir R_V is naturally isentropic, whereas the heat reservoir R_H has zero entropy creation because there is no transfer to it since all cooling duties are directed to SW streams. Similarly, all species reservoirs R_1, R_2, ..., R_nc, do not create entropy because there is no transfer to/from them in all MRUs, since all involved compounds are continuously fed via inlet streams and disposed of by outlet streams without any chemical reaction, i.e., there is no contact with species reservoirs which are left unchanged. Thus, $\dot{\Omega}_S$ is determined by only using the flow rates of entropy associated with feed, product and waste streams of the MRUs.

Results of lost exergy calculations via both ways are displayed in Tables 9.6 and 9.7, respectively for RER Approaches #1 and #2. As can be noted, $\dot{W}^{\,\mathrm{LOST}}$ and $\Delta \dot{B}$ in all cases are concordant and corroborate each other, with discrepancies of low magnitude always below 1%, thereby ensuring consistency of results.

Table 9.6 Cross-check of exergy calculations: comparison of rates of lost exergy via Eqs. (8.11) and (8.12) with RER Approach #1

MRU	Rate of W^{LOST} (kW)	Rate of ΔB (kW)	Discrepancy (%)
TP	1150.5	1142.2	0.72
FS	1617.3	1626.6	−0.58
SS	1292.5	1300.8	−0.64

Table 9.7 Cross-check of exergy calculations: comparison of rates of lost exergy via Eqs. (8.11) and (8.12) with RER Approach #2

MRU	Rate of W^{LOST} (kW)	Rate of ΔB (kW)	Discrepancy (%)
TP	1150.5	1142.2	0.72
FS	1617.3	1626.2	−0.55
SS	1292.5	1300.8	−0.64

Reference

Smith JM, Van Ness HC and Abbott MM (2001) Introduction to chemical engineering thermodynamics, 6th edn. McGraw-Hill, p. 359–361

Chapter 10
Influence of Design Parameters on Exergy Efficiencies of MRU Processes

Abstract Certain equipment design parameters have direct influence on the degree of irreversibility associated with the operation of the equipment in question, concomitantly with inverse influence on the respective size and capital cost. Typical examples are the temperature approach (TAPP) of heat exchangers and the reflux ratio (RR) of distillation columns. From the standpoint of the perspective of the exergy methodology presented in this work, it is worthwhile to assess (and verify) the chains of influences of such design parameters—like TAPP and RR—closely related to the degree of irreversibility of processes. Such analysis is made in this chapter, which shows that the greater the TAPP, the smaller the exchangers and the greater the degree of irreversibility of exchangers; the greater the degree of irreversibility of exchangers, the greater the consumption of thermal utilities and the greater the rate of exergy destruction; the greater the rate of exergy destruction, the lower the exergy efficiency of exchangers and the lower the exergy efficiency of the plant. The chain of influences is similar for the RR of a given column: the greater the RR, the smaller the distillation column and the greater its consumption of thermal utilities; the greater the column consumption of thermal utilities, the greater the column degree of irreversibility, the greater its rate of exergy destruction, the lower the exergy efficiency of the column and the lower the exergy efficiency of the plant.

Certain equipment design parameters have direct influence on the degree of irreversibility associated with the operation of the equipment in question, concomitantly with inverse influence on the respective size and capital cost. Typical examples are the temperature approach (TAPP) of heat exchangers and the reflux ratio (RR) of distillation columns.

Impacts of TAPP on the overall exergy efficiency of the process have the following chain of influences:

- The greater the TAPP, the smaller the exchangers and the greater the degree of irreversibility of exchangers.
- The greater the degree of irreversibility of exchangers, the greater the consumption of thermal utilities and the greater the rate of exergy destruction.

A. Mendonça Teixeira et al., *Monoethylene Glycol as Hydrate Inhibitor in Offshore Natural Gas Processing*, SpringerBriefs in Petroleum Geoscience & Engineering,
DOI 10.1007/978-3-319-66074-5_10

- The greater the rate of exergy destruction, the lower the exergy efficiency of exchangers and the lower the exergy efficiency of the plant.

The chain of influences is similar for the RR of a given column:

- The greater the RR, the smaller the distillation column and the greater its consumption of thermal utilities.
- The greater the column consumption of thermal utilities, the greater the column degree of irreversibility, the greater its rate of exergy destruction, the lower the exergy efficiency of the column and the lower the exergy efficiency of the plant.

From the standpoint of the perspective of the exergy methodology presented in this work, it is worthwhile to assess (and verify) the chains of influences of such design parameters—like TAPP and RR—closely related to the degree of irreversibility of processes.

To accomplish this, the common TAPP of three specific heat exchangers—ADC reboiler, SHE of FLS and the sub-cooler at the top of SDC using ChW—and, separately, the RR of ADC are monotonically increased in order to observe the respective impacts on exergy efficiencies of MRUs—via Eq. (8.13)—using both RER approaches. This sensitivity analysis is implemented for all MRUs under the following assumptions relative to the specific base case of each MRU:

- Transfer areas and overall heat transfer coefficients of exchangers are kept with values from the respective base cases.
- Temperature change of the hot exhaust gas stream kept from 600 to 300 °C as in all base cases.
- Number of stages and distillate flow rate of ADC kept with values from the respective base cases.

The results of the influence of temperature approach (TAPP) on the exergy efficiencies of all MRUs are shown on Table 10.1, where the first row of Table 10.1 corresponds to the base cases, which used thermal approach of 5 °C for the exchangers of TP, FS and SS.

As expected, the rising of TAPP from 5 to 25 °C increases the irreversibility related to heat exchanges, monotonically reducing the exergy efficiency of MRUs. With RER Approach #1 the unrealistic large efficiencies are reduced by

Table 10.1 Influence of temperature approach on exergy efficiency (%) of MRU processes

	RER Approach #1			RER Approach #2		
TAPP (°C)	TP	FS	SS	TP	FS	SS
5[a]	83.10[a]	78.96[a]	82.21[a]	12.13[a]	9.76[a]	11.48[a]
10	82.94	78.79	82.05	12.01	9.67	11.37
15	82.76	78.61	81.89	11.88	9.57	11.26
20	82.58	78.43	81.73	11.75	9.48	11.15
25	82.40	78.24	81.56	11.61	9.39	11.04

[a]Base case values

Table 10.2 Influence of reflux ratio (RR) on the exergy efficiency (%) of ADC of MRUs

	RER Approach #1			RER Approach #2		
RR	TP	FS	SS	TP	FS	SS
0.20	85.07	88.28	87.61	14.60	17.76	17.02
0.22	84.66	87.93	87.26	14.21	17.28	16.58
0.24	84.24	87.57	86.91	13.82	16.80	16.15
0.26	83.81	87.20	86.54	13.44	16.33	15.72
0.28	83.36	86.81	86.16	13.07	15.87	15.30
0.30	82.90	86.40	85.77	12.70	15.41	14.88
0.32	82.43	85.98	85.37	12.33	14.95	14.47
0.34	81.93	85.54	84.95	11.97	14.50	14.07
0.36	81.42	85.09	84.52	11.62	14.06	13.67
0.38	80.89	84.62	84.07	11.27	13.62	13.28
0.40	80.35	84.12	83.60	10.92	13.19	12.89

Table 10.3 Influence of ADC reflux ratio (RR) on overall exergy efficiency (%) of MRUs

	RER Approach #1			RER Approach #2		
RR	TP	FS	SS	TP	FS	SS
0.20	84.81	80.18	83.53	13.55	10.44	12.46
0.22	84.40	79.89	83.22	13.19	10.27	12.21
0.24	83.98	79.59	82.89	12.83	10.10	11.97
0.26	83.55	79.27	82.56	12.48	9.93	11.72
0.28	83.10	78.95	82.21	12.13	9.76	11.48
0.30	82.64	78.61	81.85	11.79	9.58	11.23
0.32	82.17	78.26	81.48	11.45	9.40	10.99
0.34	81.68	77.90	81.10	11.12	9.22	10.74
0.36	81.17	77.52	80.70	10.79	9.04	10.50
0.38	80.64	77.12	80.29	10.47	8.86	10.25
0.40	80.09	76.71	79.86	10.15	8.67	10.01

approximately almost 1% with TAPP = 25 °C, whereas with RER Approach #2, this fall is approximately of 4%.

The results of the influence of reflux ratio (RR) of ADC on the exergy efficiency of the ADCs of TP, FS and SS are seen on Table 10.2, whereas the influences of RR on the overall efficiency of TP, FS and SS MRUs follow in Table 10.3.

The results corresponding to the base cases of TP, FS and SS (Table 9.5) are recognized for RR = 0.28 on Table 10.3. As easily seen, the overall exergy efficiencies of all MRUs are much more sensitive to changes on the RR of ADC. With RER Approach #1 the unrealistic large efficiencies are reduced by approximately almost 5% as RR doubles from 0.2 to 0.4, whereas with RER Approach #2, this fall is approximately of 20%.

To explain these trends in Tables 10.2 and 10.3:

- Firstly, it must be recalled that ADC is recognized in Fig. 9.3 and especially Fig. 9.4 (which adopts the appropriate RER definition) as the main exergy sink in all MRUs.

- Secondly, from Fig. 9.4 it can be seen that the exergy efficiencies of all MRUs are "dragged" to the efficiency of ADC in consequence of its prominent role as main exergy degrader.
- Thirdly, Chap. 7 aggregates useful information on thermodynamic efficiency of distillation columns, like its strong dependence on RR and how it impacts the overall efficiency of a power consuming process. It was demonstrated that common distillation columns have low thermodynamic efficiencies that fall initially very rapidly and then asymptotically to zero (Figs. 7.4 and 7.8) as the reflux ratio increases from minimum to total reflux.
- Fourthly, Sect. 7.3 showed how the fall of the thermodynamic efficiency of a dominant (in terms of exergy destruction) distillation column can impact the overall process efficiency in the case of power consuming flowsheets like MRUs.

Chapter 11
Energy Performance Versus Exergy Performance of MRU Processes

Abstract The interrelationship between energy performance and exergy performance of a chemical process is somewhat subtle and commonly not well interpreted in general. For instance, it is possible to keep the same level of energy performance of a given operating process, but adopting some modifications—characteristically based on investing some capital into the process—to operate with a better exergy performance, as demonstrated in this chapter. In other words, an upgrade of the exergy performance does not necessarily mean that the process now uses less energy, albeit a better exergy performance usually leads to better energy usage and less energy expenditures. Another obvious fact is that making the process more costly does not necessarily imply in better exergy performance. The truth is that the achievement of a better exergy performance of a process always implies, on the one hand, that some monetary investment has to be injected into the process increasing its capital expenditure (CAPEX), size and possibly operational complexity, but, on the other hand, with the counterpart that some benefit can be expected in one or more of the following contexts related to the process performance as a whole: (1) energy degradation and energy usage; (2) energy consumption; (3) health, safety and environmental (HSE) impacts; (4) durability of equipment; (5) maintenance costs of equipment; (6) energy costs; (7) operation costs (OPEX); (8) product degradation costs; (9) waste production costs; (10) pollutant emissions; and (11) atmospheric emissions of CO_2.

The interrelationship between energy performance and exergy performance of a chemical process is somewhat subtle and commonly not well interpreted in general. For instance, it is possible to keep the same level of energy performance of a given operating process, but adopting some modifications—characteristically based on investing some capital into the process—to operate with a better exergy performance. In other words, an upgrade of the exergy performance does not necessarily mean that the process now uses less energy, albeit a better exergy performance usually leads to better energy usage and less energy expenditures. Another obvious fact is that making the process more costly does not necessarily imply in better exergy performance.

The truth is that the achievement of a better exergy performance of a process always implies, on the one hand, that some monetary investment has to be injected

A. Mendonça Teixeira et al., *Monoethylene Glycol as Hydrate Inhibitor in Offshore Natural Gas Processing*, SpringerBriefs in Petroleum Geoscience & Engineering,
DOI 10.1007/978-3-319-66074-5_11

into the process increasing its capital expenditure (CAPEX), size and possibly operational complexity, but, on the other hand, with the counterpart that some benefit can be expected in one or more of the following contexts related to the process performance as a whole (Voldsunt et al. 2014): (1) energy degradation and energy usage; (2) energy consumption; (3) health, safety and environmental (HSE) impacts; (4) durability of equipment; (5) maintenance costs of equipment; (6) energy costs; (7) operation costs (OPEX); (8) product degradation costs; (9) waste production costs; (10) pollutant emissions; and (11) atmospheric emissions of CO_2.

In order to demonstrate this concept, let us consider the three MRU processes in Chap. 5 which were analyzed in terms of exergy efficiency in Chap. 9 according to RER Approach #1 and RER Approach #2. Let us only consider the much more meaningful results of ExA with RER Approach #2. Then, some improvement is implemented into all the three MRUs to reduce exergy degradation increasing the respective exergy efficiencies according to ExA with RER Approach #2. Such process modification should be proposed so that all MRU configurations are equally benefited in terms of better exergy usage, while not improving the energy (heat and EE) consumption. That is, the energy performance is exactly the same as in the previous MRU configurations, but the exergy efficiency is improved resulting in some benefits in the MRU operation and in the offshore platform operation taken as a whole.

11.1 Modification of MRU Processes for Better Exergy Usage Under Constant Energy Usage

It is certainly possible to increment the quality of exergy usage in all three MRU processes—TP, FS, and SS—by simply altering some common operational or structural parameter of all MRUs that will entail better exergy efficiency. In the present case we seek a reduction in the MRU input rate of exergy, while maintaining its production and separation targets. This will improve the exergy efficiencies of all MRUs.

This can be implemented, for example, by reducing the temperature of the final exhaust gas leaving the Heat Recovery Water Heater (HRWH), which is responsible by the production of pressurized hot water (PHW) at 200 °C. As established in the list of MRU processing assumptions in Sect. 6.1, the temperature of the final exhaust gas leaving the HRWH was fixed at 300 °C. By reducing the final gas exhaust temperature to 200 °C, while maintaining the same flow rate of PHW leaving the HRWH at 200 °C, the same supply of heat is guaranteed to the MRUs, not affecting their heat and power consumptions. But, certainly the HRWH intake of hot gas exhaust at 600 °C can be reduced by approximately 25%. This will reduce the intake of exergy into the MRUs, while maintaining their operational performances and targets, therefore increasing the exergy efficiency.

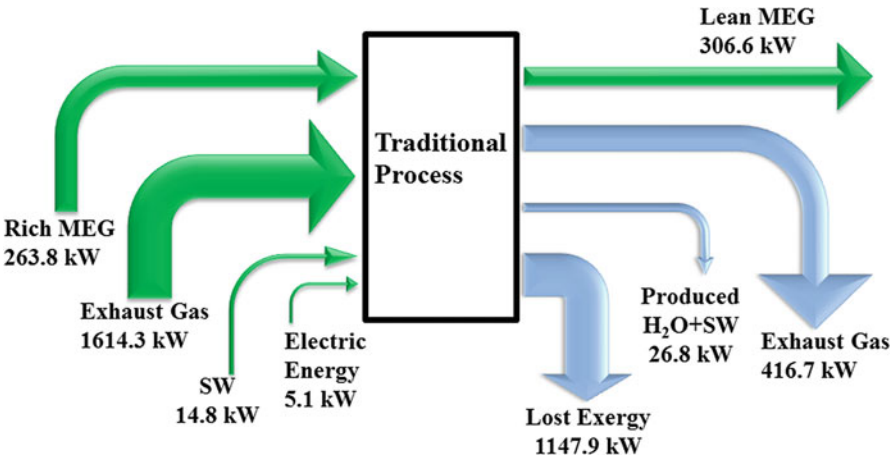

Fig. 11.1 New Sankey diagram for traditional process (TP) (RER Approach #2)

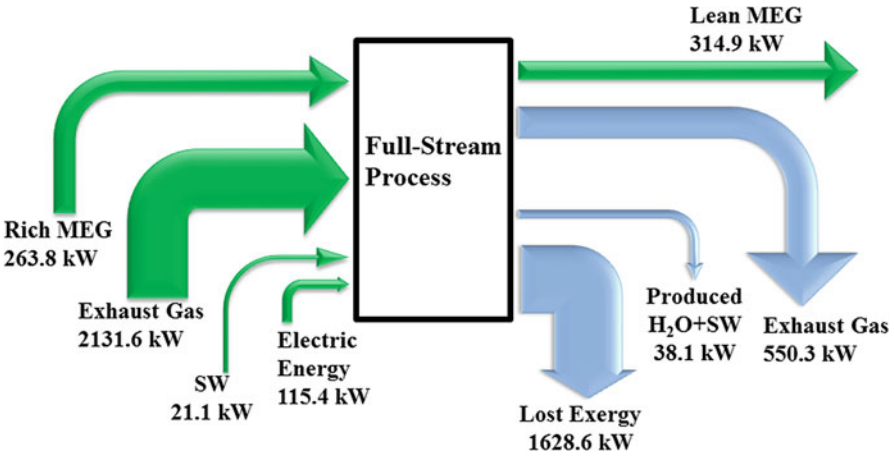

Fig. 11.2 New Sankey diagram for full-stream process (FS) (RER Approach #2)

Figures 11.1, 11.2, and 11.3 depict the new Sankey diagrams of exergy usage by the three respective MRUs TP, FS, and SS using RER Approach #2. The corresponding new and old exergy efficiencies are shown in Table 11.1. Table 11.1 also reports the old and new flow rates of hot exhaust gas (at 600 °C) needed by all MRUs, showing that a certain reduction is observed in the consumption of this resource after the implementation of the HRWH expansion.

It is evident that, despite not leading to a gain in terms of energy performance, this HRWH modification implies a severe increase in the equipment cost, because it now has to have a much better geometry and greater heat transfer area to cool the gas exhaust to 200 °C, while maintaining the produced PHW at 200 °C with the same flow rate.

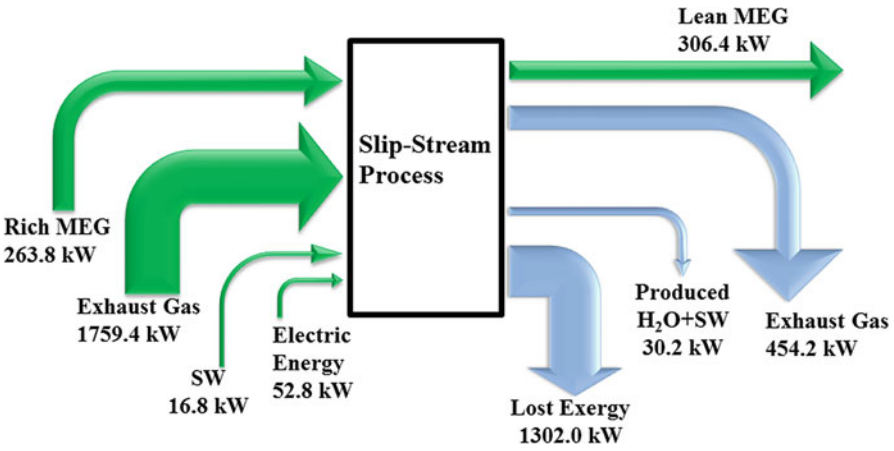

Fig. 11.3 New Sankey diagram for slip-stream process (SS) (RER Approach #2)

Table 11.1 Old and new exhaust gas flow rates and exergy efficiencies of MRUs

MRU	Old exhaust gas flow rate (ton/h)	New exhaust gas flow rate (ton/h)	Old exergy efficiency (%)	New exergy efficiency (%)
TP	19.1	13.7	12.13	16.15
FS	24.0	18.1	9.76	12.44
SS	19.9	15.0	11.48	14.64

On the other hand, there are real benefits to the oil and gas offshore platform as a whole and to the environment, namely: (1) lower hot exhaust consumption by the MRU means that a greater flow rate of this hot resource is available to other uses in the platform; and (2) the environmental impact of the emission of residual hot gas exhaust by the MRU has now a lesser importance because the exhaust is released relatively colder at 200 °C with a lower flow rate.

Table 11.1 shows that this modification in the HRWH (entailing additional CAPEX) cuts the consumption of hot gas exhaust by approximately 25%, with the consequence that the input flow rate of exergy to all MRUs has decreased by approximately 25%. Taken into account the formula of exergy efficiency in Eq. (8.13), this implies that all MRU exergy efficiencies increase by about 25% relatively to the previous respective values.

In other words, the Energy Performances of all MRUs were kept constant, but all Exergy Performances were improved. The indirect consequences of this HRWH modification are that the hot utility gas exhaust at 600 °C (consumed by all MRUs) is spared and the final emission of used gas exhaust is reduced, both in terms of temperature as well as in terms of flow rate. New Sankey diagrams reporting exergy flows of MRUs TP, FS, and SS in Figs. 11.1, 11.2, and 11.3, should be compared with the respective old ones Figs. 9.8, 9.9, and 9.10 before the adoption of the HRWH modification.

Reference

Voldsunt M, Nguyen T-V, Elmegaard B, Ertesvåg I S, Røsjorde A, Jøssang K, Kjelstrup S. “Exergy destruction and losses on four North Sea offshore platforms: a comparative study of the oil and gas processing plants”. Energy 74, 2014, 45–78. http://dx.doi.org/10.1016/j.energy.2014.02.080

Chapter 12
Concluding Remarks

Abstract The need to avoid hydrate formation is undeniable in offshore natural gas fields, especially in deep-water environments, where favorable conditions for hydrate formation are easily found. In this context, MEG injection is an approved technology to successfully displace the hydrates equilibrium loci to lower temperatures in ultra-deep subsea gas production pipelines. Further, Rich MEG has to be processed in MEG Recovery Units (MRU) in order to be recovered as Lean MEG to be pumped back as refreshed THI, saving costs. Also, as distillation-based processes, MRUs are very intensive in terms of heat consumption. Energy is related to properties that depend only on the present state of the material in the system at hand. On the other hand, Exergy is a property that depends both on the state of the material in the system and on the definition of the Reference Environment Reservoir (RER). Thus, two choices of MEG state in the RER were investigated so as to perform Exergy Analysis for three MRU technologies designed to operate on offshore NG production rigs: Traditional Process (TP), Full-Stream Process (FS), and Slip-Stream Process (SS). This chapter brings the main conclusions of this book, which covered several qualitative and quantitative aspects related to hydrate inhibition and offshore MRUs, studied from their fundamental aspects to engineering aspects and from Energy Performance to Exergy Performance assessments by handling advanced topics like Exergy Analysis through many approaches, including classical Thermodynamic Analysis of separation processes.

The need to avoid hydrate formation is undeniable in offshore natural gas fields, especially in deep-water environments, where favorable conditions for hydrate formation are easily found. In this context, MEG injection is an approved THI technology to successfully displace the hydrates equilibrium loci to lower temperatures in ultra-deep subsea gas production pipelines.

Further, Rich MEG has to be processed in MEG Recovery Units (MRU) in order to be recovered as Lean MEG to be pumped back as refreshed THI, saving costs. Another fact is that as distillation-based technologies, MRUs are very intensive in terms of heat consumption.

Consequently, in offshore platforms, where space and energy resources are limited, besides determining energy requirements—Energy Performance—it is

A. Mendonça Teixeira et al., *Monoethylene Glycol as Hydrate Inhibitor in Offshore Natural Gas Processing*, SpringerBriefs in Petroleum Geoscience & Engineering,
DOI 10.1007/978-3-319-66074-5_12

also of importance to perform a Thermodynamic Analysis to assess degradation of energy quality, which can be done by Exergy Analysis—Exergy Performance.

Energy is related to properties that depend only on the present state of the material in the system at hand. On the other hand, Exergy is a property that depends both on the state of the material in the system and on the definition of the Reference Environment Reservoir (RER). Thus, two choices of MEG state in the RER were investigated so as to perform Exergy Analysis for three MRU technologies designed to operate on offshore NG production rigs: Traditional Process (TP), Full-Stream Process (FS), and Slip-Stream Process (SS).

To accomplish this, firstly the PFDs of the MRUs under consideration were solved within a professional simulation environment to obtain the Energy Performance of all MRUs—i.e. heat and power consumptions and CO_2 emissions—and also all distributions of mass and energy flow rates along the MRUs.

To access the Exergy Analyses of MRUs, two RER Approaches were chosen:

- Usual RER Approach #1, a two-phase environment where the gas phase corresponds to the dry-basis standard atmosphere in VLE with pure liquid water at 25 °C and 1 atm containing traces of MEG in the gas phase under oxidative chemical equilibrium with CO_2, H_2O, and O_2.
- Novel RER Approach #2, again a two-phase environment consisting of dry-basis atmospheric air in VLE with liquid water containing MEG at infinite dilution, but not in chemical equilibrium with air species.

Both approaches calculated the same rate of lost exergy for the same MRU and yielded consistent results (cross-check consistency test, Sect. 9.4).

However, RER Approach #1 seems inappropriate because it leads to too high values of exergy flow rates of streams, which are much higher than the corresponding values of rates of lost exergy. This masks results and hinders the discrimination of performances of units and processes in terms of exergy degradation.

On the other hand, RER Approach #2 defines the RER condition of MEG as a liquid infinitely diluted in water, not in chemical equilibrium with air species. The corresponding exergy flow rates of streams are much lower now, with greater evidence of exergy losses and better discrimination of exergy efficiencies.

Hence, RER Approach #2 could clearly indicate the main points of exergy destruction, as originally intended by Exergy Analysis. Further, exergy efficiencies of MRUs with RER Approach #2 presented values around 10–11% which are very reasonable values for distillation-based processes as demonstrated in the two distillation examples of Chap. 7. Despite the stringent separation targets for water disposal and minimum MEG losses (minimum water purity of 99.99% w/w), the MRU distillations ADC and SDC are not too hard separations, because the atmospheric or subatmospheric relative volatilities MEG-H_2O are very large and easily shown to be greater than 20.

RER Approach #1, although consistent and correct, failed to provide discrimination of Exergy Performances and realistic results, whereas the proposed novel

RER Approach #2 was able to provide much more realistic and meaningful exergy efficiency values.

Therefore, setting an appropriate RER definition is highlighted in order to achieve a successful Exergy Analysis. By means of Exergy Analysis with appropriate RER choice, commercial MRUs were weighted with the respective main exergy sinks accurately identified and the respective exergy efficiencies correctly determined.

A comprehensive sensitivity study was also performed in Chap. 10 so as to get insights on how MRU exergy efficiencies respond with the increase of crucial design parameters—temperature approach for heat exchangers and reflux ratio of ADC—whose values are directly translated as degree of irreversibility in the respective operations, i.e., the greater their values, the lower the process exergy efficiency.

By last, the Exergy Performance is confronted with the Energy Performance in the context of offshore MRUs. Chapter 11 shows that these two concepts are interconnected, but in a subtle way. A simple example was solved in terms of Exergy Analysis showing that the Energy Performance of MRUs could be kept constant, while the Exergy Performance is upgraded by investing in a costlier system for Heat Recovery Water Heater (HRWH). This brings indirect long-term benefits like less environmental impact of final gas exhausts and better use of available resources.

In summary, this book covers several qualitative and quantitative aspects related to hydrate inhibition and offshore MEG Recovery Units—MRUs. MRUs are studied from their fundamental aspects to engineering aspects and from Energy Performance to Exergy Performance assessments by handling advanced topics like Exergy Analysis through many approaches, including classical Thermodynamic Analysis of separation processes. Thus, this book addresses a self-contained global comprehension on the subject of MEG recovery on offshore platforms.

Index

A. Mendonça Teixeira et al., *Monoethylene Glycol as Hydrate Inhibitor in Offshore Natural Gas Processing*, SpringerBriefs in Petroleum Geoscience & Engineering,
DOI 10.1007/978-3-319-66074-5